Principles and Theory of Radar Interferometry

Paul A Rosen

Jet Propulsion Laboratory

August 8, 2011
UNAVCO Short Course

Outline of Tutorial

I. Quick Review of Radar Imaging Fundamentals

- A. Basic Principles of SAR
- B. Range and Azimuth Compression
- C.Strip Mode vs ScanSAR vs Spotlight
- D. Doppler and its Implications

II. Geometric Aspects of Interferometric Phase Measurement

- A. Interferometric Phase for Topographic Mapping
- B. Interferometric Phase for Deformation Mapping
- C. Sensitivity of Topographic Phase Measurements
- D. Sensitivity of Deformation Phase Measurements
- E. Comparison of Various Interferometric Mapping Schemes

III. Interferometric Correlation

- A. Random and Deterministic Portions of the Interferometric Phase
- B. SNR and Interferometric Correlation
- C. Geometric Decorrelation and Range Spectral Shift
- D. Temporal Decorrelation
- E. Volumetric Decorrelation
- F. Other Error Sources

IV. Interferometric Processing

- A. Processing Flow
- B. Interferogram Formation
- C. Image Co-registration
- D. Baseline Determination
- E. Phase Unwrapping
- F. Height Determination
- G. Deformation Signal Extraction

The Radar Concept

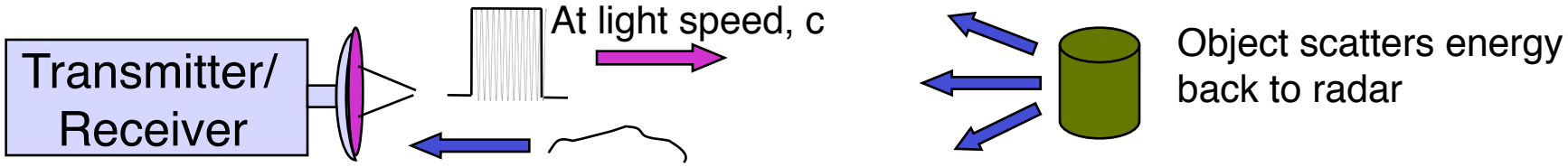

- Much like sound waves, radar waves carry information that echoes from distant objects
- The time delay of the echo measures the distance to the object
- The changes of the message in the echo determines the object characteristics

Wave Properties of Light

- Radar waves, like lightwaves, are electromagnetic energy that propagates

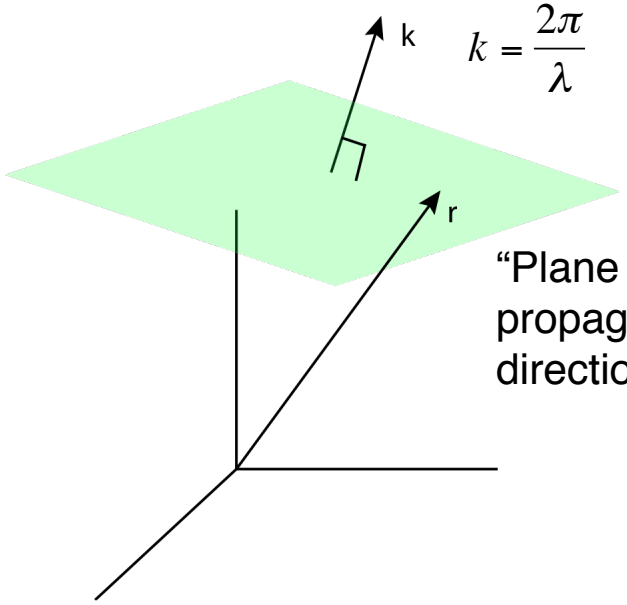

$$k = \frac{2\pi}{\lambda}$$

"Plane wave" propagating in direction k

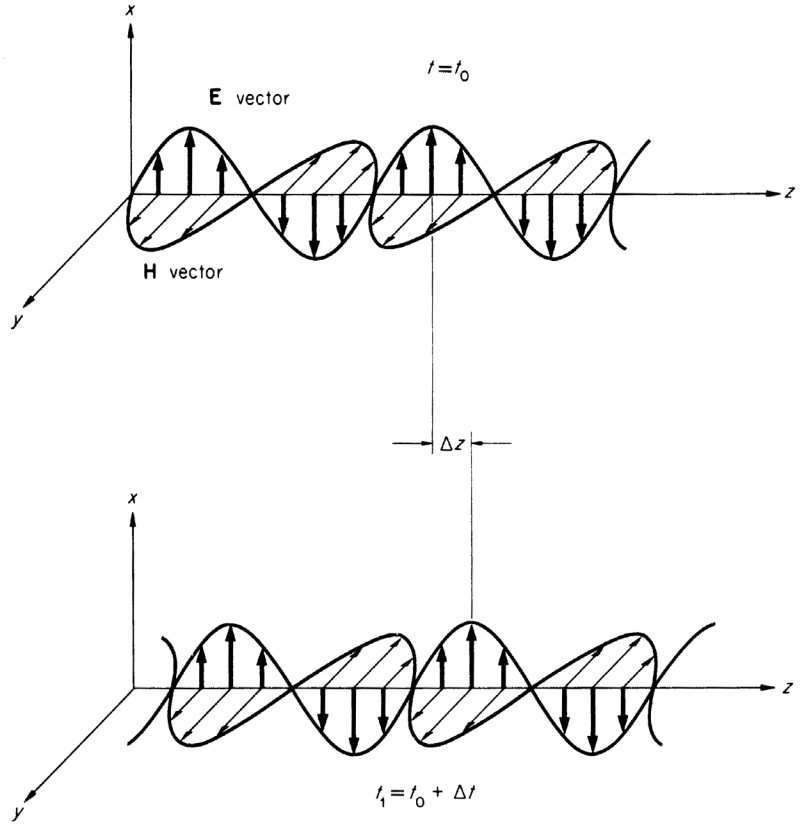

Energy propagates →

"Phase" ↘ frequency ↘

$$E(x,y,z,t) = E_0 e^{j\phi(x,y,z,t)} = E_0 e^{j(\omega t - \vec{k}\cdot\vec{r})}$$

Radar and Light Waves

- Radars operate at microwave frequencies, an invisible part of the electromagnetic spectrum
- Microwaves have wavelengths in the millimeter to meter range
- Like lasers, radars are coherent and nearly a pure tone

Millimeters to meters wavelength

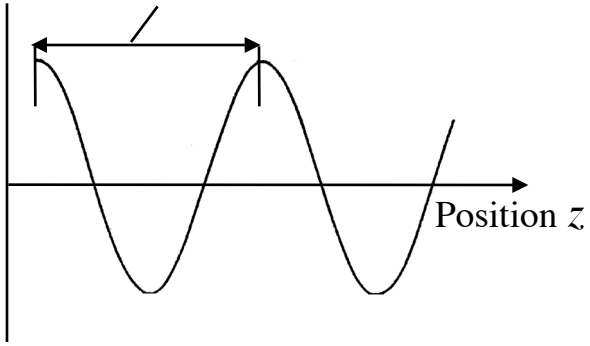

Common Radar Frequency Bands

Band	X	C	S	L	P
Wavelength (cm)	3	6	12	24	75
Frequency (G-cycles/s)	10	5	2.5	1.2	0.4

The Electromagnetic Spectrum

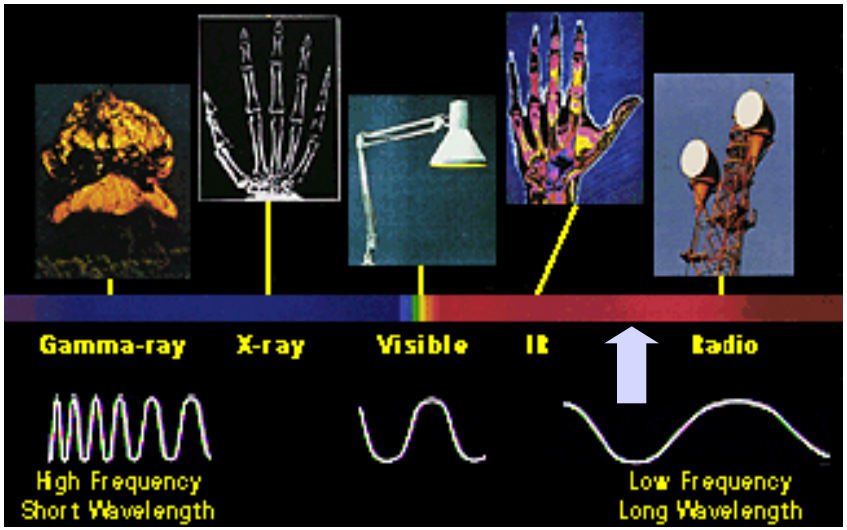

tiny 100's μm mm's to m's

Radar on a Moving Platform

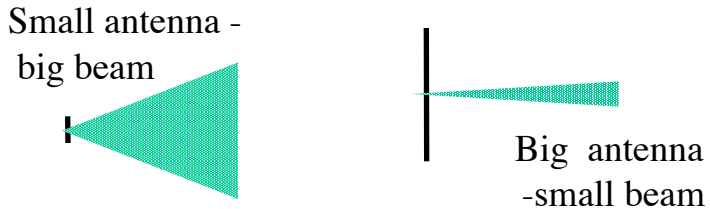

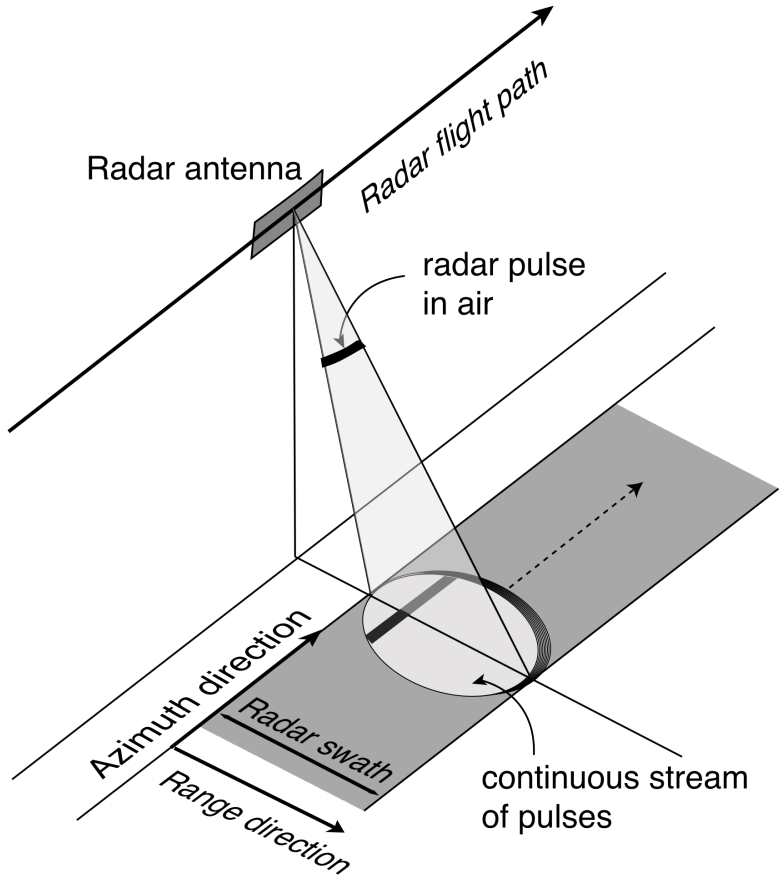

- Pulses are transmitted from the radar platform as it moves along its flight path
- Each pulse has finite extent in time, illuminating a narrow strip of ground as it sweeps through the antenna beam
- Some of the energy from the ground is scattered back to the radar instrument

Antenna Beamwidth

$$\theta_{3dB} = \frac{\lambda}{L}$$

Footprint Size on Ground

$$\Delta X_{az} \approx \rho\theta_{3dB_{az}} = \frac{\rho\lambda}{L_{az}}$$

$$\Delta X_{\rho} \approx \rho\theta_{3dB_{\rho}} = \frac{\rho\lambda}{L_{\rho}}$$

Achieving resolution in range

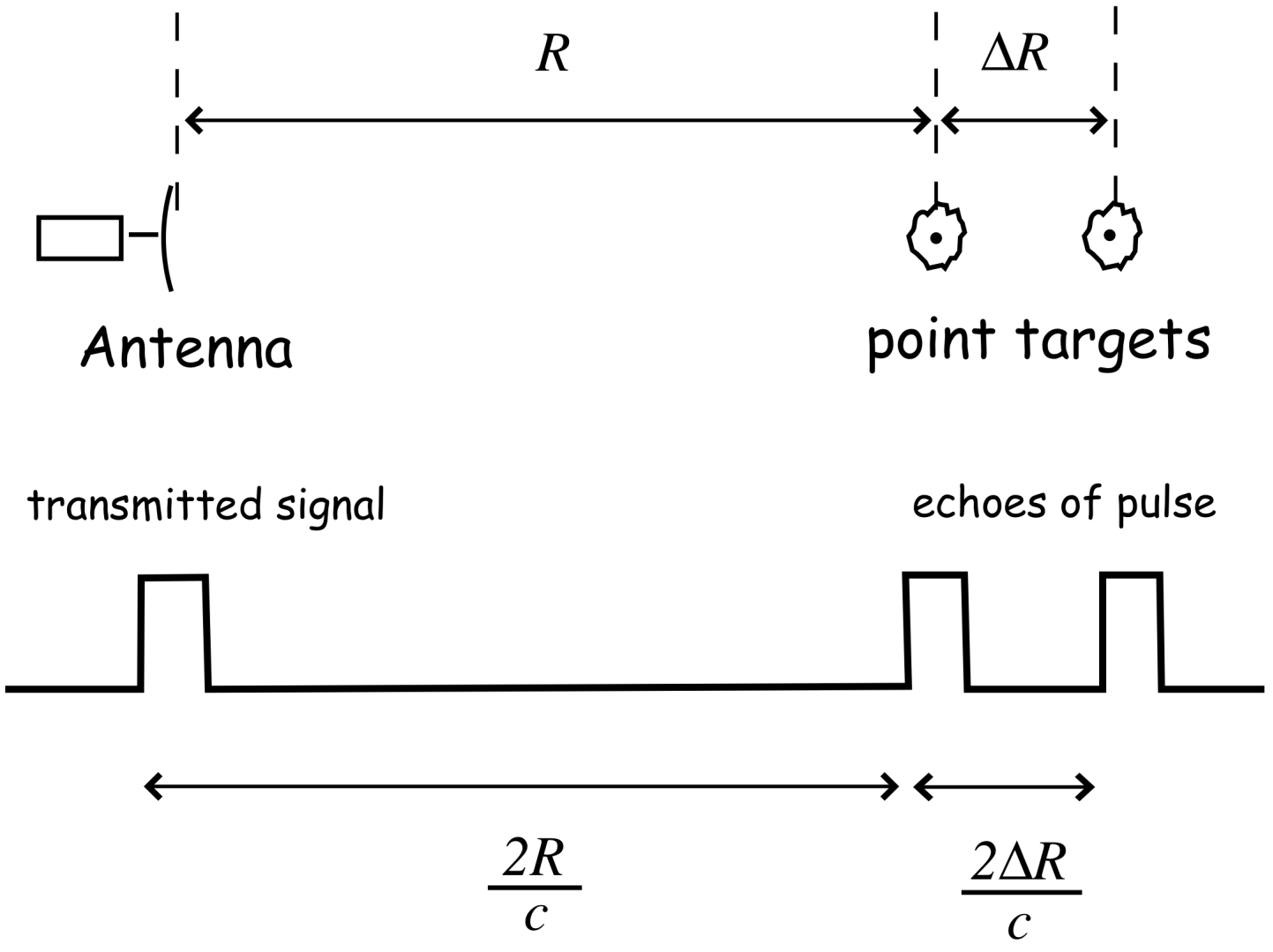

If possible, use a narrow pulse to resolve close targets

Achieving resolution in range

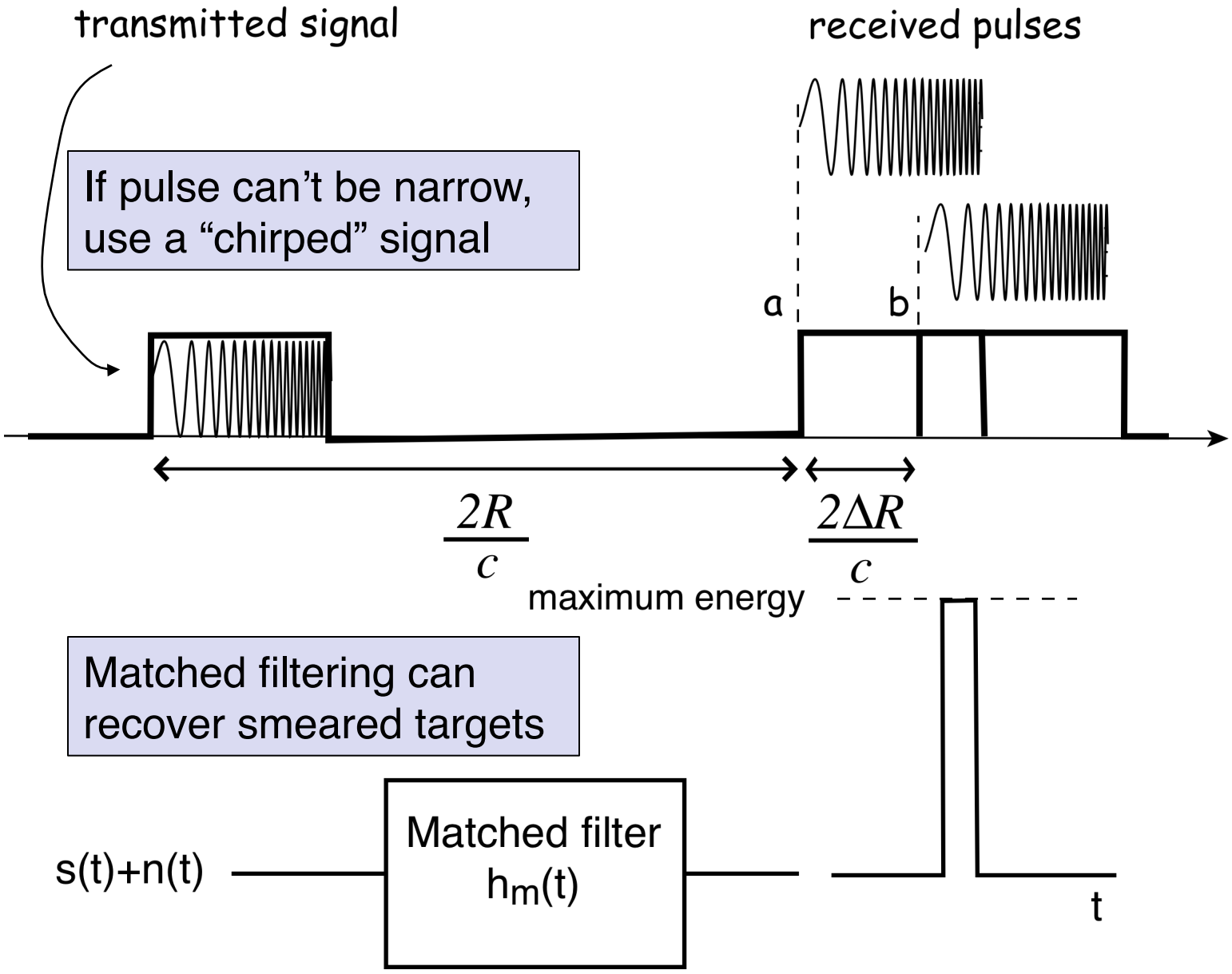

Matched Filtering of Received Echo

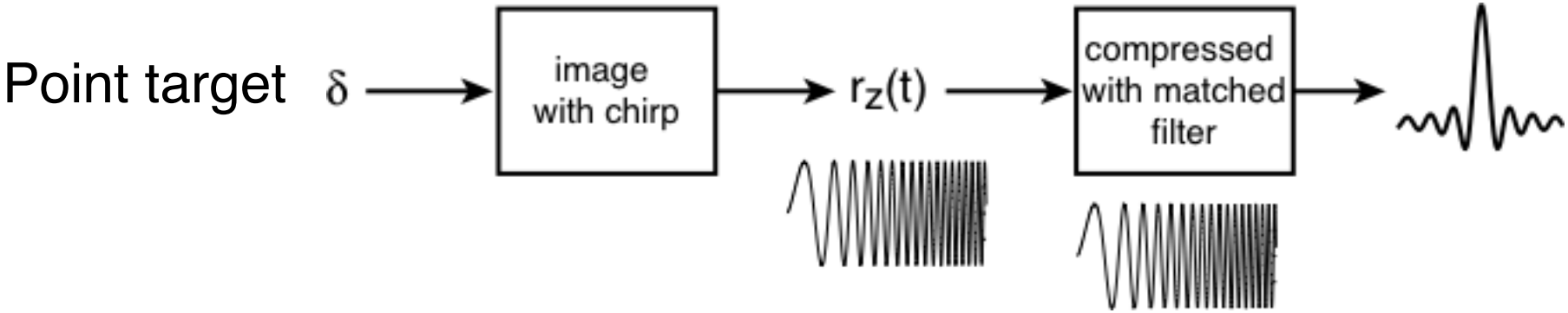

In general, the ground surface can be though of as a distribution of point targets, so the received echo, r(t), is a convolution of ground and chirp signal

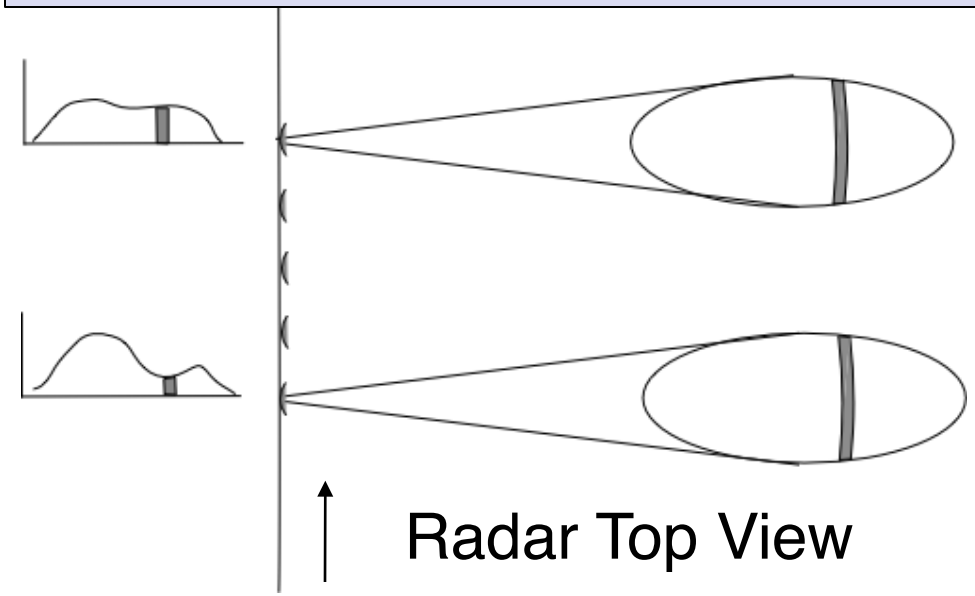

- Transmitted pulses are usually coded waveforms with significant bandwidth
- Matched filtering allows recovery of fine resolution features with a low peak-power pulse train

Raw Signal of a Point Target

Range →

Pulse Number →

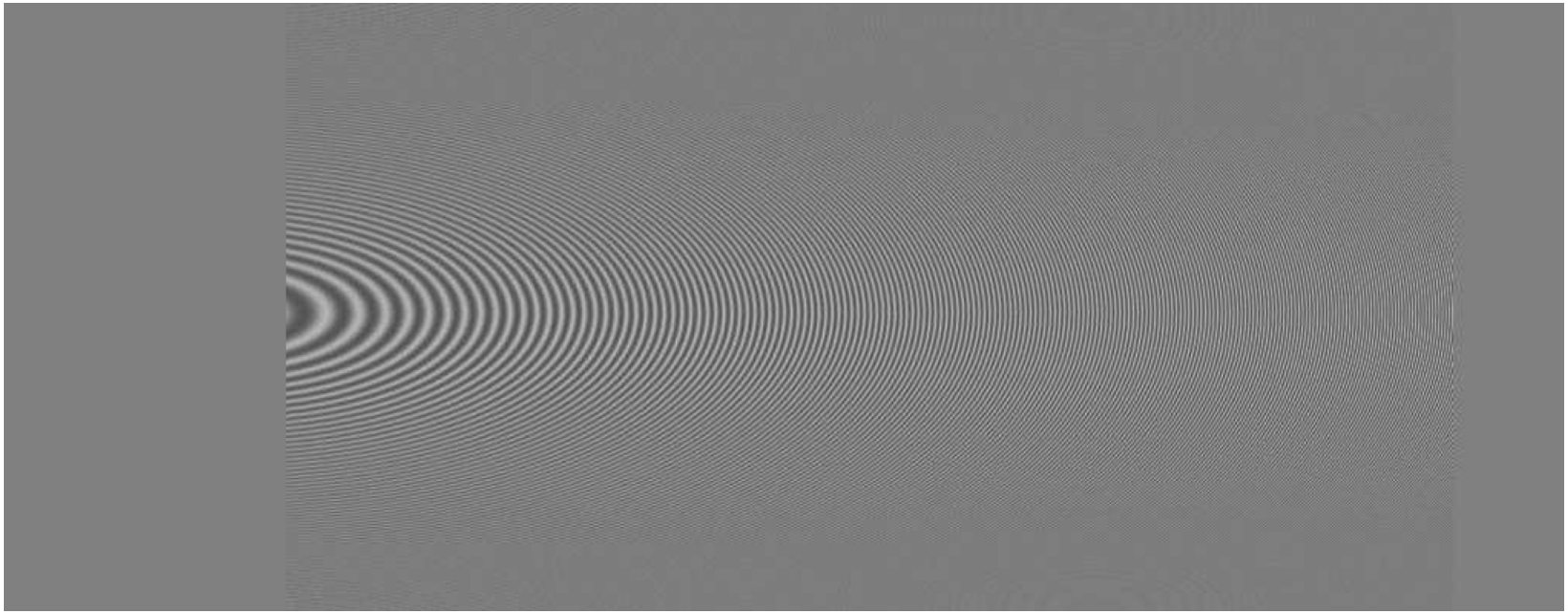

This “image” shows a sequence of simulated pulse echoes from a single point target

Range Compression of a Point Target; after Matched filtering

Range →

Pulse Number →

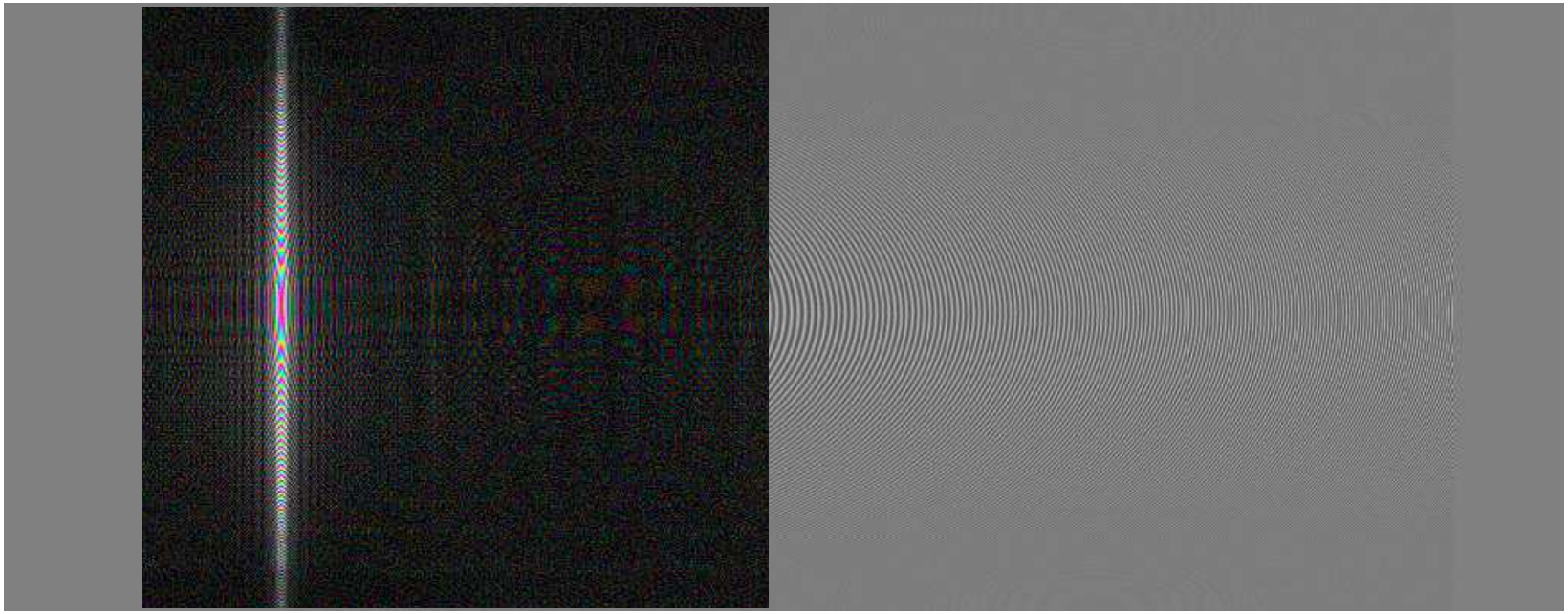

This “image” shows the simulated pulse echoes after range compression matched filtering

SAR Imaging Concept

Real Aperture Imaging

Cross-Track resolution achieved by short or coded pulses

Along-Track resolution limited by beamwidth

Synthetic Aperture Imaging

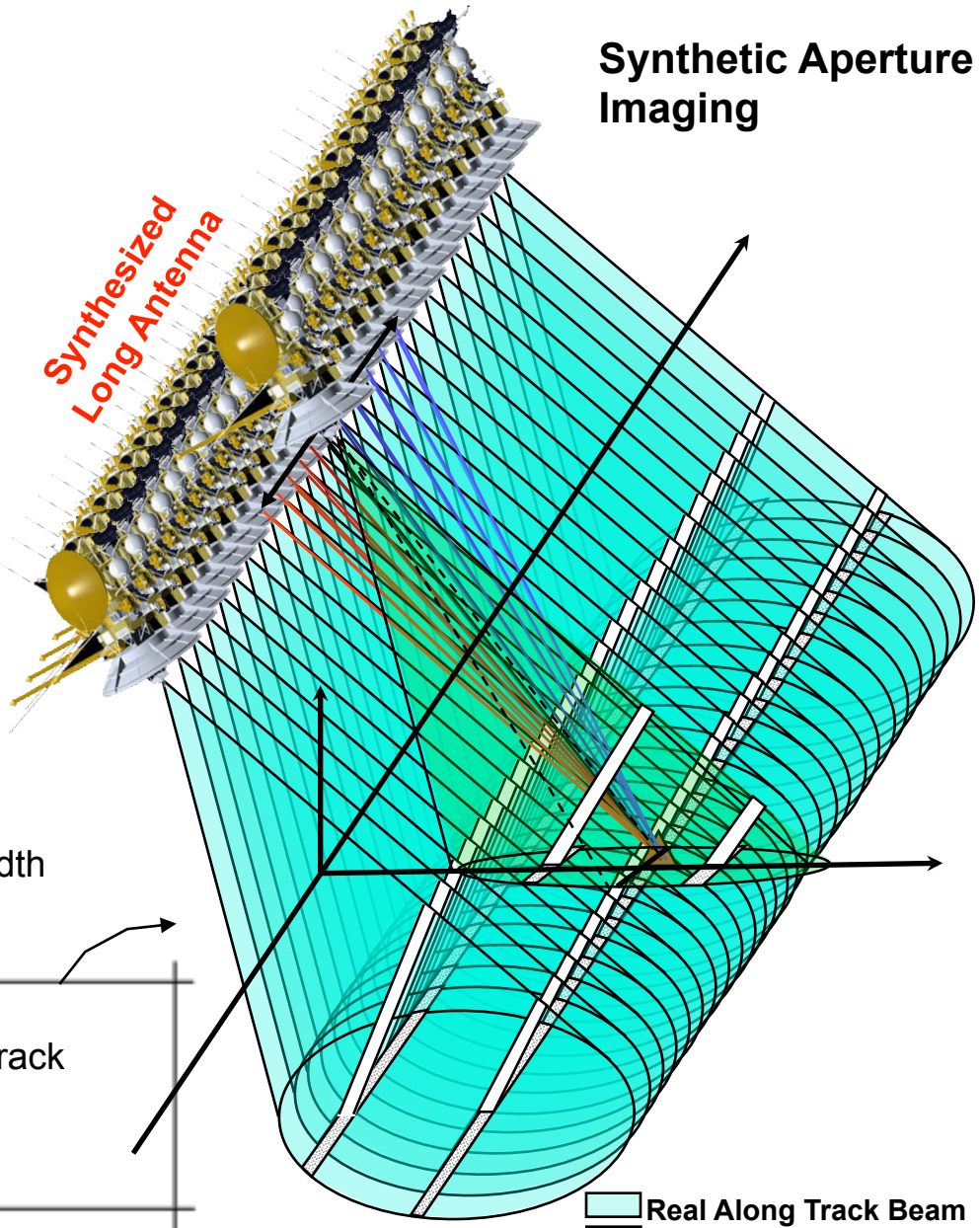

Along-Track resolution achieved by coherently combining echoes from multiple pulses along-track

- Resolution proportional to antenna length
- Independent of Range/Frequency

The Doppler Shift

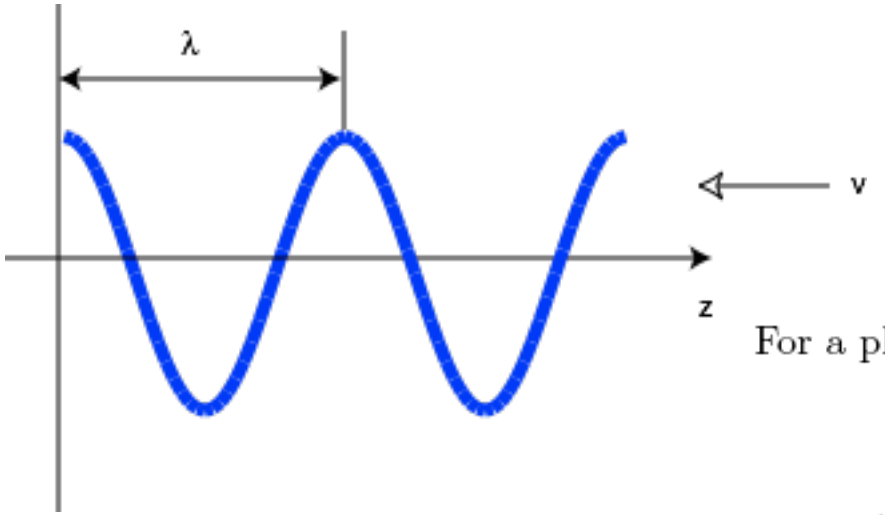

Phase of a wave is invariant with reference frame. As a result, the frequency in a moving frame must adjust to compensate for relative velocity

For a plane wave propagating in an arbitrary direction $\hat{k}$, $\vec{k} = k\hat{k}$,

$$\phi = (\omega t - \vec{k} \cdot \vec{r})$$

For fixed $\vec{r}$,

$$\frac{\partial \phi}{\partial t} = \omega$$

For $\vec{r}$ in linear motion, such that $\vec{r} = \vec{r_0} + \vec{v}t$,

$$\begin{aligned} \omega' = \frac{\partial \phi}{\partial t} &= \omega - \vec{k} \cdot \vec{v} \\ &= \omega - \frac{\omega}{c}\hat{k} \cdot \vec{v} \\ &= \omega \left(1 - \frac{\hat{k} \cdot \vec{v}}{c}\right) \end{aligned}$$

Doppler in SAR Imaging

$$
\begin{aligned}
R(x) &= \sqrt{R_0^2 + (x - x_0)^2} \\
&\approx R_0 \left(1 + \frac{(x - x_0)^2}{2R_0^2}\right) \\
&\approx R_0 + \frac{(x - x_0)^2}{2R_0}
\end{aligned}
$$

Dropping the constant term

$$
\begin{aligned}
\phi(t) &= -\frac{\pi}{F^2} v^2 (t - t_0)^2 \\
\omega(t) &= -2\pi \frac{v^2}{F^2} (t - t_0) \\
f_D(t) &= -\frac{v^2}{F^2} (t - t_0)
\end{aligned}
$$

$$F^2 = \lambda R_0 / 2.$$

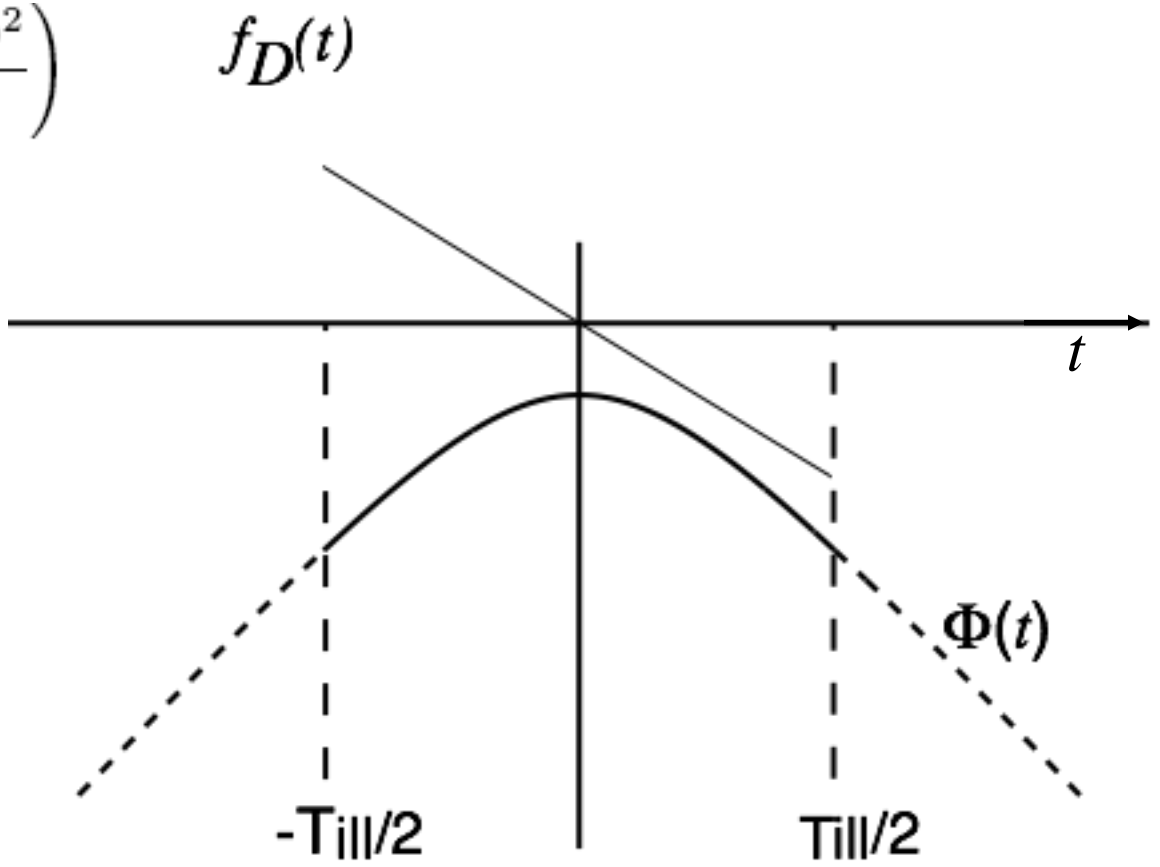

Range-Doppler Coordinates

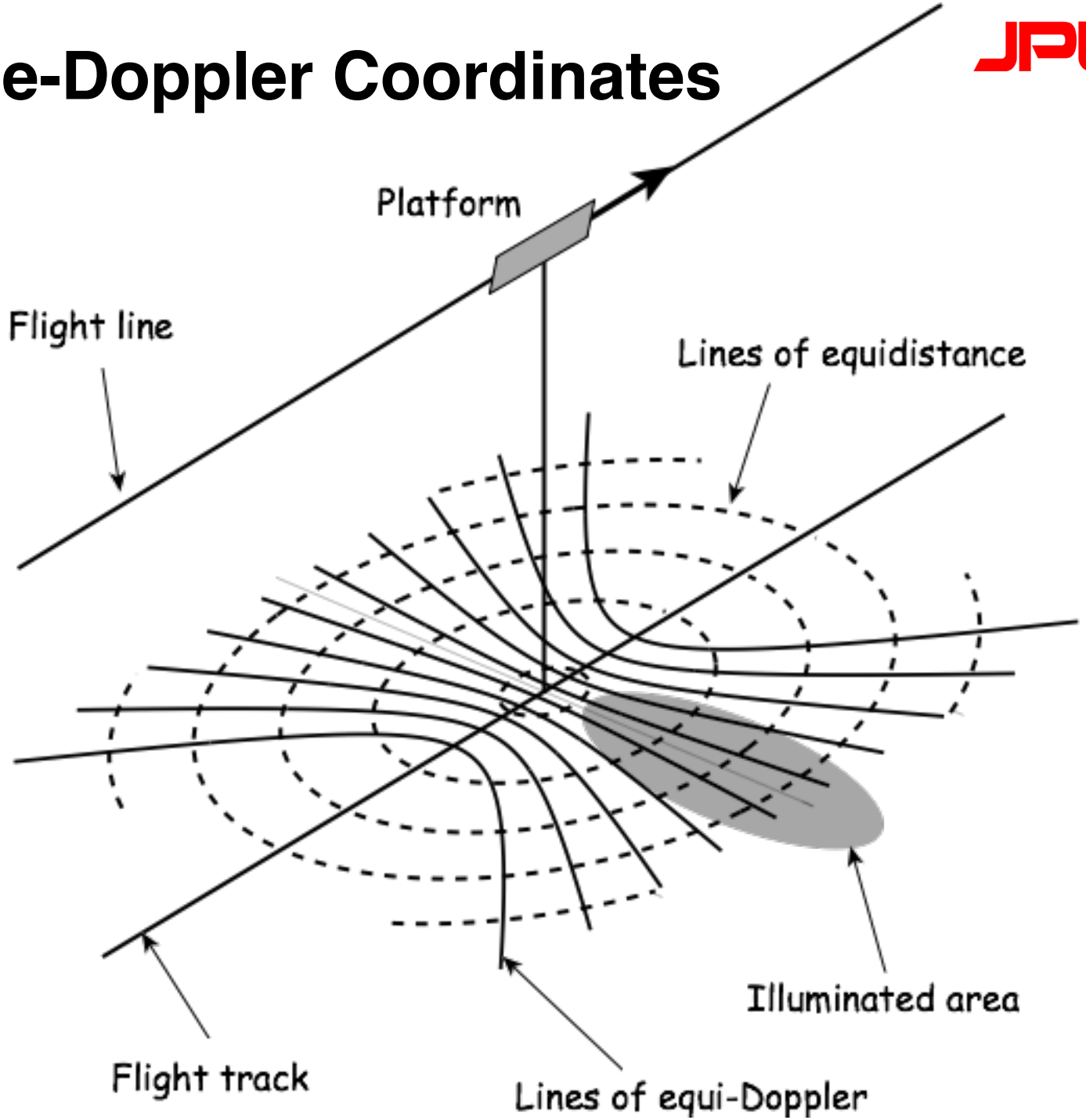

Doppler and Squint

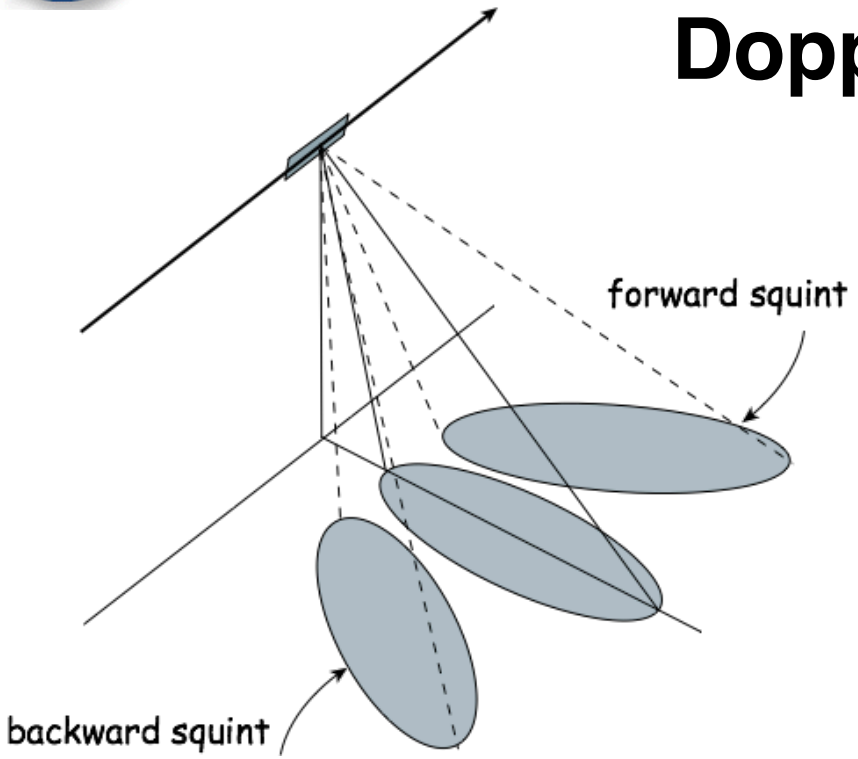

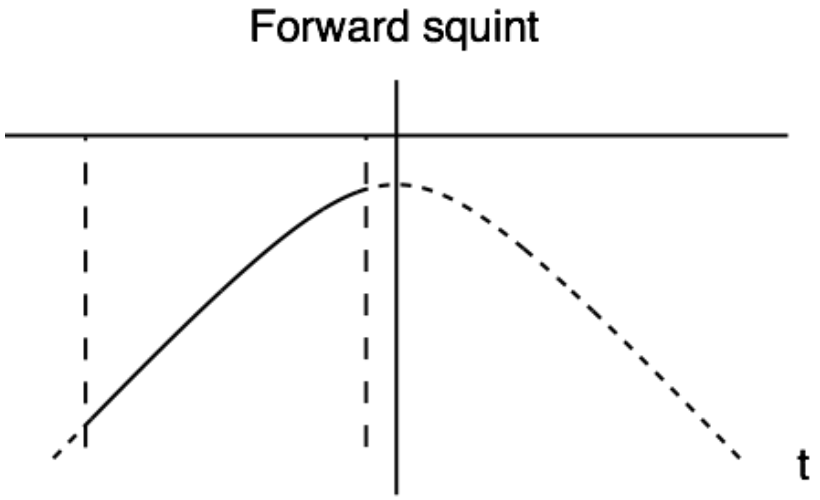

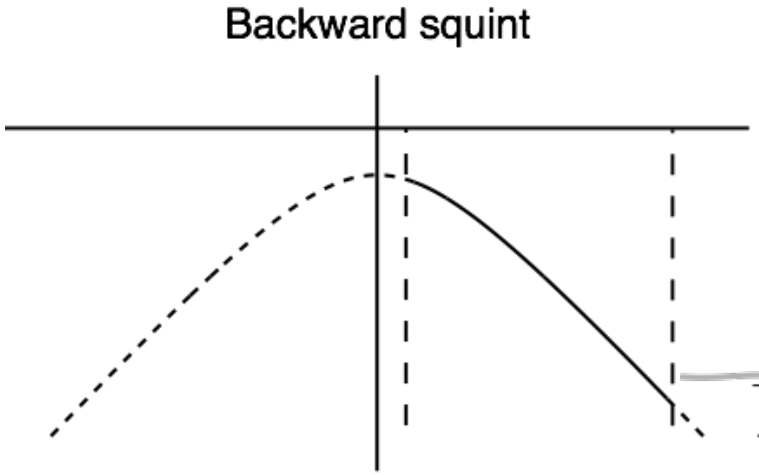

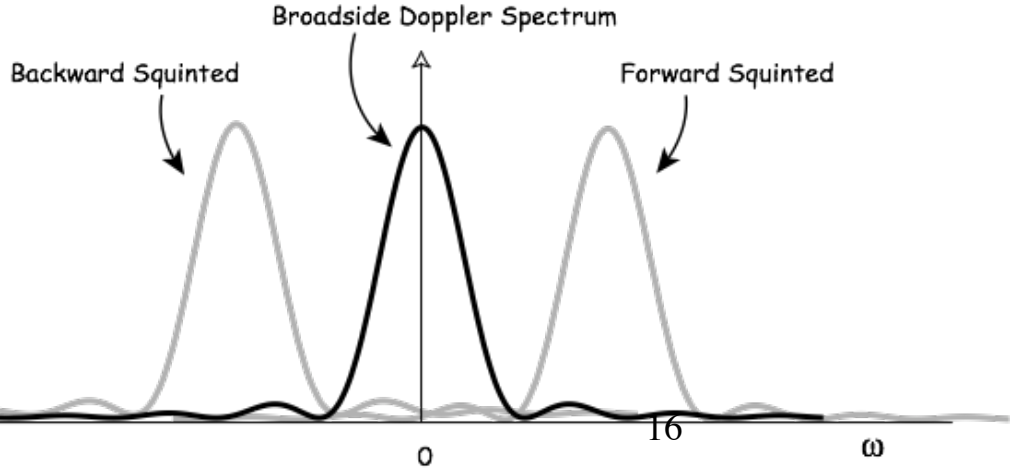

Azimuth Resolution from Aperture Synthesis

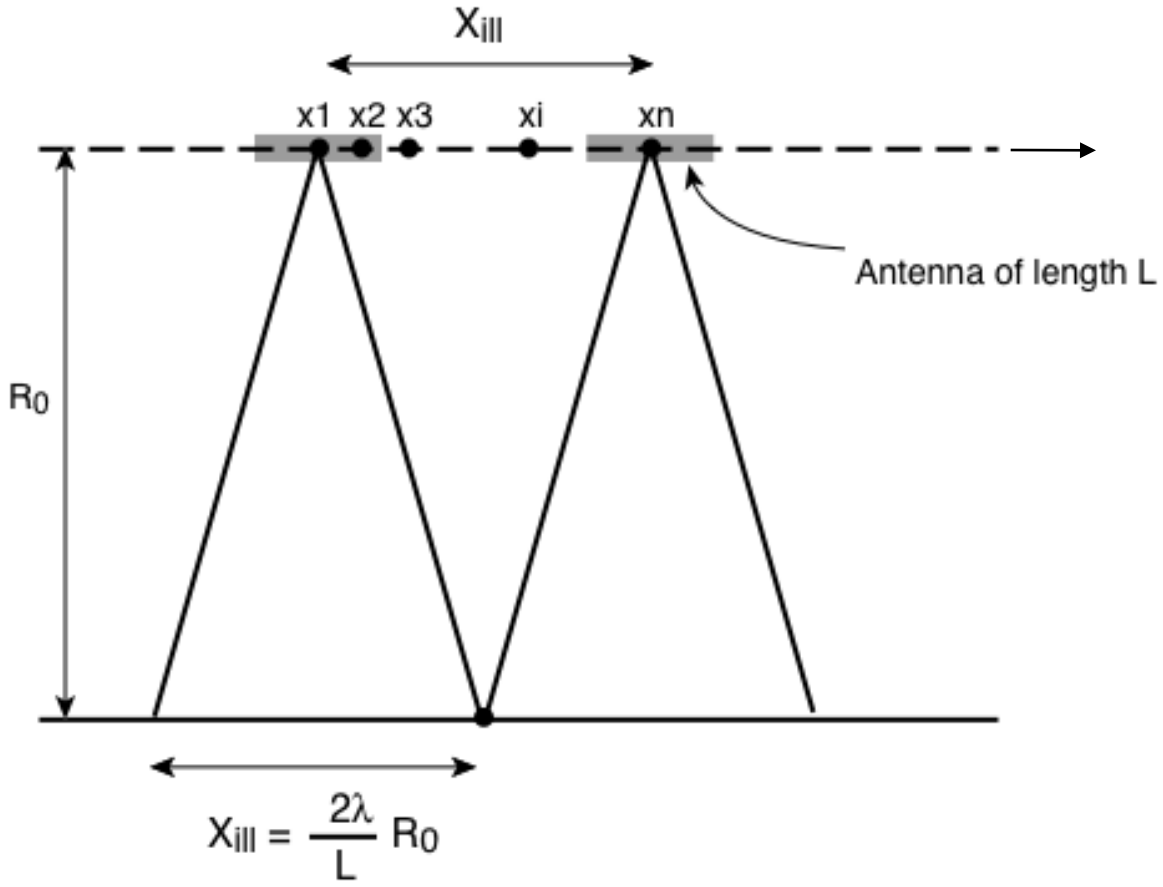

- The synthetic aperture X_{ill} lengthens as R0 increases…
- …which decreases the azimuth synthetic aperture's angular beamwidth (λ/X_{ill}) in proportion…
- …but the spatial resolution on the ground ($\lambda R_0/X_{ill} = L/2$) is constant
- Aperture synthesis processing is very similar to matched filtering in range

Raw Signal of a Point Target

Range →

Pulse Number →

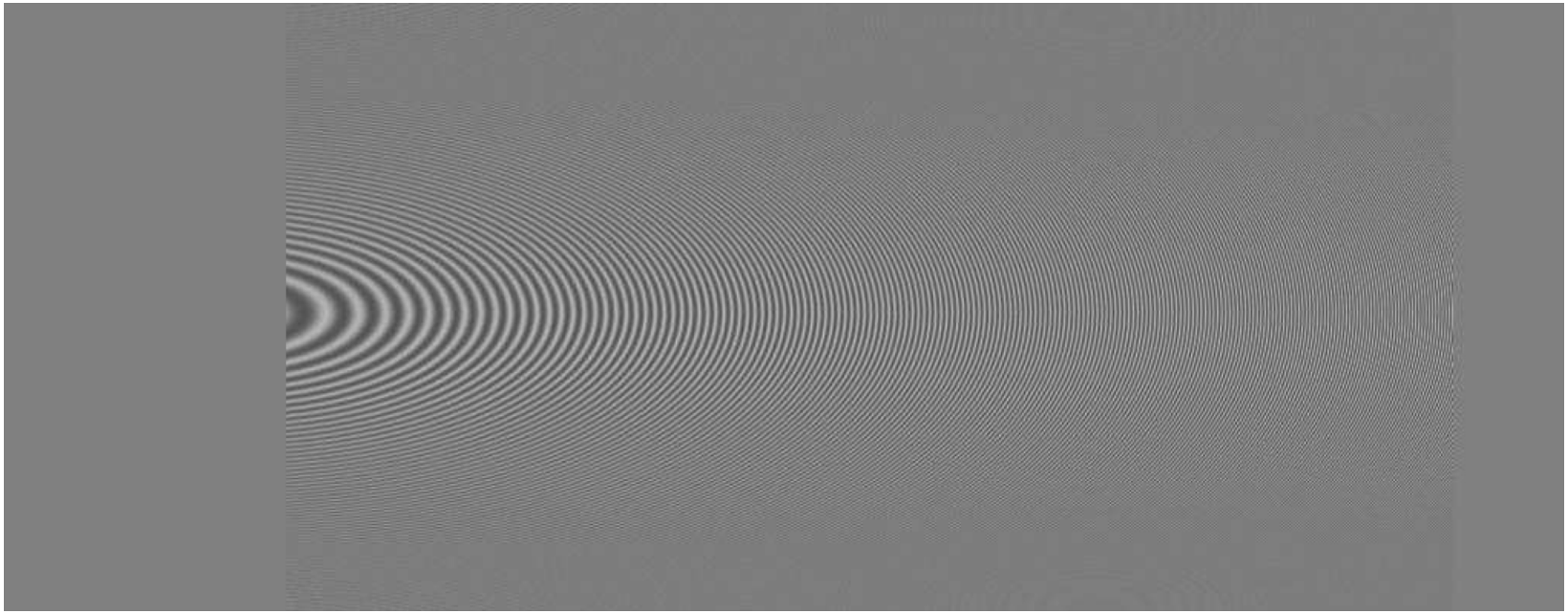

This “image” shows a sequence of simulated pulse echoes from a single point target

Range Compression of a Point Target; after Matched filtering

Range →

Pulse Number →

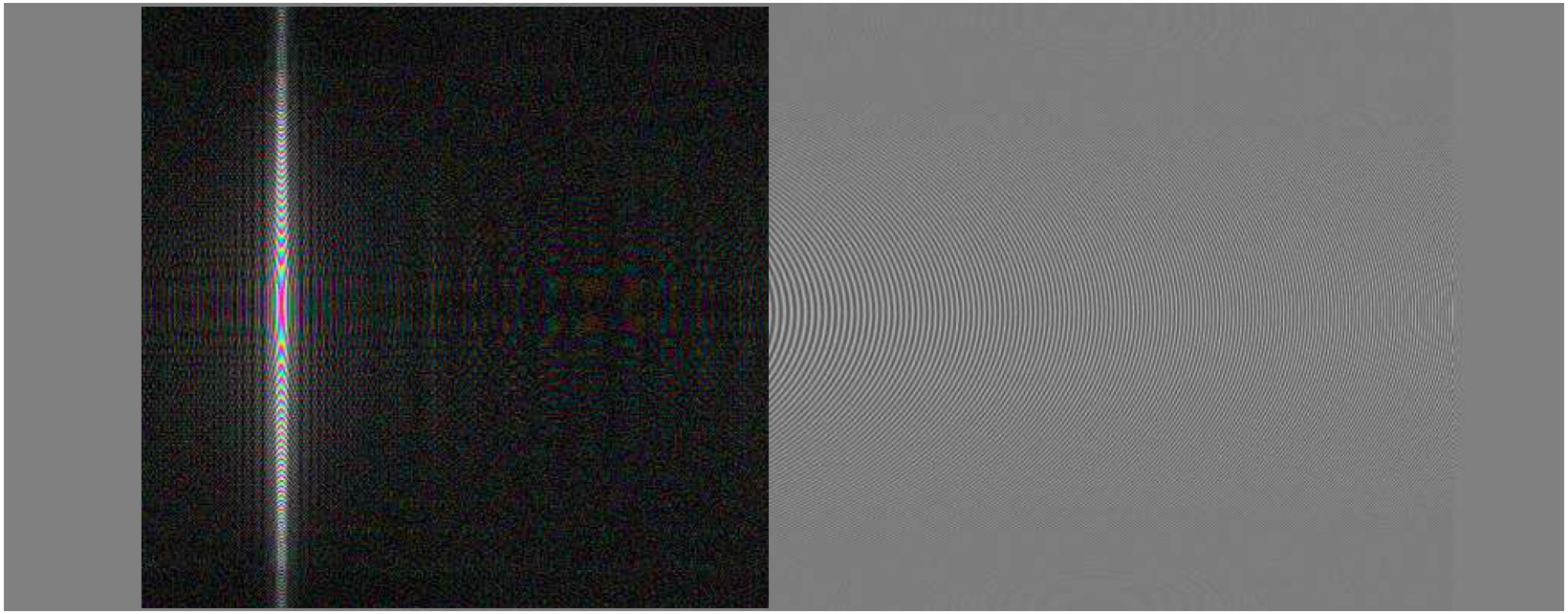

This “image” shows the simulated pulse echoes after range compression matched filtering

Point Target after Azimuth Compression Matched filtering

Range →

Pulse Number →

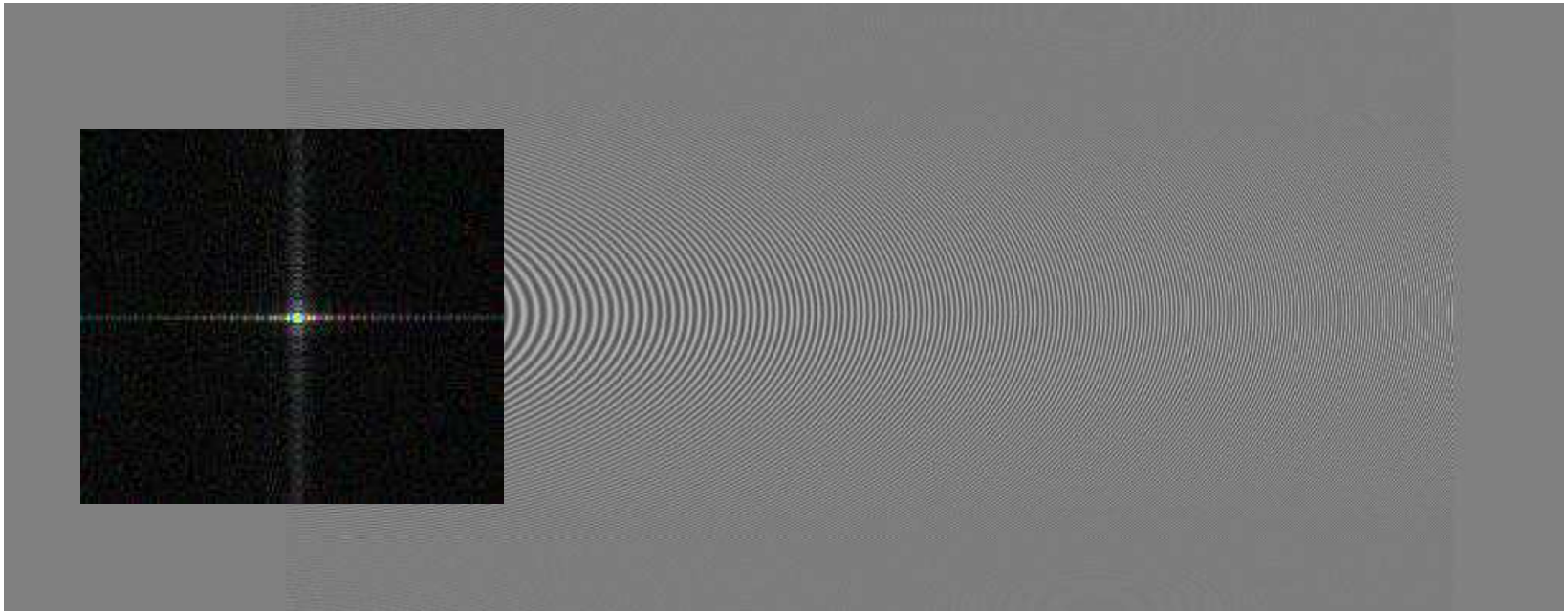

This “image” shows the simulated pulse echoes after range compression matched filtering

Cassini Example of Image Processing

- Range: Pulse segments convolved with *matched filter*
  - Estimate of Doppler shifted, base-banded echo from point target at boresight.
  - DC bin zeroed out.

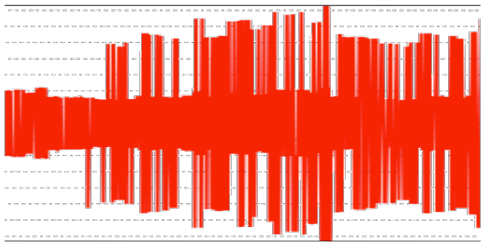

convolved with

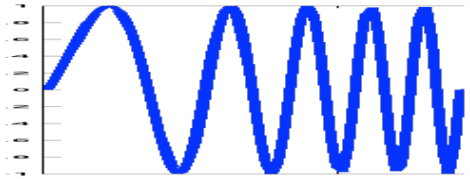

yields

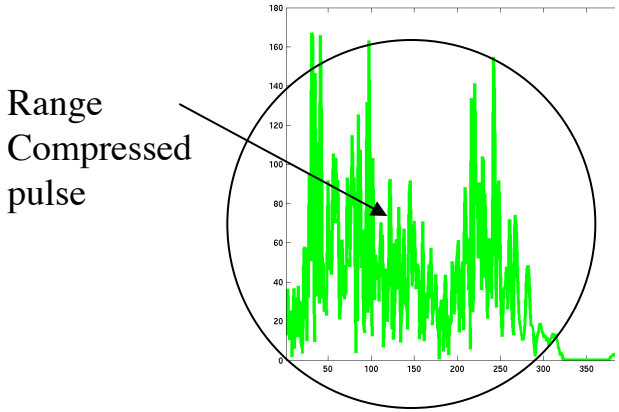

- Azimuth
  - Input: Each range bin sampled once per pulse
  - Convolved with azimuth matched filter
    - Linear FM chirp at Doppler centroid

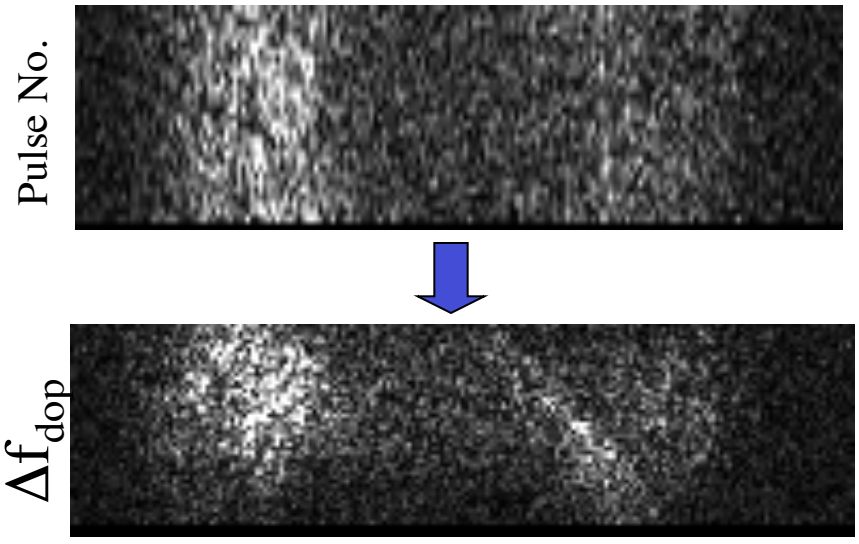

5 beams mosaicked together, after geolocation, averaging, and noise subtraction

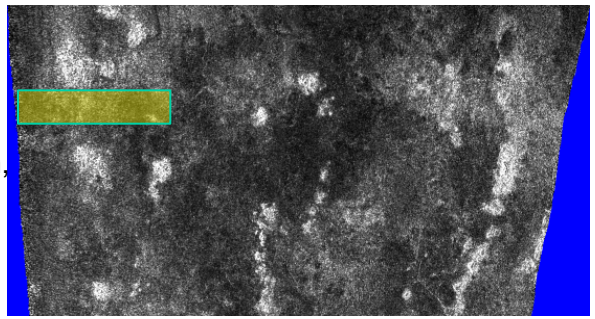

Conventional SAR modes

- Strip-mode SAR
  - Standard SAR mode
  - Send a pulse of energy; receive echo; repeat
  - One pulse transmit and receive at a time
  - Swath width limited by radar ambiguities
- ScanSAR
  - Wider swath low resolution SAR mode
  - Execute sequence as follows:
    - Send a pulse of energy; receive echo; repeat 50-100 times
    - Repoint the beam across-track to position 2 electrically (almost instantaneous)
    - Send a pulse of energy; receive echo; repeat 50-100 times
    - Repoint the beam across-track to position 3 electrically (almost instantaneous)
    - Send a pulse of energy; receive echo; repeat 50-100 times
  - Again, one pulse transmit and receive at a time
  - ScanSAR trades resolution (in along-track dimension) for swath: low impact on data rate
  - Generally poorer ambiguity and radiometric performance than Strip SAR

StripSAR

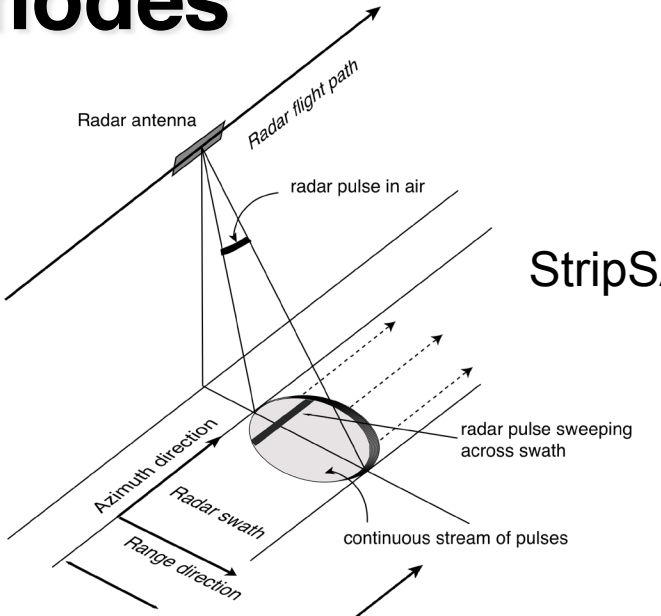

ScanSAR

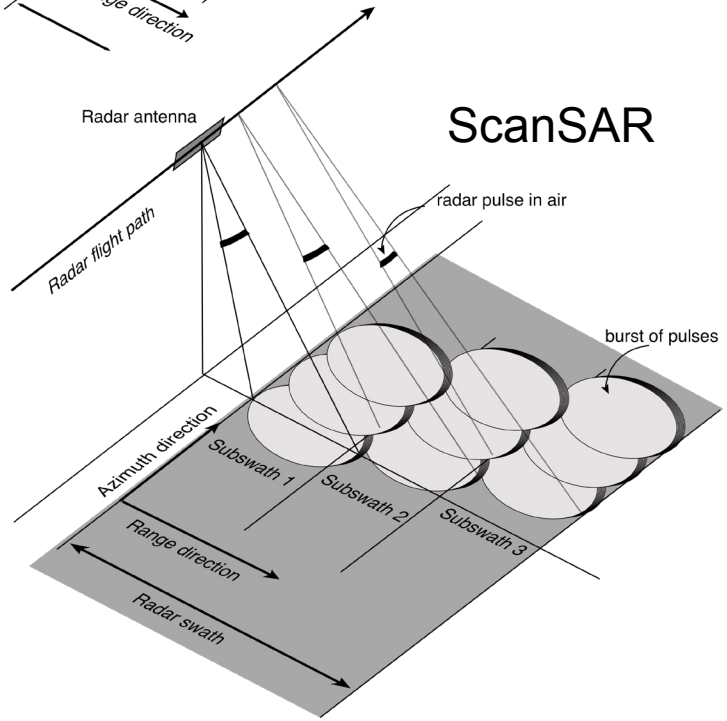

ScanSAR Imaging and Burst Geometry

In ScanSAR the look angle for a burst of pulses changes for each dwell period

burst of pulses in alternating dwells…

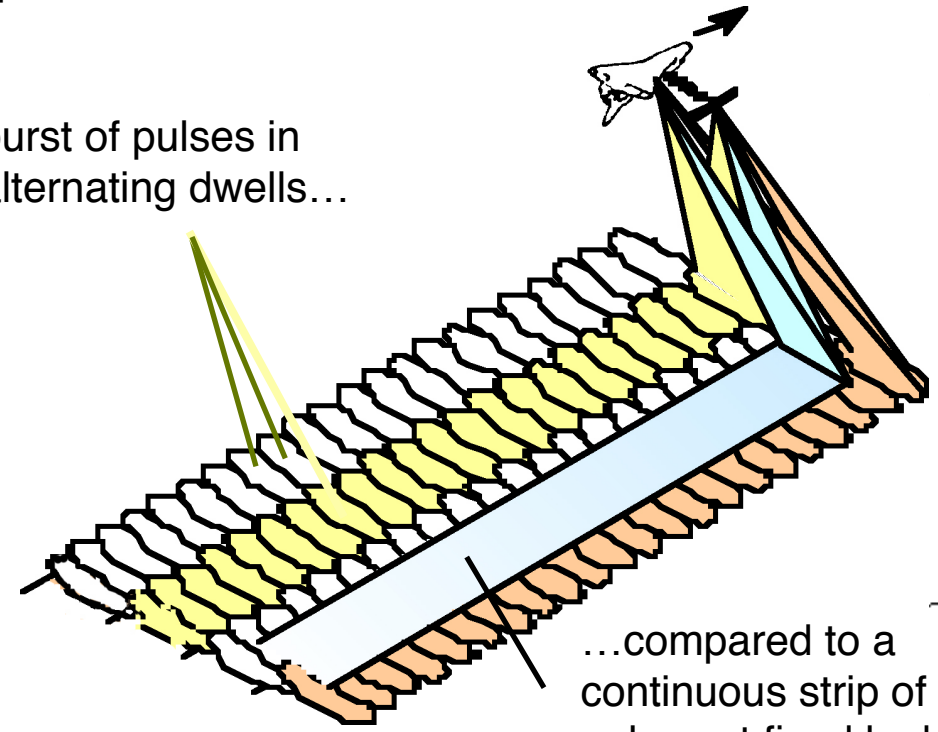

…compared to a continuous strip of pulses at fixed look angle

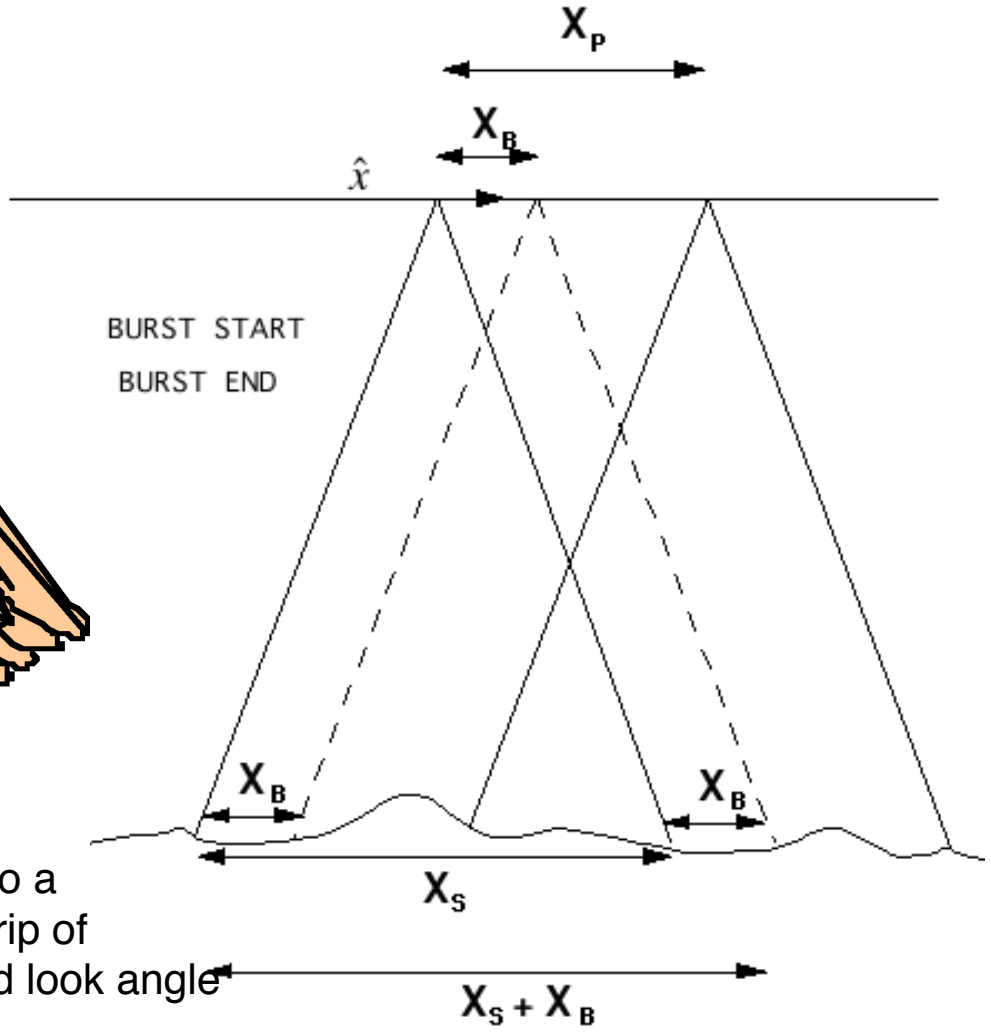

Illustration of Burst Combination

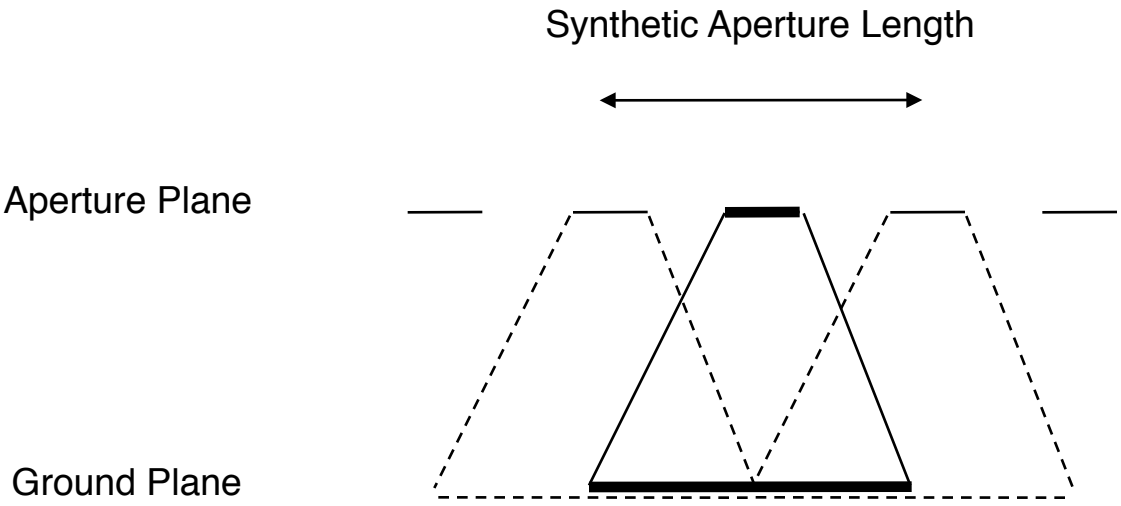

Images formed from each burst overlap in the ground plane.

Images are incoherently added (in power) to recover looks in processing.

Strip versus ScanSAR images (no radiometric calibration)

Standard Strip Mode Amplitude (4 looks; then 4x4 more)

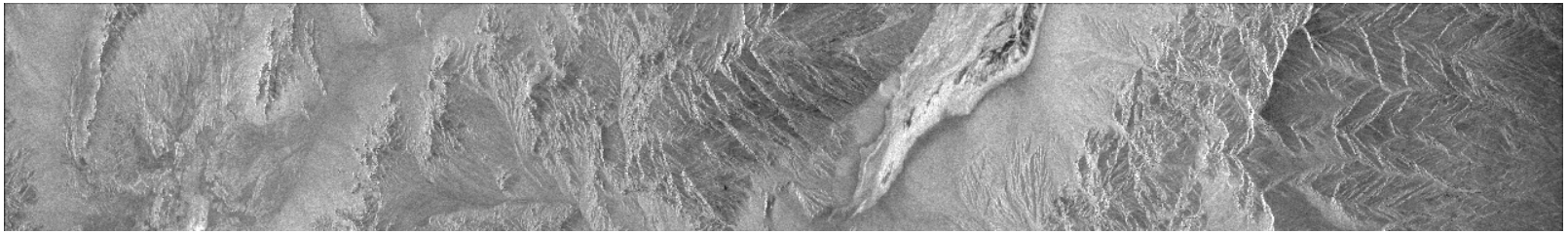

Burst Processed Amplitude (1/4 aperture; 2 looks; then 4x4 more)

Note Amplitude Scalloping

What Radar Can Tell Us

- Transmitted radar signals have known characteristics
  - Amplitude
  - Polarization
  - Phase and Time Reference
  - Wavelength, or Frequency
- A distant object that scatters the radar signal back toward the receiver alters the amplitude, polarization, and phase, differently for different wavelengths
- Comparison of the received signal characteristics to the transmitted signal allows us to understand the properties of the object.
- This is the principle of active remote sensing.

Radar Imaging Properties

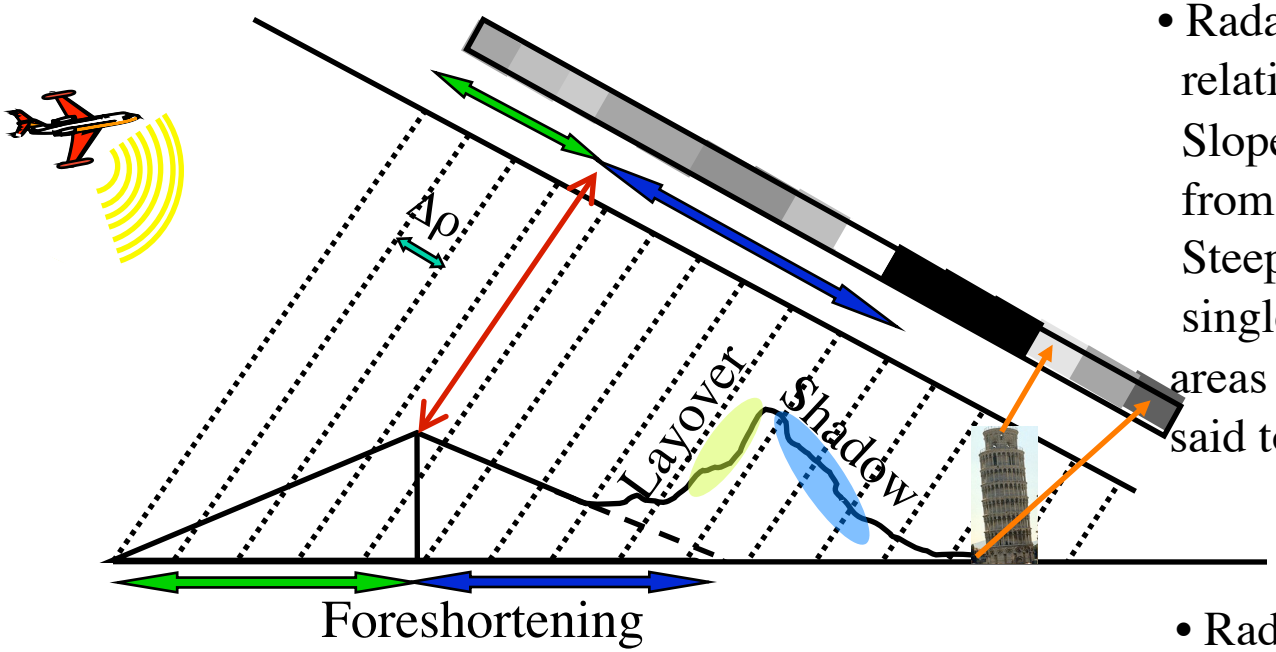

- Radar images are distorted relative to a planimetric view. Slopes facing toward or away from the radar appear foreshortened. Steep slopes are collapsed into a single range cell called layover and areas occulted by other areas are said to be shadowed.

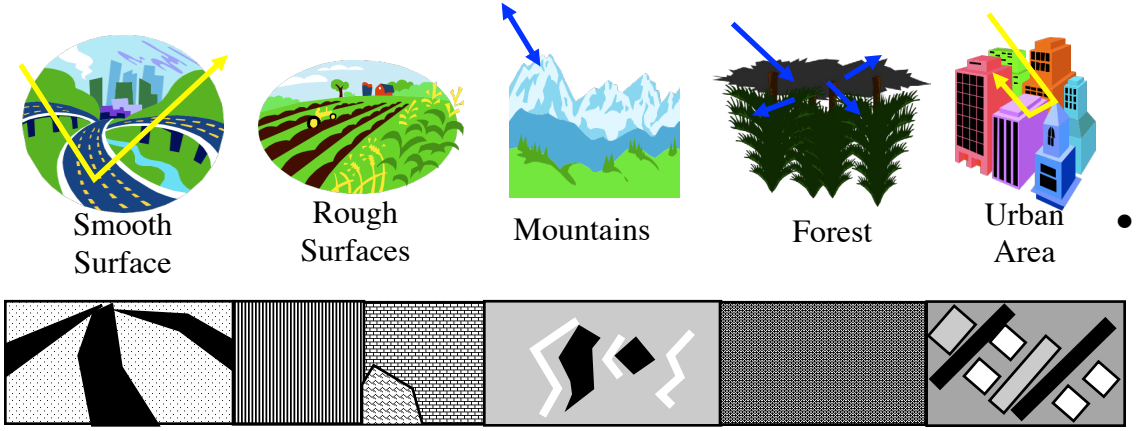

- Radar is primarily sensitive to the structure of objects being imaged whereas optical images are primarily sensitive to chemistry.
- The scale of objects relative to the radar wavelength determines how smooth an object appears to the radar and how bright or dark it is in the imagery.

Wavelength - A Measure of Surface Scale

Light interacts most strongly with objects on the size of the wavelength

L (24 cm) C (6 cm) X (3 cm)

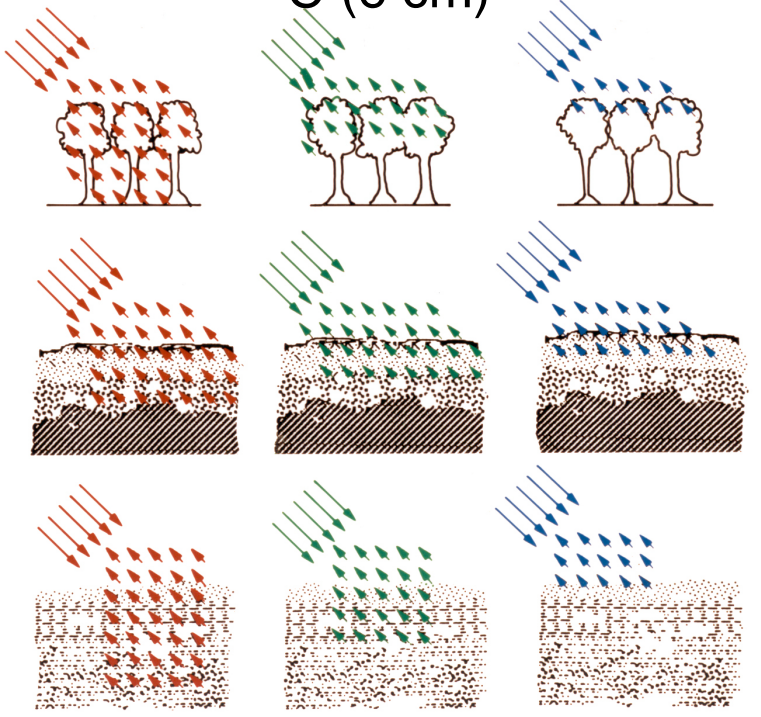

Forest: Leaves reflect X-band wavelengths but not L-band

Dry soils: Surface looks rough to X-band but not L-band

Ice: Surface and layering look rough to X-band but not L-band

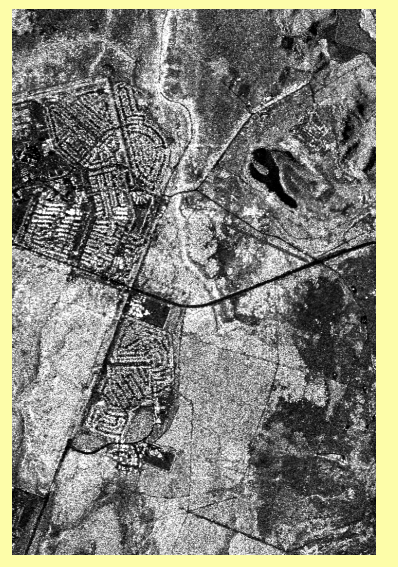

Polarization - A Measure of Surface Orientations and Properties

Wave Polarization

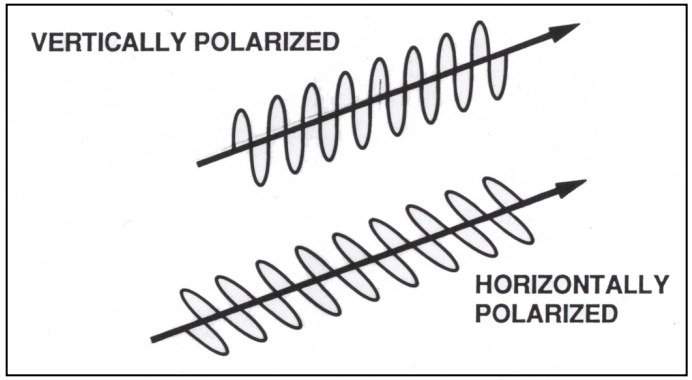

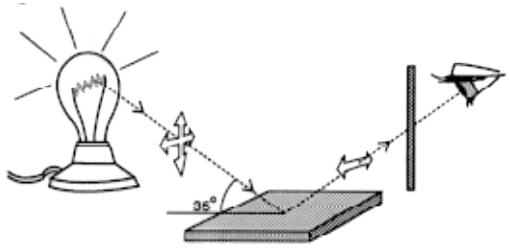

Mostly horizontal polarization is reflected from a flat surface.

Polarization Filters

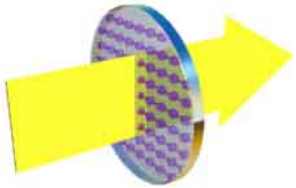

Vertical polarization passes through horizontally arranged absorbers.

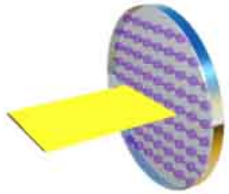

Horizontal polarization does not pass through horizontally arranged absorbers.

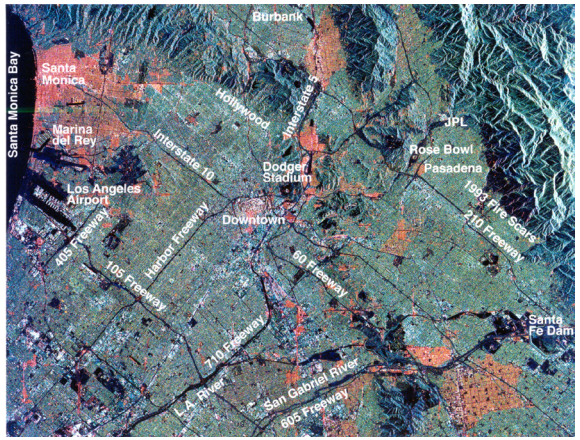

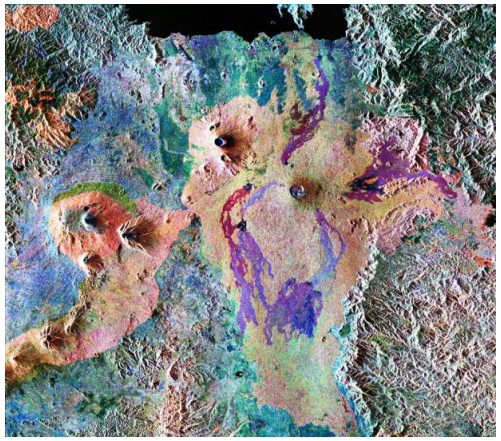

Color figures from www.colorado.edu/physics/2000

Death Valley

(HH-Red, HV – Green, VV – Blue)

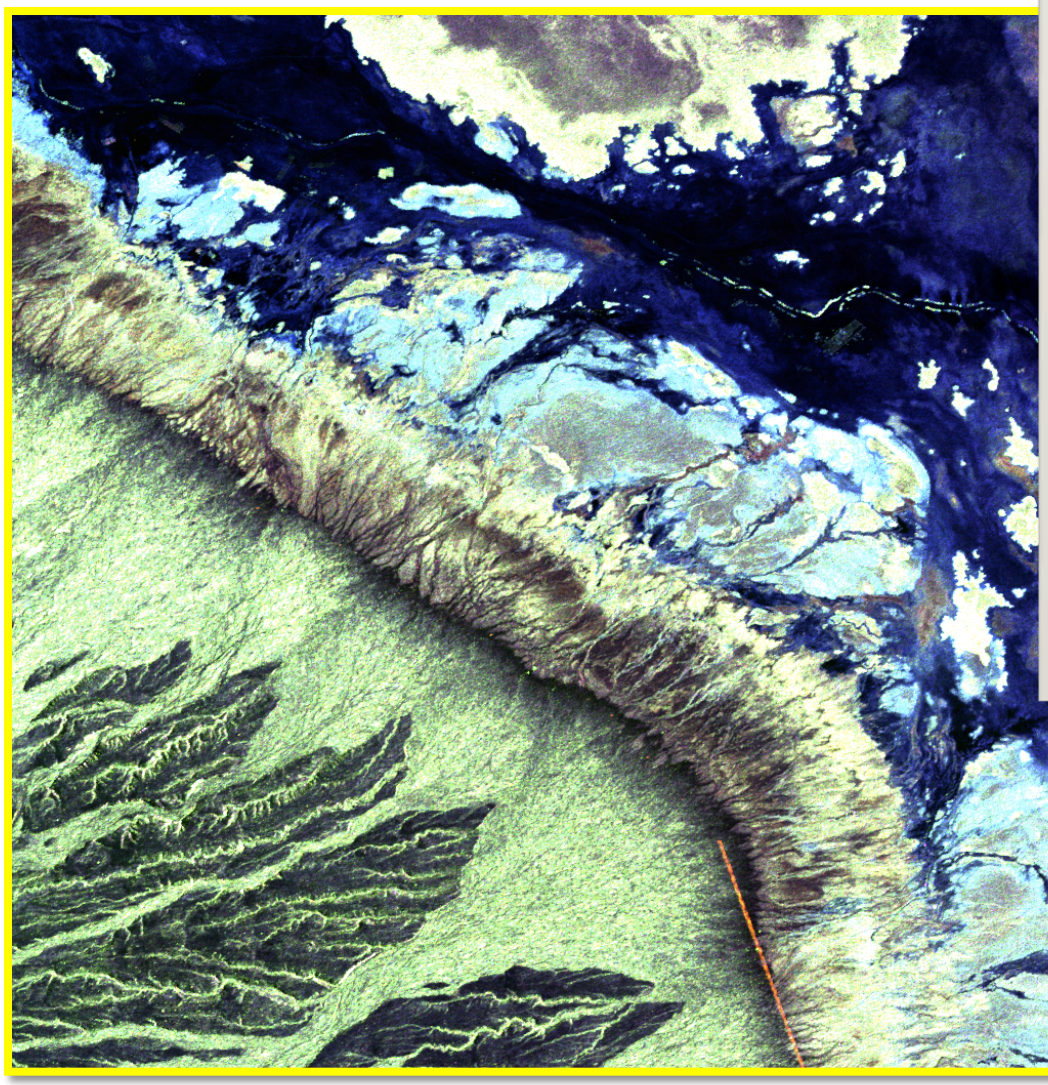

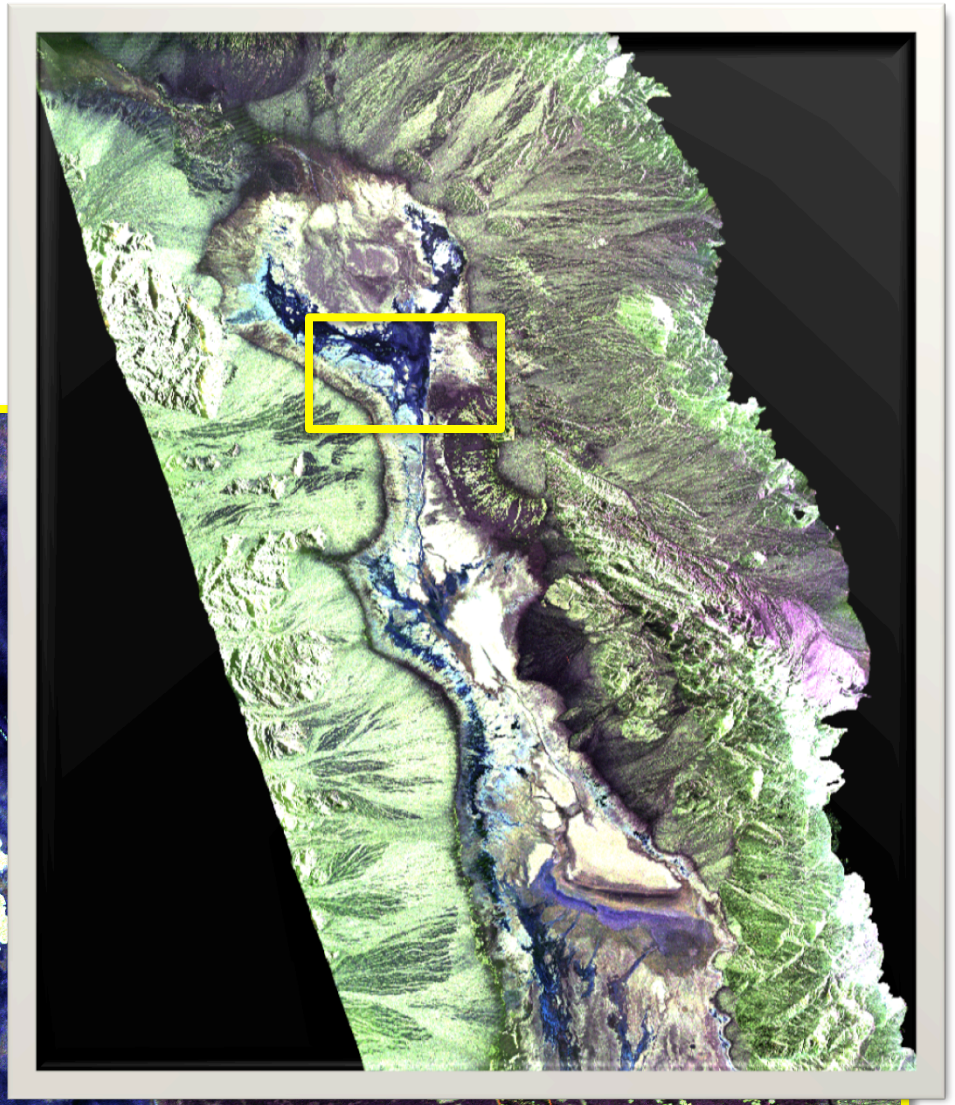

Speckle and Radiometric Accuracy

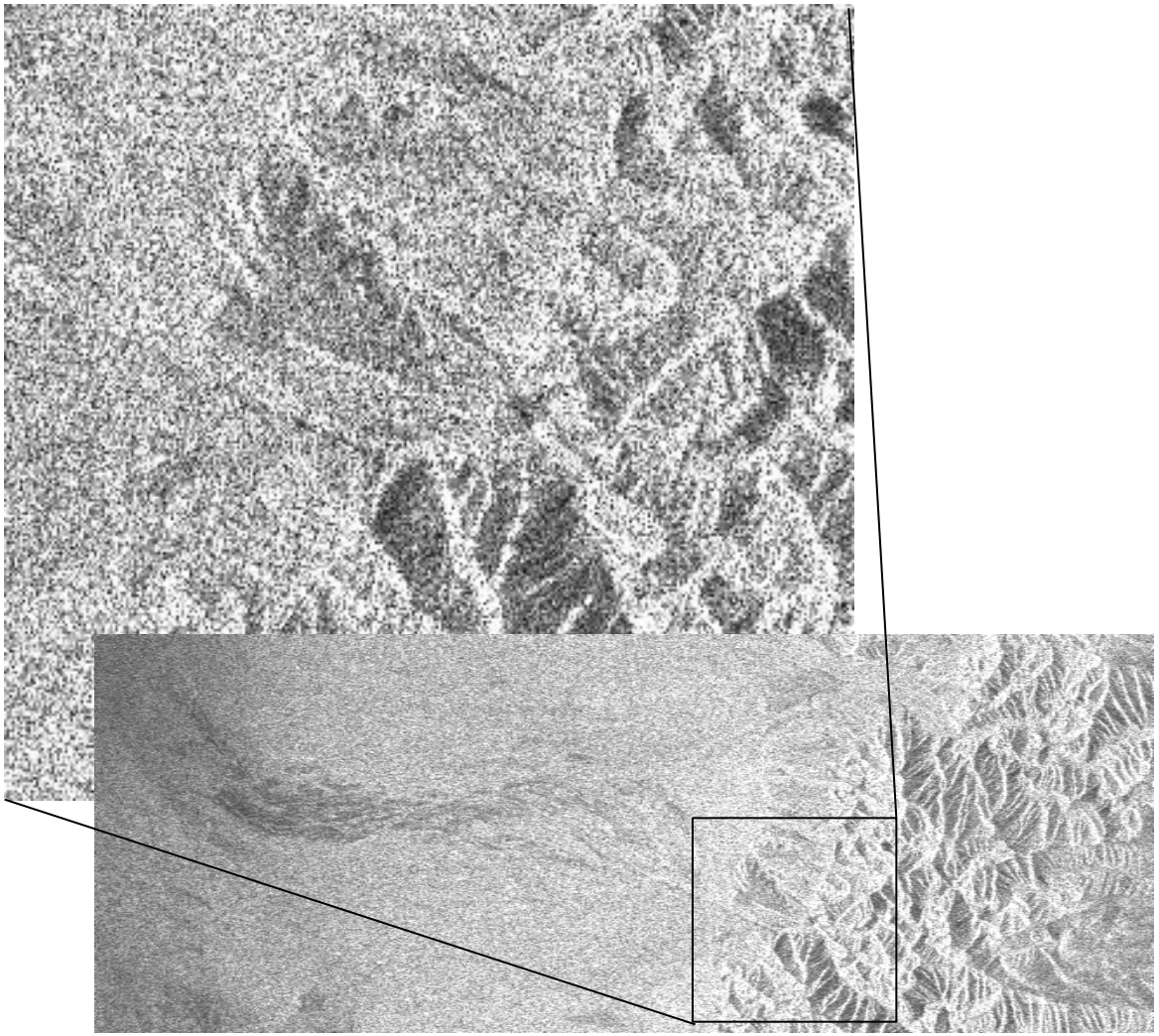

Natural “laser” speckle masks intrinsic radar backscatter which contains surface information, independent of SNR!

Spatial averaging (looks) reduces the speckle and draws out the natural backscatter reflectivity

Spatial Averaging or Looks

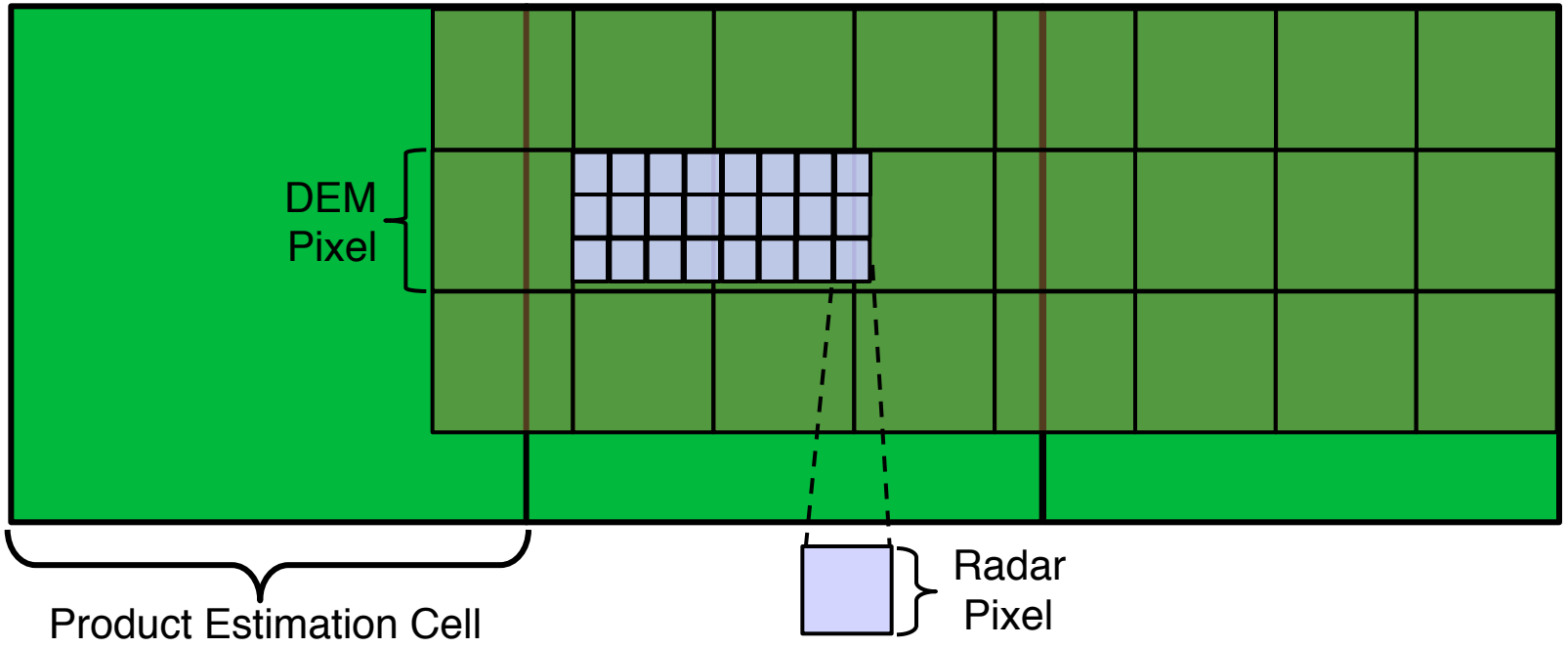

Phase - A Measure of the Range and Surface Complexity

The phase of the radar signal is the number of *cycles of oscillation* that the wave executes between the radar and the surface and back again.

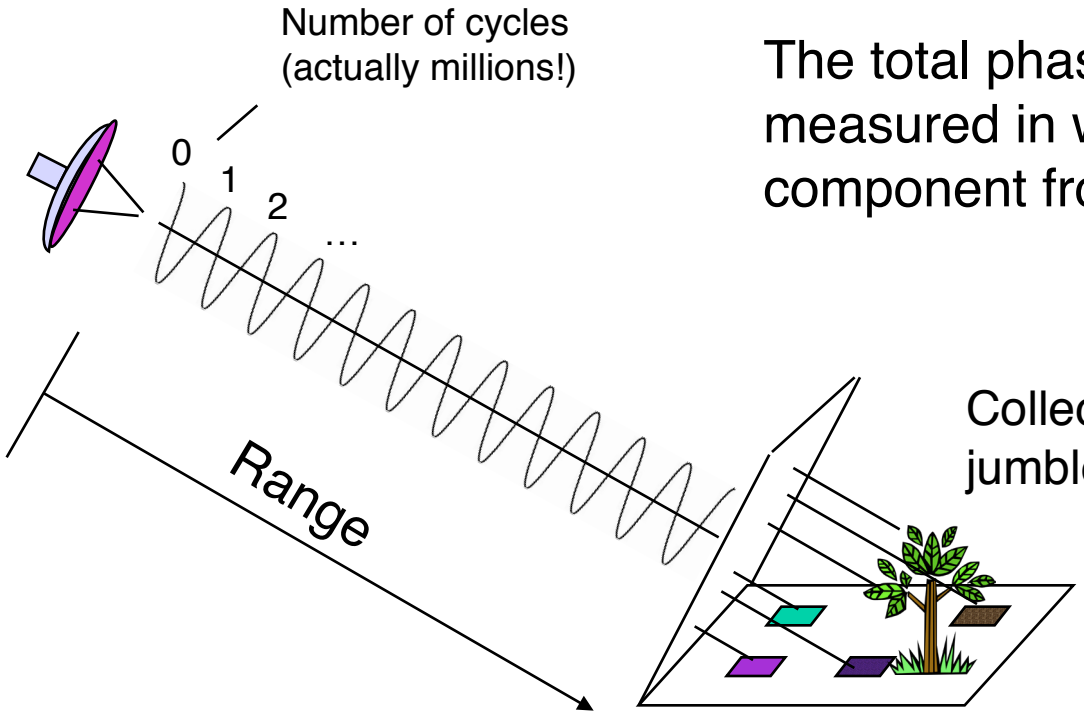

The total phase is two-way range measured in wave cycles + random component from the surface

Collection of random path lengths jumbles the phase of the echo

Only *interferometry* can sort it out!

What is Radar Interferometry?

- Radar interferometry can be broadly defined by use of phase measurements to precisely measure the relative distance to an object when imaged by synthetic aperture radar from two or more observations separated either in time or space.
  - Interferometric phase is simply another means of measuring (relative) distance.

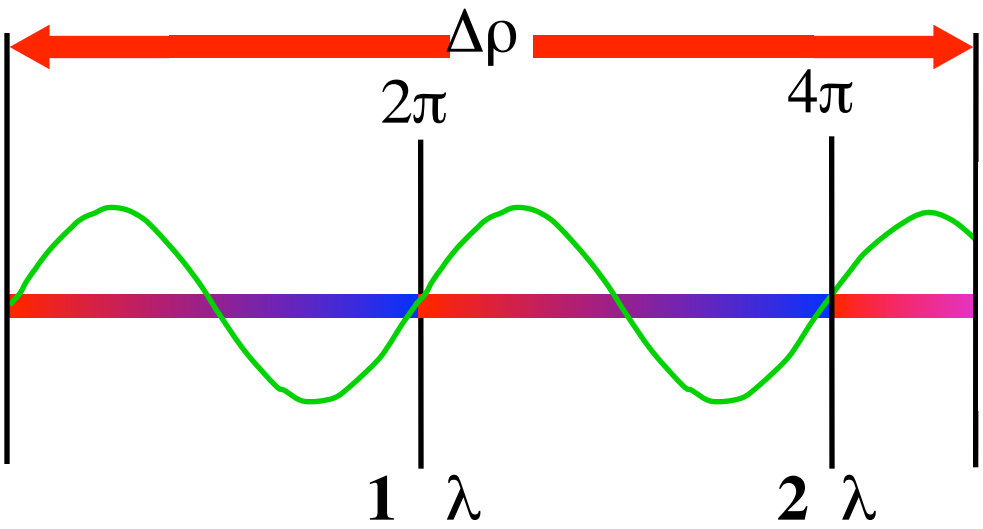

$$\phi = \underbrace{2\pi}_{\text{Radians per wavelength}} \underbrace{\frac{\Delta\rho}{\lambda}}_{\text{Number of wavelengths}}$$

- Phase measurements in interferometric systems can be made with degree level accuracy, and with typical radar wavelengths in 3-80 cm range this corresponds to relative range measurements having millimeter accuracy.

Interference Concept

- Interference occurs when the phase of two different waves is not aligned. The observed intensity, I, is the time average of the sum of the wave fields

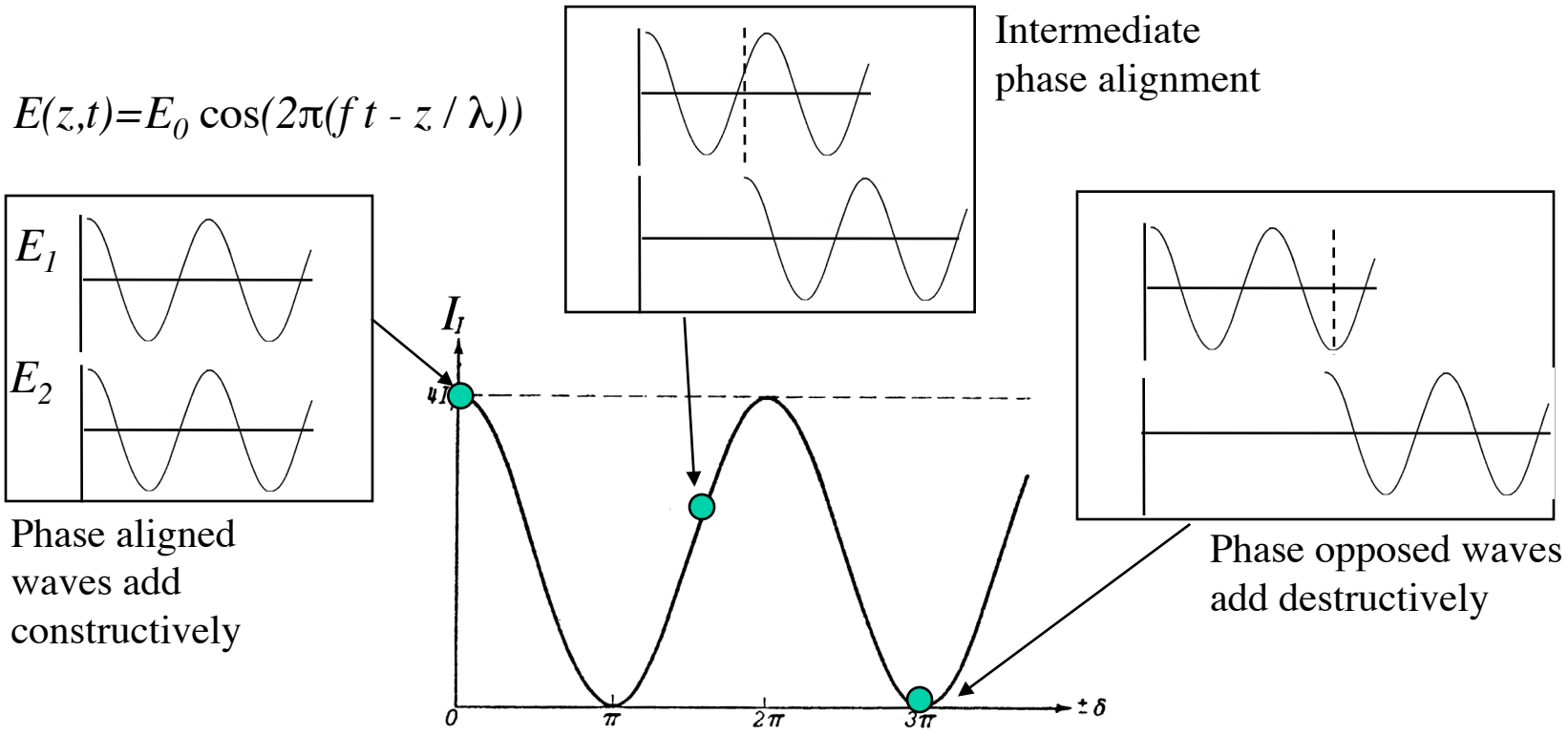

Fig. 7.1. Interference of two beams of equal intensity; variation of intensity with phase difference.

Young's Interferometer

- In Young's experiment, a point source illuminates two separated vertical slits in an opaque screen. The slits are very narrow and act as line sources. For this case, the pattern of intensity variations on the observing screen is bright/dark banding.

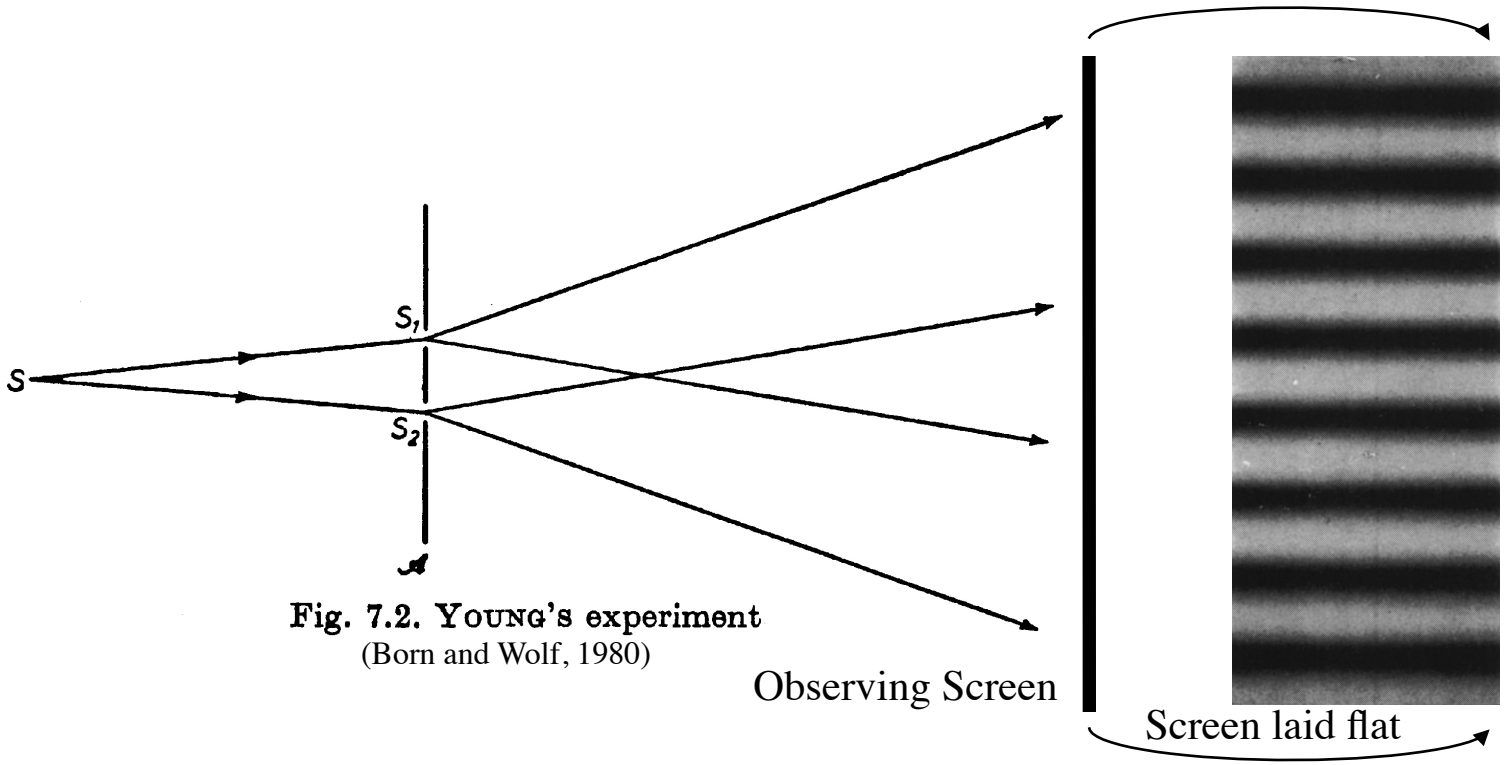

Fig. 7.2. YOUNG's experiment
(Born and Wolf, 1980)

Young's Interferometer Geometry

- The brightness variations can be understood in terms of the relative phase of the interfering waves at the observing screen
- The spacing of fringes is set by the slit separation
- Phase = $2 \pi x d / a \lambda$
- $x_{max} = m a \lambda / d$, m = 0, 1, 2 , ...

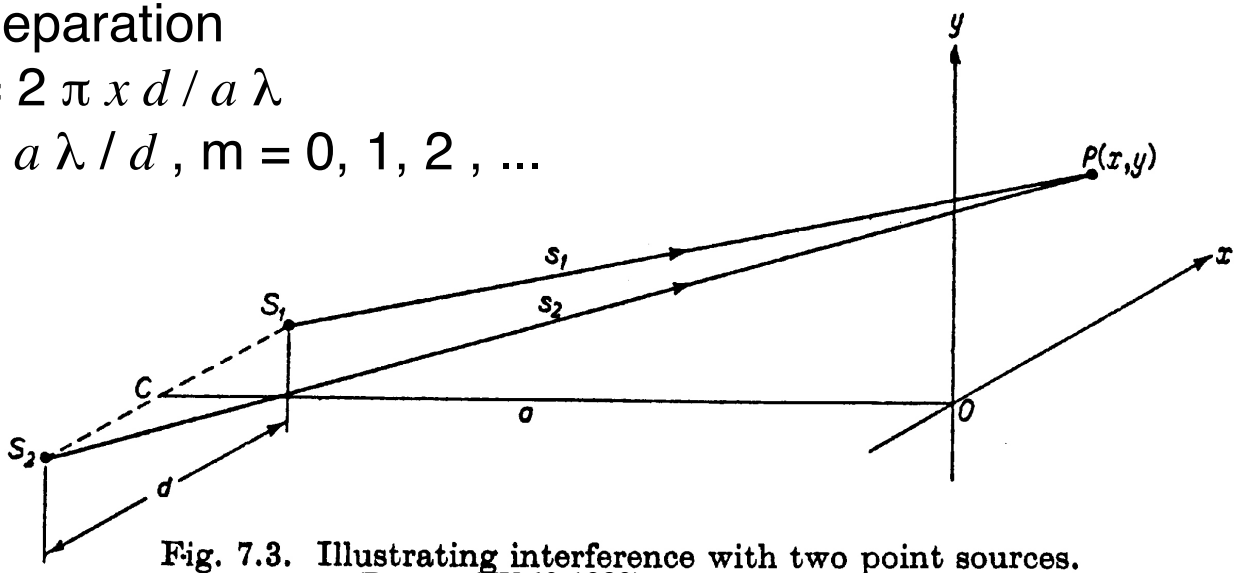

Fig. 7.3. Illustrating interference with two point sources.
(Born and Wolf, 1980)

Radar Interferometry

- Radar Interferometry is a simple extension of the Young's interferometry concept
- Radar has a coherent source much like a laser
- The two radar (SAR) antennas act as coherent point sources
- Because the wavelengths are so long, the signal can easily be digitized and processed coherently, measuring the phase information directly.
- When imaging a surface, the phase fronts from the two sources interfere.
- The surface topography slices the interference pattern.

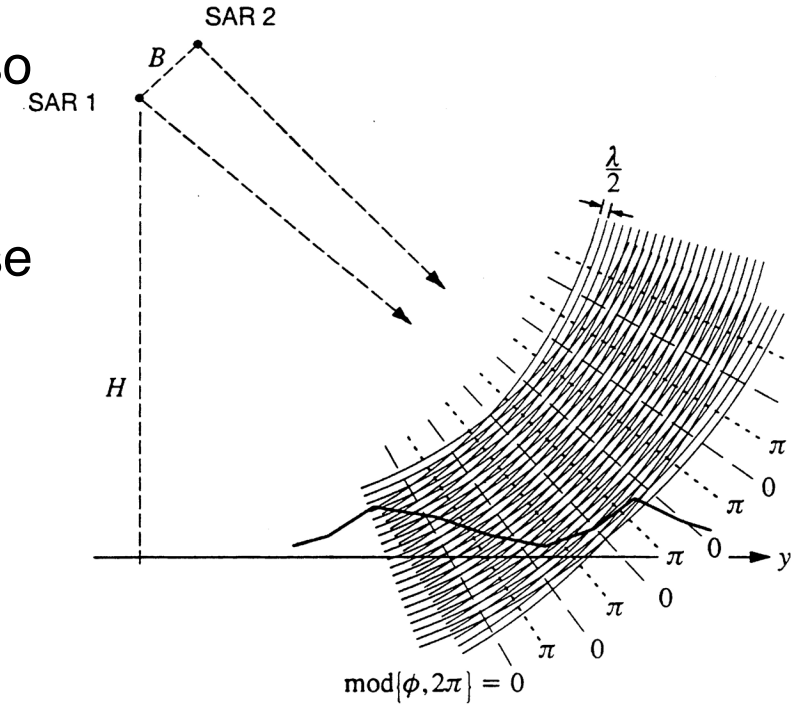

- The measured phase differences record the topographic information.

Radar Interferometry Example

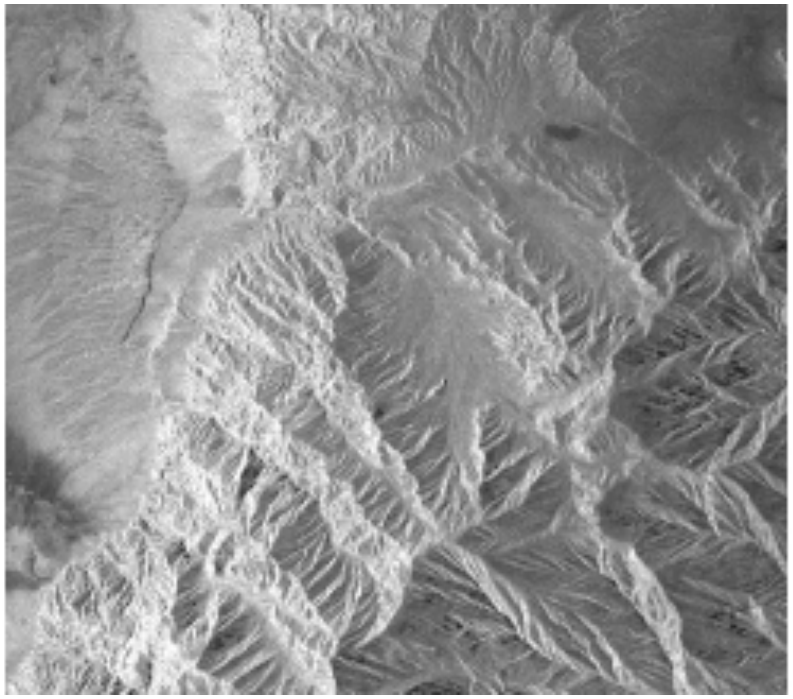

Standard Radar Image

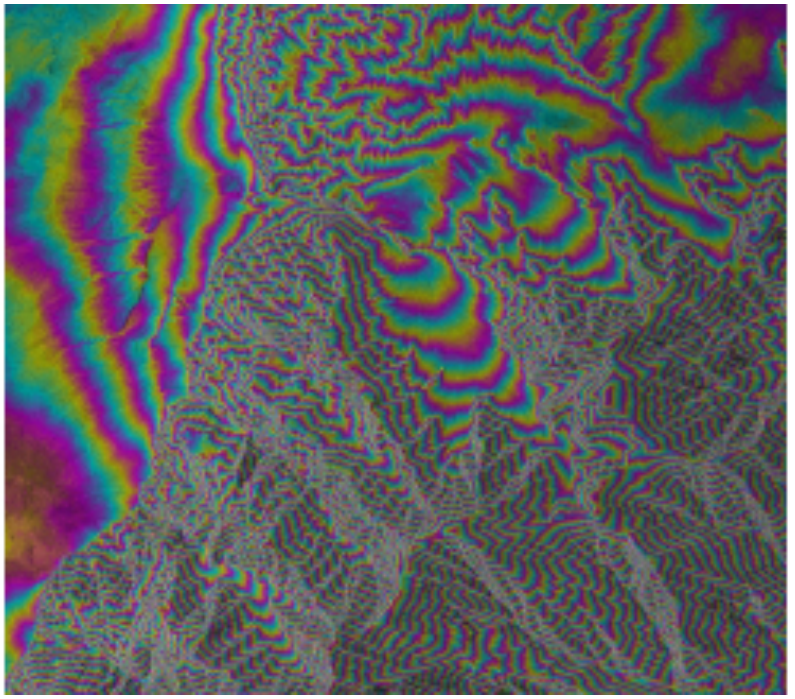

Interference fringes follow the topography

One cycle of color represents 1/2 wavelength of path difference

Types of Radar Interferometry

- Two main classes of interferometric radars are separated based on the geometric configuration of the baseline vector, i.e. the vector separating the antenna locations in the interferometric pair. These are:
  - Cross-Track interferometers used for topographic and surface deformation measurements whereby the antennas are nominally separated in the cross-track direction.
  - Along-Track interferometers used to measure radial velocity whereby the antennas are separated in the along-track direction.

Cross-Track Interferometer

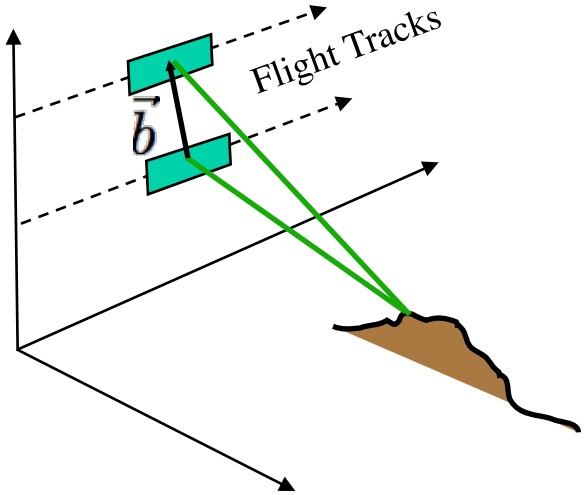

- Dual antenna single pass interferometers
- Single antenna repeat pass interferometers
  ==> Topography and Deformation

Along-Track Interferometer

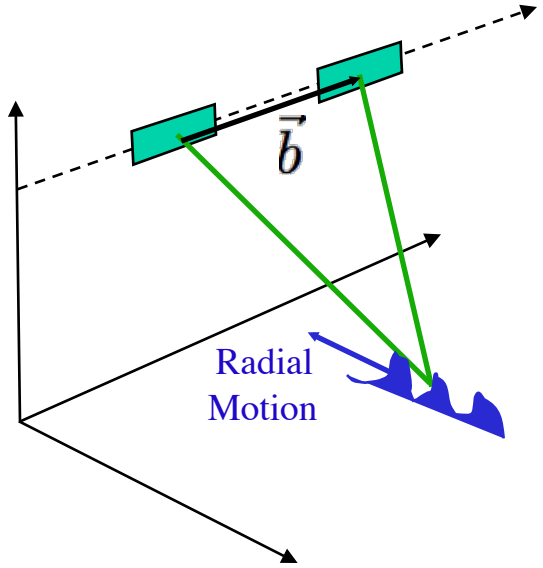

- Dual antenna single pass interferometer
- Along-track separation
  ==> Radial velocity

Interferometry Applications

- Mapping/Cartography
  - Radar Interferometry from airborne platforms is routinely used to produce topographic maps as digital elevation models (DEMs).
    - 2-5 meter circular position accuracy
    - 5-10 m post spacing and resolution
    - 10 km by 80 km DEMs produced in 1 hr on mini-supercomputer
  - Radar imagery is automatically geocoded, becoming easily combined with other (multispectral) data sets.
  - Applications of topography enabled by interferometric rapid mapping
    - Land use management, classification, hazard assessment, intelligence, urban planning, short and long time scale geology, hydrology
- Deformation Mapping and Change Detection
  - Repeat Pass Radar Interferometry from spaceborne platforms is routinely used to produce topographic *change* maps as digital displacement models (DDMs).
    - 0.3-1 centimeter relative displacement accuracy
    - 10-100 m post spacing and resolution
    - 100 km by 100 km DDMs produced rapidly once data is available
  - Applications include
    - Earthquake and volcano monitoring and modeling, landslides and subsidence
    - Glacier and ice sheet dynamics
    - Deforestation, change detection, disaster monitoring

Interferometry for Topography

Measured phase difference:

$$\Delta\phi = -\frac{2\pi}{\lambda}\delta\rho$$

Triangulation:

$$\sin(\theta - \alpha) = \frac{(\rho + \delta\rho)^2 - \rho^2 - B^2}{2\rho B}$$

$$z = h - \rho\cos\theta$$

Critical Interferometer Knowledge:
- Baseline, (B, α), to mm's
- System phase differences, to deg's

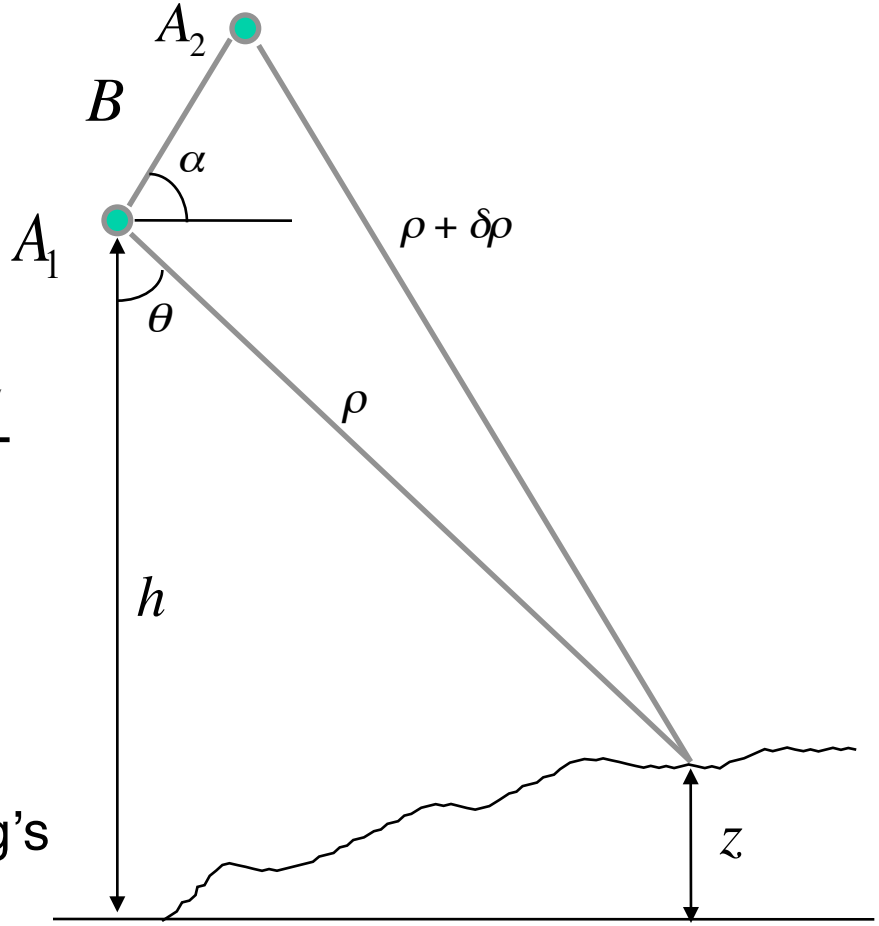

Data Collection Options

For single pass interferometry (SPI) both antennas are located on the same platform. Two modes of data collection are common:

- *single-antenna-transmit mode* - one antenna transmits and both receive
- *ping-pong mode* - each antenna transmits and receives its own echoes effectively doubling the physical baseline.

Classic

$$\Delta\phi = \frac{2\pi}{\lambda}(\rho_2 + \rho_1) - \frac{2\pi}{\lambda}(\rho_1 + \rho_1)$$

$$= \frac{2\pi}{\lambda}(\rho_2 - \rho_1)$$

$$\Delta\phi = \frac{2\pi p}{\lambda}\delta\rho, \quad p = 1$$

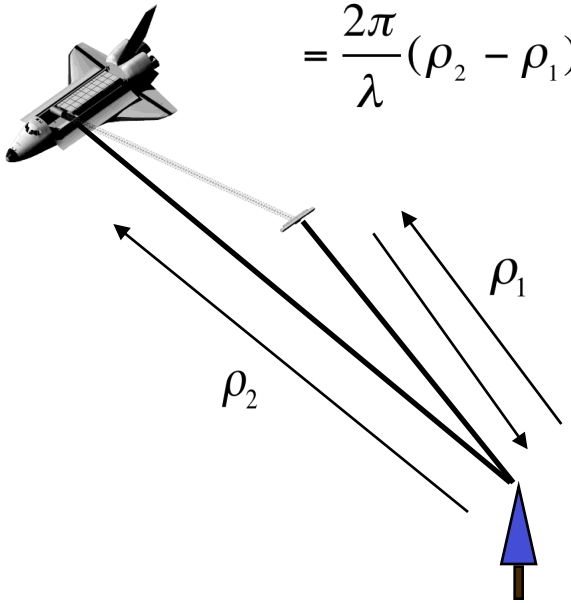

Ping-Pong

$$\Delta\phi = \frac{2\pi}{\lambda}(\rho_2 + \rho_2) - \frac{2\pi}{\lambda}(\rho_1 + \rho_1)$$

$$= \frac{4\pi}{\lambda}(\rho_2 - \rho_1)$$

$$\Delta\phi = \frac{2\pi p}{\lambda}\delta\rho, \quad p = 2$$

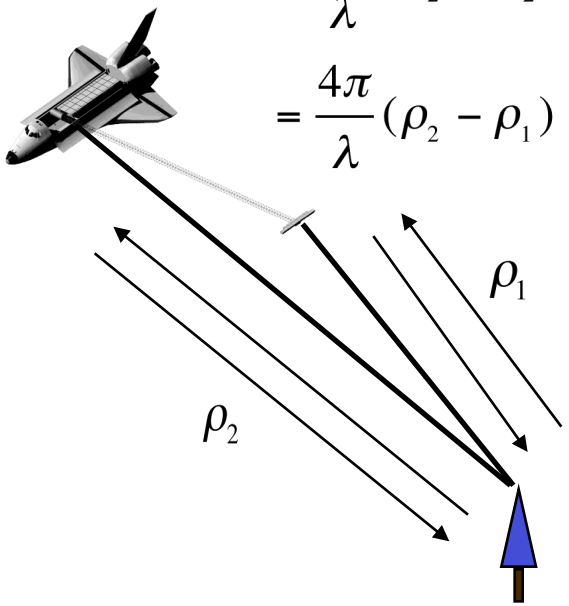

JPL

Height Reconstruction

- Interferometric height reconstruction is the determination of a target's position vector from known platform ephemeris information, baseline information, and the interferometric phase.

$\vec{P}$ = platform position vector

ρ = range to target

$\hat{\ell}$ = unit vector pointing from platform to target

$\vec{T}$ = target location vector

BASIC EQUATION

$$\vec{T} = \vec{P} + \rho\,\hat{\ell}$$

- Interferometry provides a means of determining $\hat{\ell}$

Interferometric Geometry

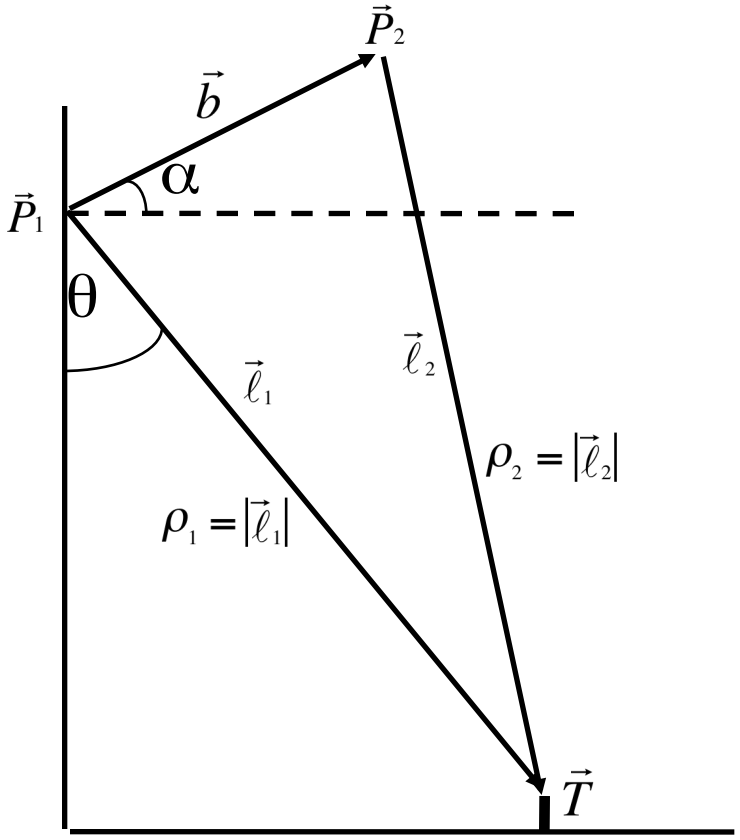

$$\vec{b} = \vec{P}_2 - \vec{P}_1 = \vec{\ell}_1 - \vec{\ell}_2$$

$$\vec{\ell}_2 = \vec{\ell}_1 - \vec{b}$$

$$b = |\vec{b}| = \langle \vec{b}, \vec{b} \rangle^{\frac{1}{2}}, \quad \hat{\ell}_1 = \frac{\vec{\ell}_1}{|\vec{\ell}_1|} = \frac{\vec{\ell}_1}{\rho_1}$$

$$\Delta\phi = \frac{2\pi p}{\lambda}(\rho_2 - \rho_1) = \frac{2\pi p}{\lambda}\left(|\vec{\ell}_2| - |\vec{\ell}_1|\right)$$

$$= \frac{2\pi p}{\lambda}\left(\langle \vec{\ell}_2, \vec{\ell}_2 \rangle^{\frac{1}{2}} - \rho_1\right)$$

$$= \frac{2\pi p}{\lambda}\left(\langle \vec{\ell}_1 - \vec{b}, \vec{\ell}_1 - \vec{b} \rangle^{\frac{1}{2}} - \rho_1\right)$$

$$= \frac{2\pi p}{\lambda}\left(\left(\rho^2{}_1 - 2\langle \vec{\ell}_1, \vec{b} \rangle + b^2\right)^{\frac{1}{2}} - \rho_1\right)$$

$$= \frac{2\pi p}{\lambda}\rho_1\left(\left(1 - \frac{2\langle \hat{\ell}_1, \vec{b} \rangle}{\rho_1} + \left(\frac{b}{\rho_1}\right)^2\right)^{\frac{1}{2}} - 1\right)$$

- p equals 1 or 2 depending on system

2-D Height Reconstruction - Flat Earth

- Before considering the general 3-D height reconstruction it is instructive to first solve the two dimensional problem.

Assume that b << ρ and let $\hat{\ell}_1 = \frac{\vec{\ell}_1}{|\vec{\ell}_1|} = \frac{\vec{\ell}_1}{\rho}$. Taking a first order Taylor's expansion of

$$\Delta\phi = \frac{2\pi p}{\lambda}\rho_1\left(\left(1 - \frac{2\langle\hat{\ell}_1,\vec{b}\rangle}{\rho_1} + \left(\frac{b}{\rho_1}\right)^2\right)^{\frac{1}{2}} - 1\right)$$

the interferometric phase can be approximated as

$$\Delta\phi \approx -\frac{2\pi p}{\lambda}\langle\hat{\ell}_1,\vec{b}\rangle$$

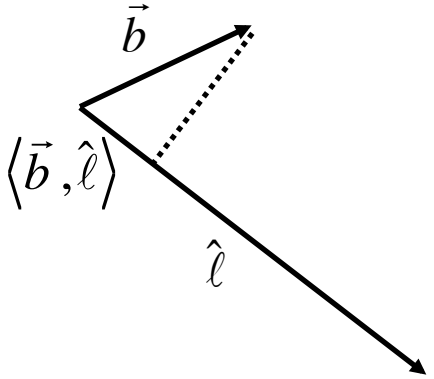

With $\vec{b} = (b\cos(\alpha), b\sin(\alpha))$ and $\hat{\ell} = (\sin(\theta), -\cos(\theta))$ then

$$\Delta\phi = -\frac{2\pi p}{\lambda} b\sin(\theta - \alpha)$$

2-D Height Reconstruction - Flat Earth II

- Let $\vec{P}$ = (y_o, h) be the platform position vector, then

$$\vec{T} = \vec{P} + \rho\,\hat{\ell}$$
$$= (y_o, h) + \rho\,(\sin(\theta), -\cos(\theta))$$
$$= (y_o + \rho\,\sin(\theta), h - \rho\,\cos(\theta))$$

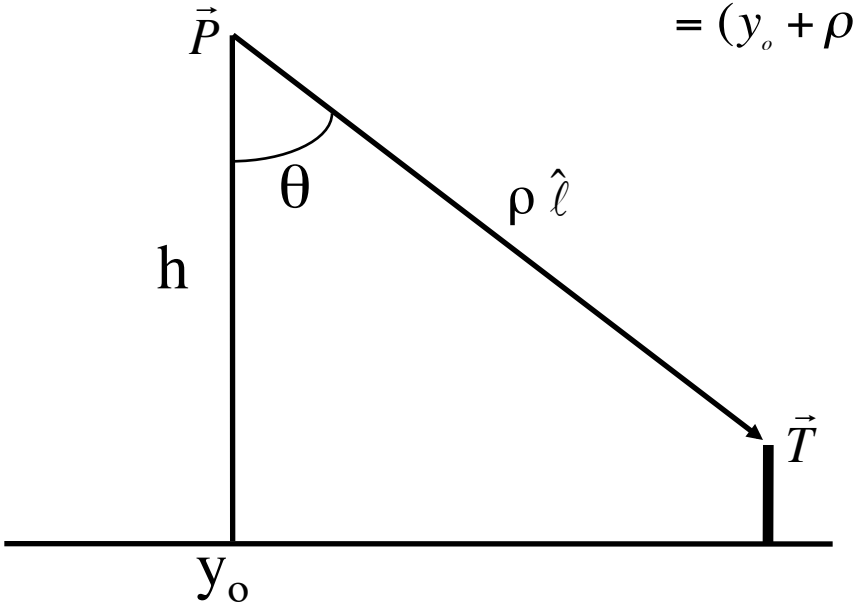

- Solving for θ in terms of the interferometric phase, $\Delta\phi$, yields

$$\theta = \sin^{-1}\left(\frac{-\lambda\Delta\phi}{2\pi p b}\right) + \alpha$$

Phase Gradient

- For a number of applications including flight planning and unwrapping studies it is desirable to be able to compute the interferometric phase gradient for an arbitrarily sloped surface, look geometry and baseline.
- The interferometric phase is well approximated for most applications by

$$\phi \approx -\frac{2\pi p}{\lambda}\left\langle \vec{b}, \hat{l} \right\rangle \qquad (\phi \Leftrightarrow \Delta\phi)$$

where $\vec{b}$ is the baseline vector, $\hat{l}$ a unit vector pointing to the target and λ is the wavelength.

- The phase gradient is

$$\nabla\phi = \begin{bmatrix} \frac{\partial\phi}{\partial s} \\ \frac{\partial\phi}{\partial\rho} \end{bmatrix} = -\frac{2\pi p}{\lambda}\begin{bmatrix} \left\langle \vec{b}, \frac{\partial\hat{l}}{\partial s} \right\rangle \\ \left\langle \vec{b}, \frac{\partial\hat{l}}{\partial\rho} \right\rangle \end{bmatrix}$$

where s is the along track coordinate and ρ is the range.

Phase Gradient Observations

- There in a change in phase with respect to range regardless of whether the terrain is sloped in the range direction or not. The phase rate, or fringe rate, with respect to a flat surface is called the flat surface (or spherical earth) fringe frequency.

$$\frac{\partial \phi}{\partial \rho} = \frac{2\pi p}{\lambda} \frac{b\cos(\theta - \alpha)}{\rho \tan(\theta - \psi_c)} = \frac{2\pi p}{\lambda} \frac{b_\perp}{\rho \tan(\theta - \psi_c)}$$

$(\phi \Leftrightarrow \Delta\phi)$

- Note that the fringe rate depends on the local slope and the perpendicular baseline length.
- The fringe rate in the azimuth or along track direction is zero unless there is an azimuth slope. It also depends on the magnitude of the local slope and the perpendicular baseline length

$$\frac{\partial \phi}{\partial s} = \frac{2\pi p}{\lambda} \frac{b\cos(\theta - \alpha)}{\rho} \sin\theta \tan\psi_s = \frac{2\pi p}{\lambda} \frac{b_\perp}{\rho} \sin\theta \tan\psi_s$$

Flattened Phase

- Often when looking at interferograms or prior to unwrapping it is desirable to remove the flat earth fringes so that the resulting fringes will follow the local topography. This process is call flattening and the resulting phase is called the flattened phase.
- The flattened phase is given by

$$\Delta\phi_{flat} = -\frac{4\pi}{\lambda}\left(\langle\hat{\ell},\vec{b}\rangle - \langle\hat{\ell}_o,\vec{b}\rangle\right)$$

where $\hat{\ell}$ is the look vector to a point and $\hat{\ell}_o$ is the corresponding look vector to the flat surface at the same range.

- Making the usual 2 dimensional simplifications

$$\begin{aligned}\Delta\phi_{flat} &= \frac{4\pi}{\lambda}b(\sin(\theta-\alpha)-\sin(\theta_o-\alpha)) \\ &\approx \frac{4\pi}{\lambda}b\cos(\theta-\alpha)\delta\theta\end{aligned}$$

Flattened Phase II

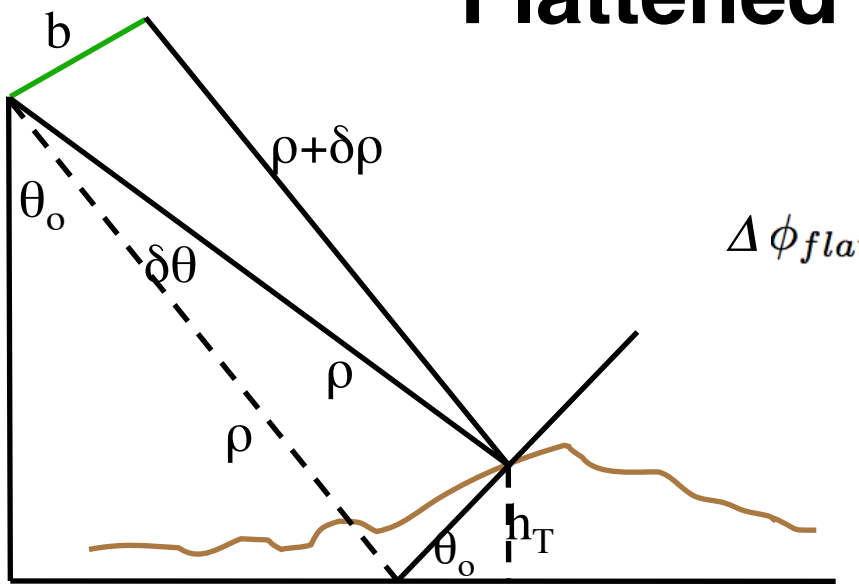

$$\Delta\phi_{flat} = \frac{4\pi}{\lambda} b(\sin(\theta-\alpha) - \sin(\theta_o - \alpha))$$
$$\approx \frac{4\pi}{\lambda} b\cos(\theta-\alpha)\delta\theta$$

From the figure we have

$$\delta\theta \approx \frac{h_T}{\rho \sin\theta_o}$$

which gives

$$\Delta\phi_{flat} = \frac{4\pi}{\lambda} b_\perp \delta\theta$$
$$= \frac{4\pi}{\lambda} b_\perp \frac{h_T}{\rho \sin\theta_o}$$

Thus the topographic portion of the interferometric phase is a function of the perpendicular baseline length.

Sensitivity of Height with Respect to Phase

Sensitivity to Phase

$$\frac{\partial \vec{T}}{\partial \phi} = \frac{-\lambda\rho}{2\pi p b \cos(\theta - \alpha)} \begin{bmatrix} 0 \\ \cos\theta \\ \sin\theta \end{bmatrix}$$

Ambiguity Height

$$h_a = 2\pi \frac{\partial T_z}{\partial \phi} = \frac{-\lambda\rho \sin(\theta)}{pb\cos(\theta - \alpha)}$$

$p=1,2$

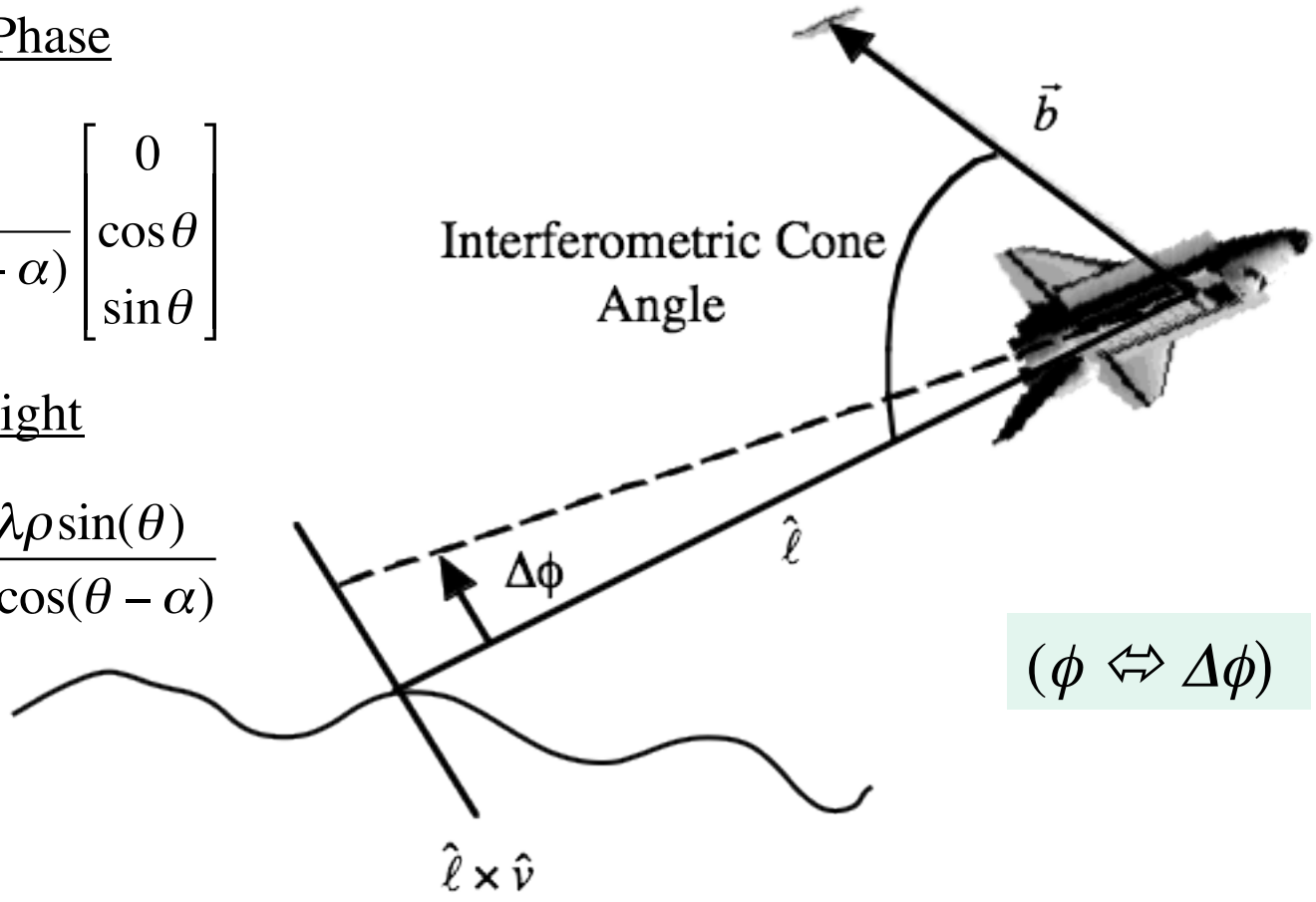

$(\phi \Leftrightarrow \Delta\phi)$

- Observe that $\frac{\partial \vec{T}}{\partial \phi}$ is parallel to $\hat{\ell} \times \hat{v}$.

3-D Height Reconstruction

- The full three dimensional height reconstruction is based on the observation that the target location is the intersection locus of three surfaces
  - range sphere $\left|\vec{P}-\vec{T}\right|=\rho$
  - Doppler cone $f=\frac{2}{\lambda}\left\langle \vec{v},\hat{\ell}\right\rangle$
  - phase cone* $\Delta\phi=-\frac{2\pi p}{\lambda}\left\langle \vec{b},\hat{\ell}\right\rangle$

Doppler and phase cones give two angles defining spherical coordinate system

- The cone angles are defined relative to the generating axes determined by
  - velocity vector — Doppler cone
  - baseline vector — phase cone

* Actually the phase surface is a hyperboloid, however for most applications where the phase equation above is valid, the hyperboloid degenerates to a cone.

Height Reconstruction Geometry

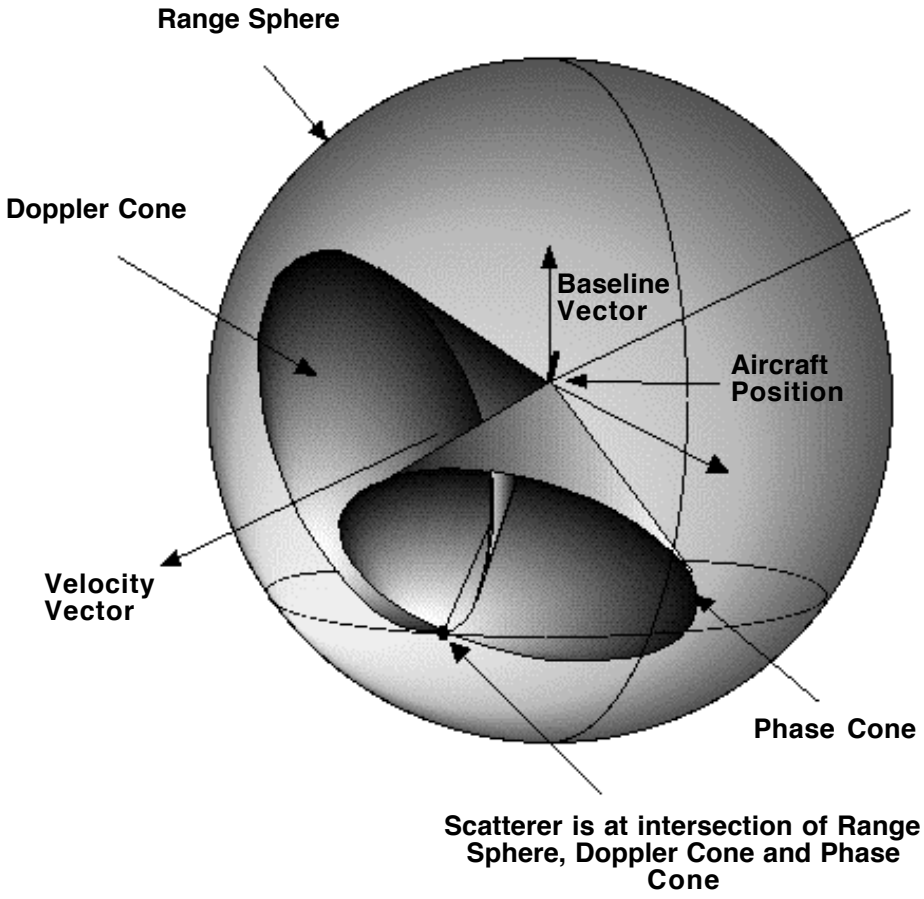

Shuttle Radar Topography Mission

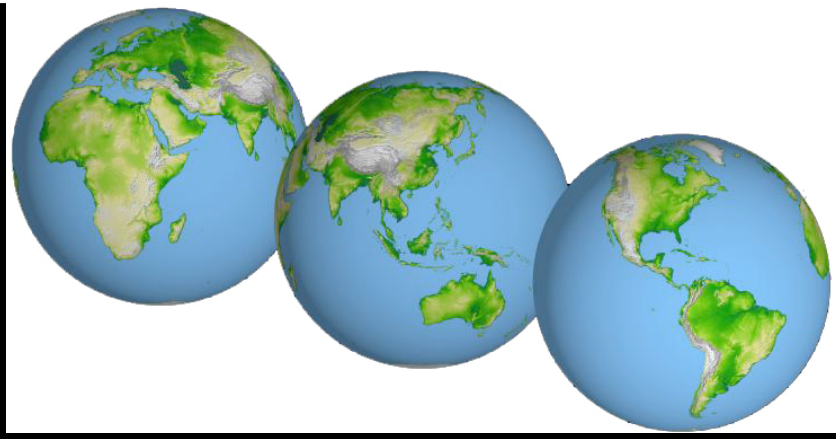

This research was carried out at the Jet Propulsion Laboratory, California Institute of Technology, under a contract with the National Aeronautics and Space Administration

Mission Overview

Launch

Feb 11, 2000 - STS99

225 km C-band interferometric swaths map all landmass between ±60° latitude at least twice

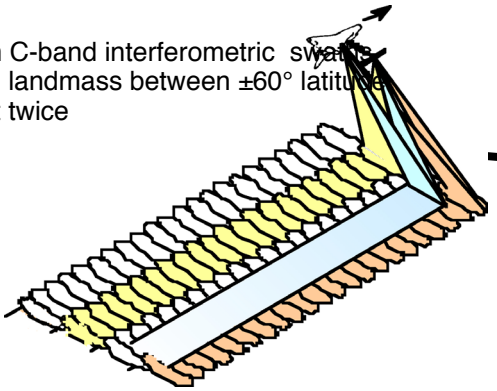

12 Tbytes data recorded on-board on 330 tape cassettes

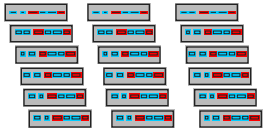

Data returned with Shuttle to Ground Data Processing Facility

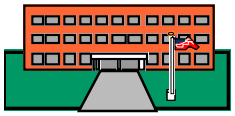

Three year processing

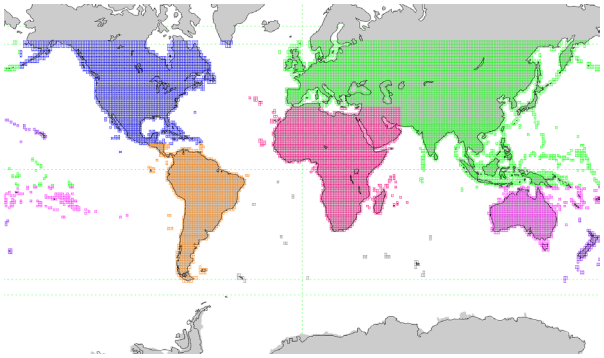

Digital elevation data delivered in 1°x1° mosaiced cells

NIMA

NIMA data validation, editing and distribution to military users

USGS science for a changing world

EDC for public distribution

SRTM Patch Processing Example

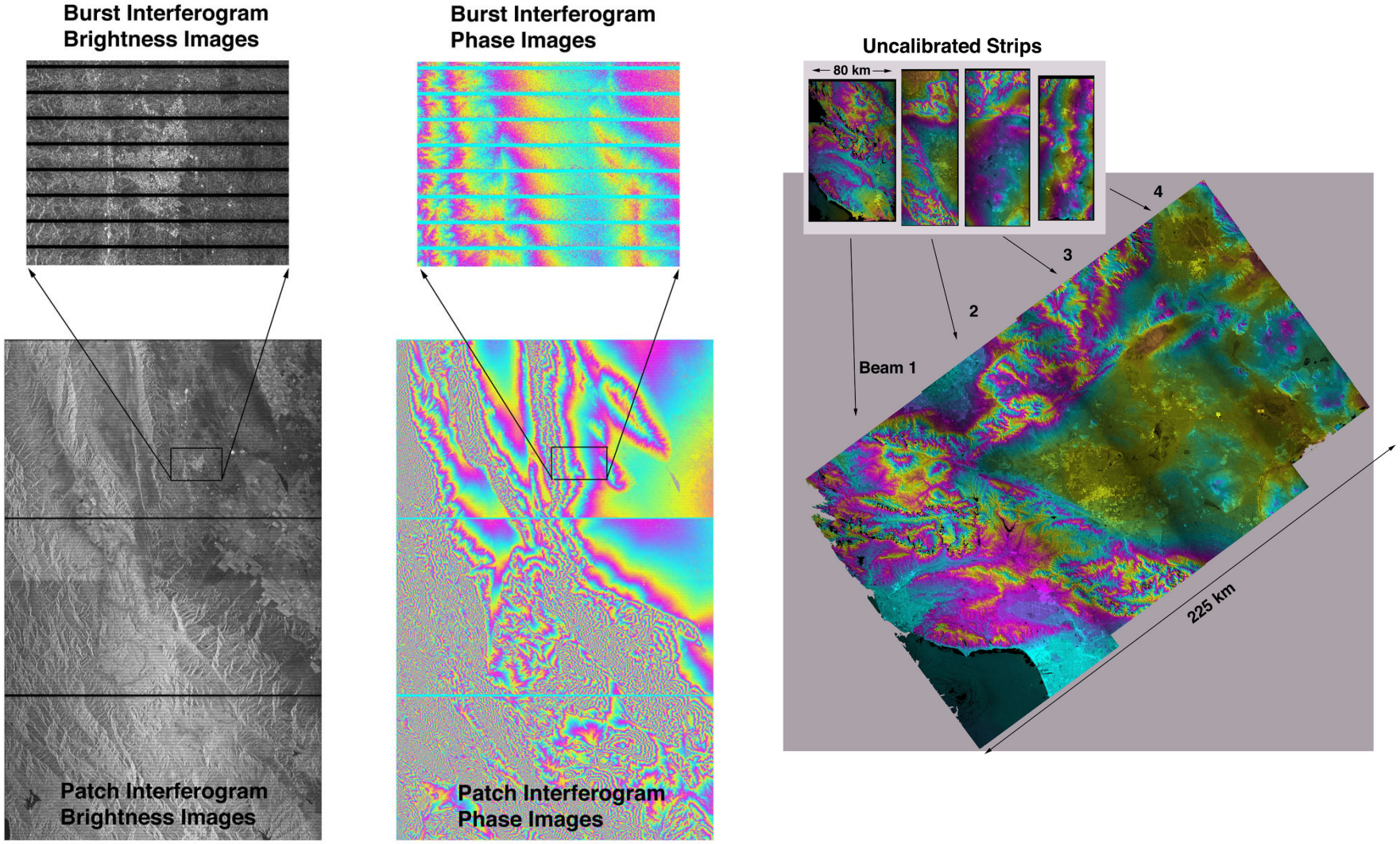

Need for Motion Compensation

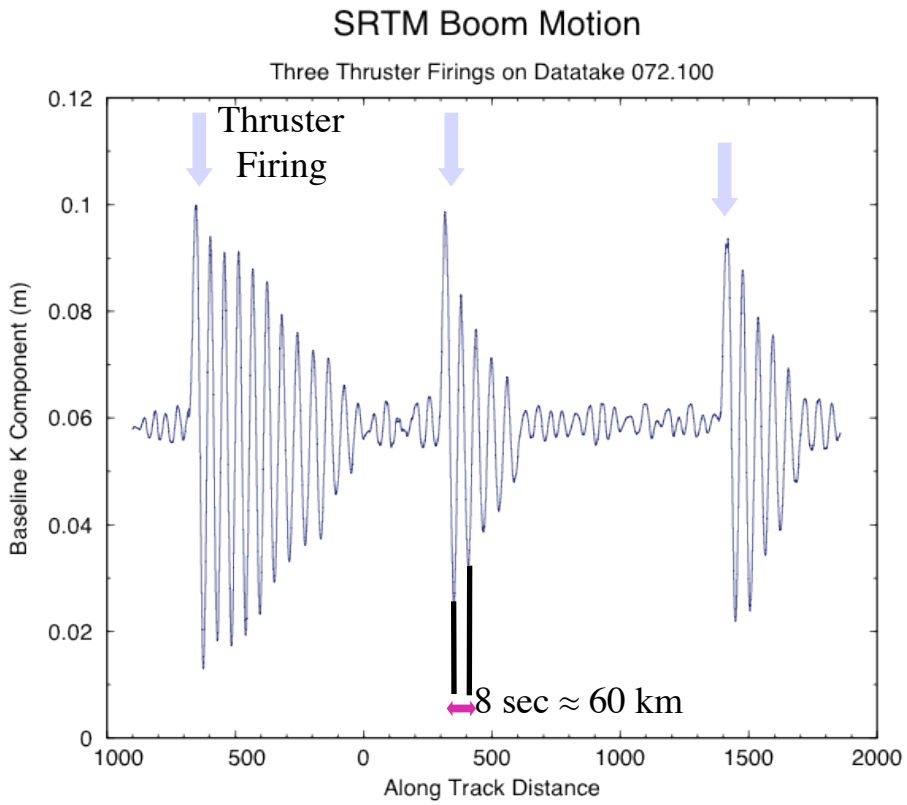

Plot of Baseline K Component

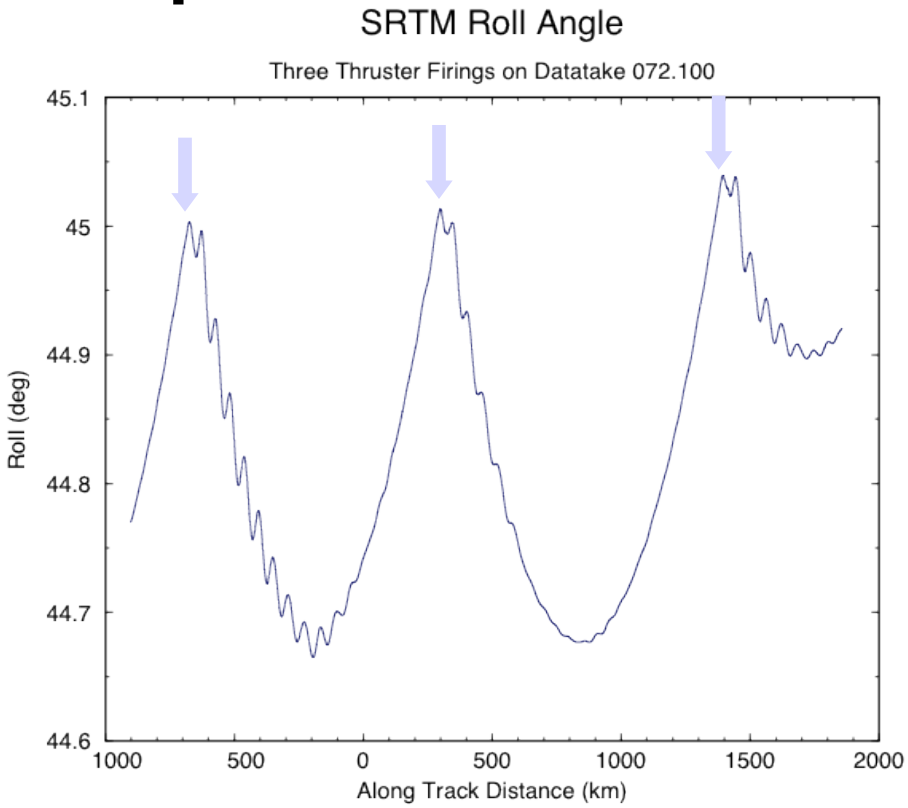

Plot of Roll Angle

- Motion compensation is required to account for boom dynamics as well as shuttle attitude changes. Left uncompensated these motions would generate hundreds of meters of height error.

SRTM Hardware Configuration

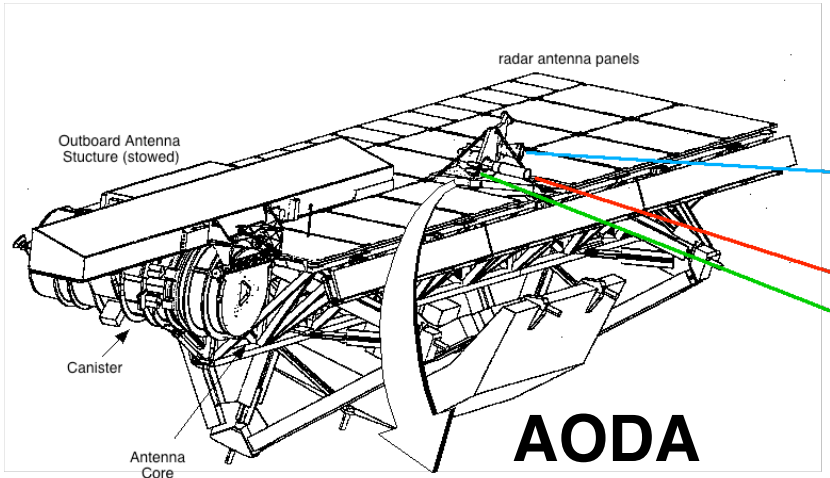

AODA

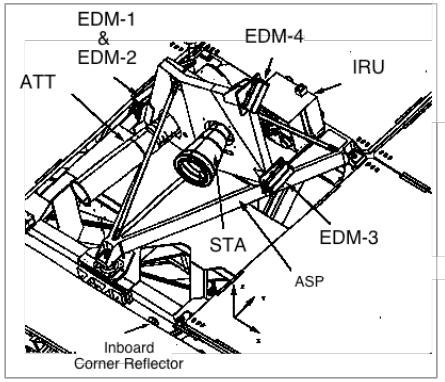

STA looks at stars

ATT looks at OTA

OTA

EDMs look at corner reflector array

Mast

Outboard Antenna Stucture (deployed)

GPS antenna (1 of 2)

flight segment

ground segment

GPSR-1

GPSR-2

SIU

to GPS antennas

to ASP sensors & OTA

commands & data

APC-1

APC-2

commands & data

global GPS ground receiver network (accessible via Internet)

JSC-Houston

ATMA

data

JPL-Pasadena

AGDP

GIPSY

SRTM Resolution Improvement

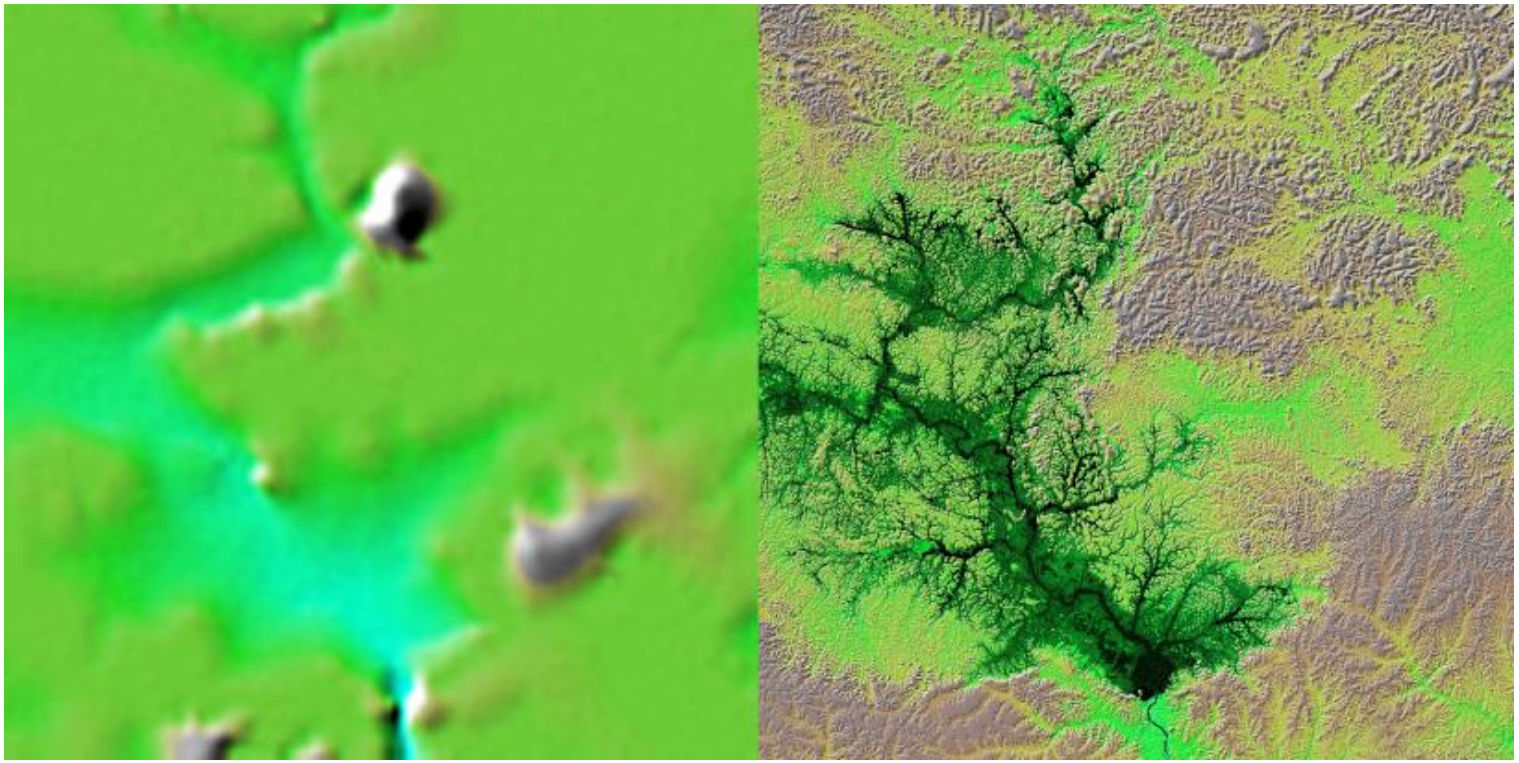

GTOPO30 DEM

SRTM DEM with radar image overlay

Lake Balbina,
Brazil

SRTM Look at Central America

SRTM Views Global Landscapes

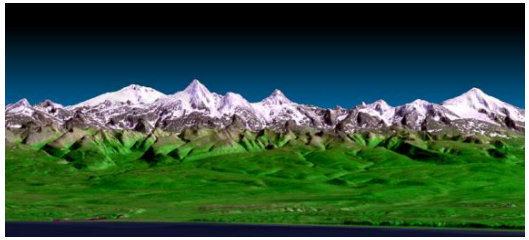

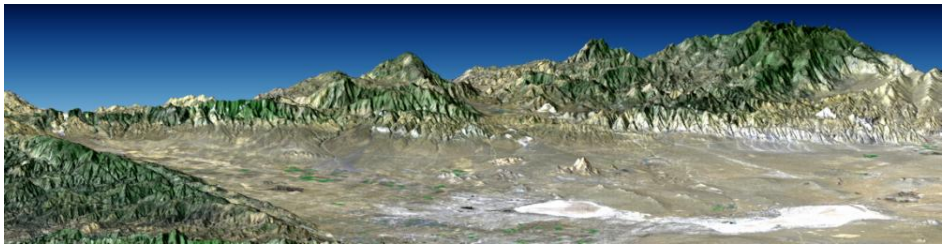

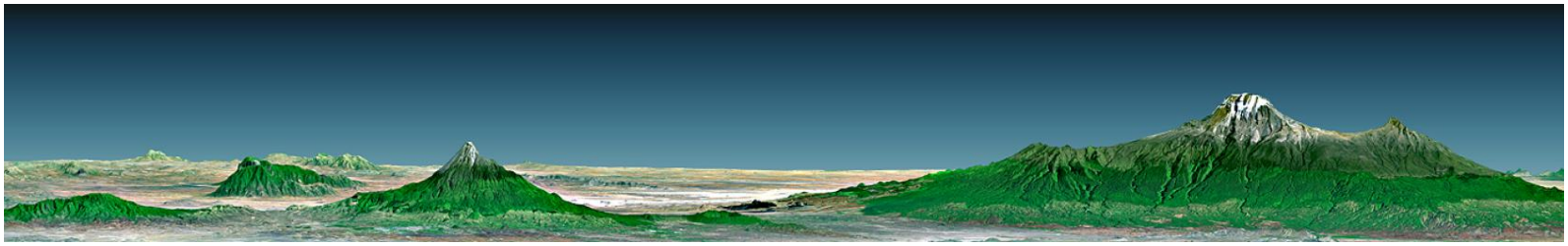

SRTM Performance Summary

- Based on over hundreds of millions of comparisons, SRTM has a absolute height accuracy of 9.0m or better over a 1^{o}x1^{o} cell, at the 90% confidence level.

- Using the kinematic GPS data, probably the best ground truth data available, SRTM meets the absolute height requirement by a factor of 3.

- **Both the absolute and relative SRTM height accuracy requirements are met.**

- Using the kinematic GPS data, SRTM's horizontal accuracy is better than 10 meters and we believe the results are consistent with no horizontal offset.

- **Both the absolute and relative SRTM horizontal accuracy requirements are met.**

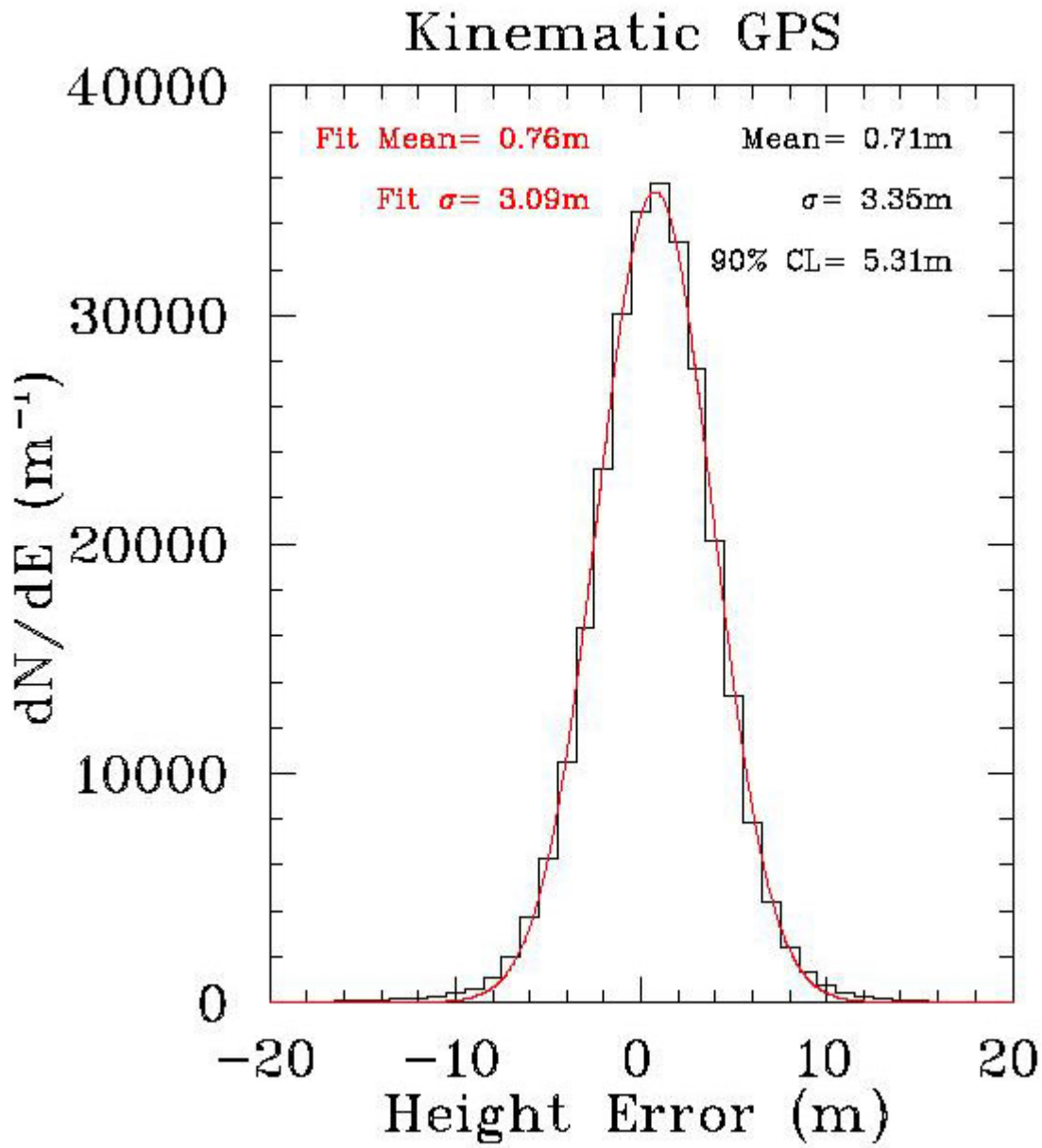
Kinematic GPS
Fit Mean= 0.76m
Fit σ= 3.09m
Mean= 0.71m
σ= 3.35m
90% CL= 5.31m
dN/dE (m⁻¹)
40000
30000
20000
10000
0
−20
−10
0
10
20
Height Error (m)

Data Collection Options

For single pass interferometry (SPI) both antennas are located on the same platform. Two modes of data collection are common:

- *single-antenna-transmit mode* - one antenna transmits and both receive
- *ping-pong mode* - each antenna transmits and receives its own echoes effectively doubling the physical baseline.

Classic

$$\Delta\phi = \frac{2\pi}{\lambda}(\rho_2 + \rho_1) - \frac{2\pi}{\lambda}(\rho_1 + \rho_1)$$

$$= \frac{2\pi}{\lambda}(\rho_2 - \rho_1)$$

$$\Delta\phi = \frac{2\pi p}{\lambda}\delta\rho, \quad p = 1$$

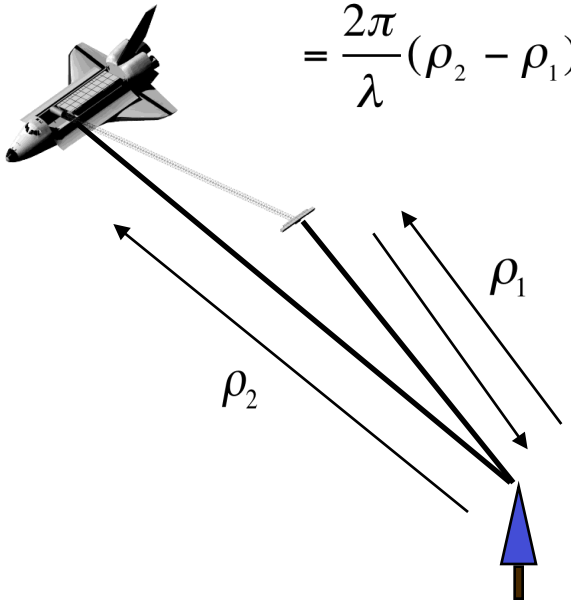

Ping-Pong

$$\Delta\phi = \frac{2\pi}{\lambda}(\rho_2 + \rho_2) - \frac{2\pi}{\lambda}(\rho_1 + \rho_1)$$

$$= \frac{4\pi}{\lambda}(\rho_2 - \rho_1)$$

$$\Delta\phi = \frac{2\pi p}{\lambda}\delta\rho, \quad p = 2$$

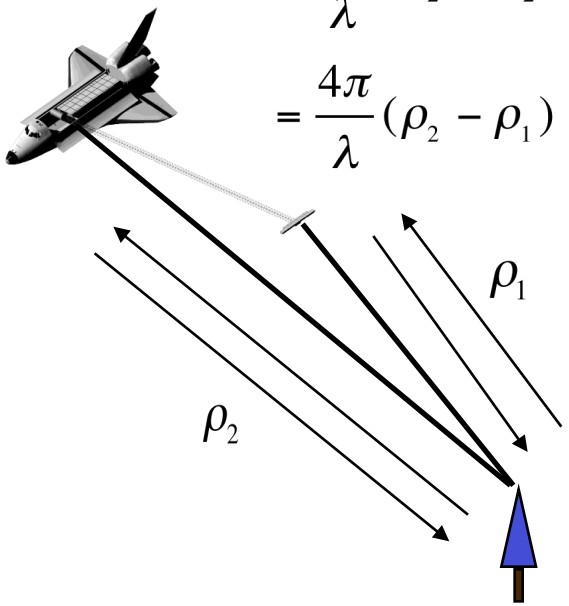

Data Collection Options II

Interferometric data can also be collected in the repeat pass mode (RPI). In this mode two spatially close radar observations of the same scene are made separated in time. The time interval may range from seconds to years. The two observations may be made different sensors provided they have nearly identical radar system parameters.

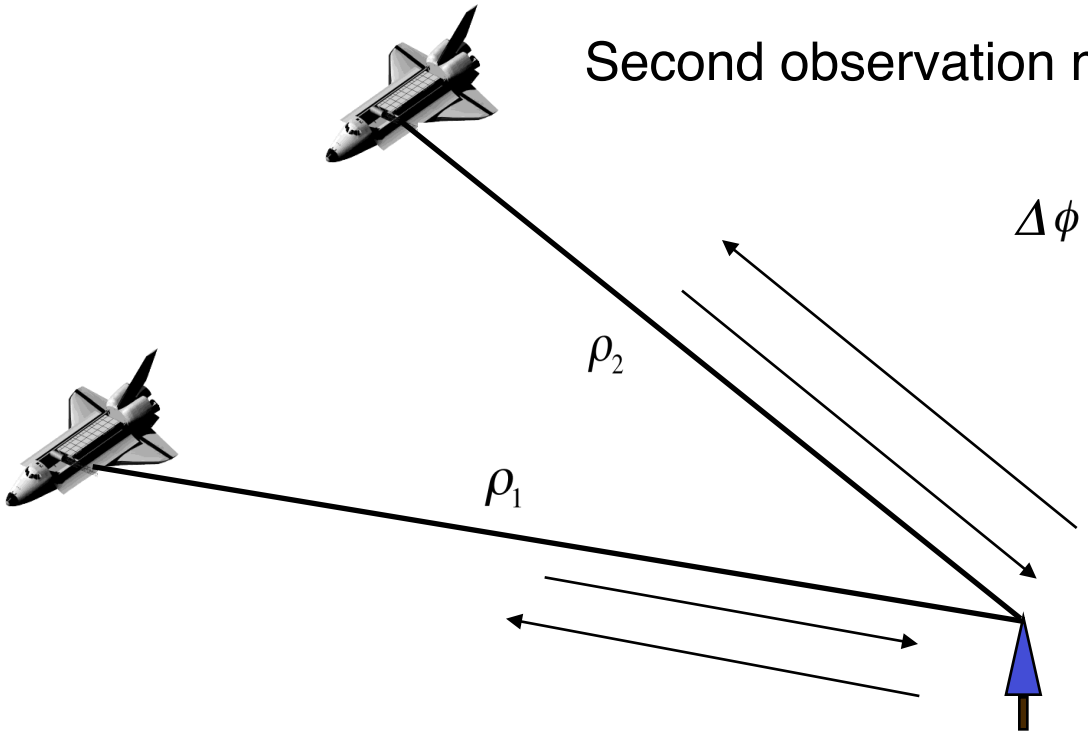

Second observation made at some later time.

$$\Delta\phi = \frac{2\pi}{\lambda}(\rho_2 + \rho_2) - \frac{2\pi}{\lambda}(\rho_1 + \rho_1)$$

$$= \frac{4\pi}{\lambda}(\rho_2 - \rho_1)$$

$$\Delta\phi = \frac{2\pi p}{\lambda}\delta\rho,$$

$$p = 2$$

Differential Interferometry

When two observations are made from the same location in space but at different times, the interferometric phase is proportional to any change in the range of a surface feature directly.

$$\Delta\phi = \frac{4\pi}{\lambda}(\rho(t_1) - \rho(t_2)) = \frac{4\pi}{\lambda}\Delta\rho_{\text{change}}$$

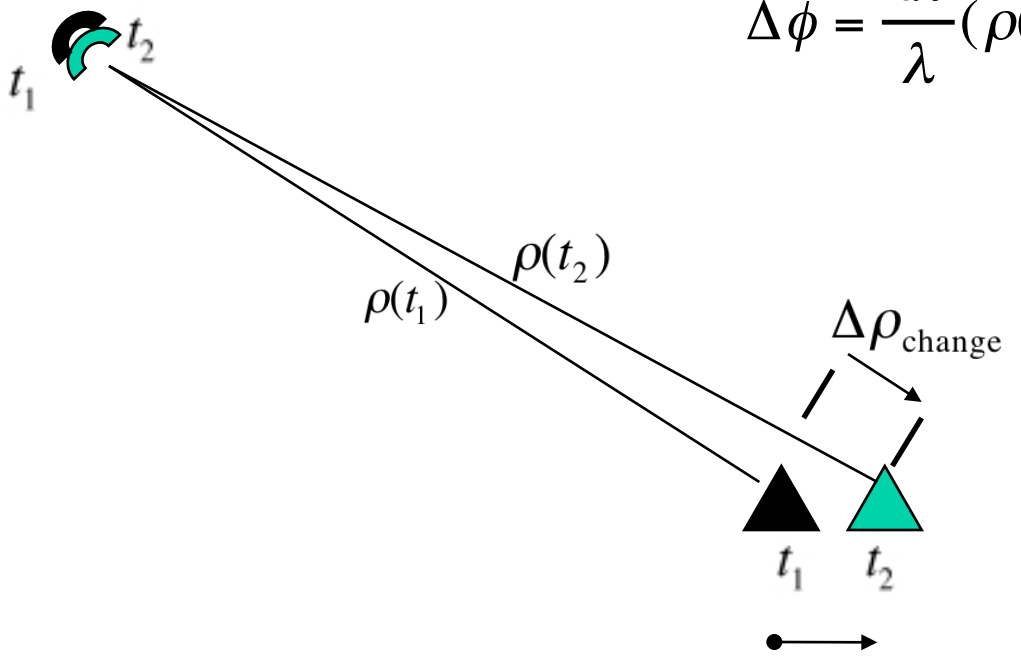

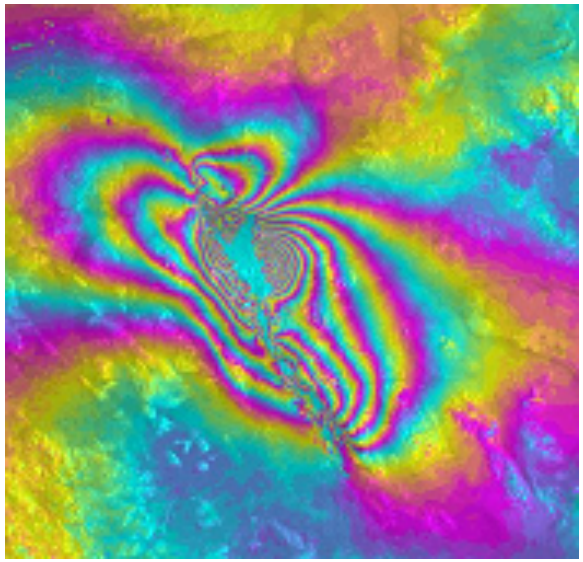

Differential Interferometric Phase

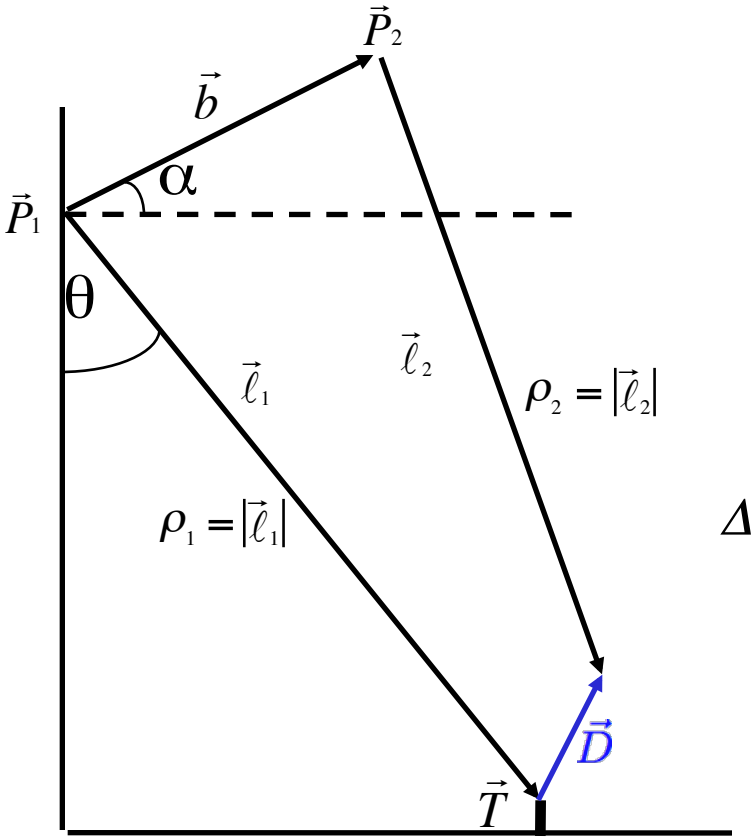

$$\vec{b} = \vec{P}_2 - \vec{P}_1 = \vec{\ell}_1 - \vec{\ell}_2$$

$$\vec{\ell}_2 = \vec{T} + \vec{D} - \vec{P}_2 = \vec{\ell}_1 + \vec{D} - \vec{b}$$

$$b = |\vec{b}| = \langle \vec{b}, \vec{b} \rangle^{\frac{1}{2}} \quad , \quad \hat{\ell}_1 = \frac{\vec{\ell}_1}{|\vec{\ell}_1|} = \frac{\vec{\ell}_1}{\rho_1}$$

$$\Delta\phi = \frac{2\pi p}{\lambda}(\rho_2 - \rho_1) = \frac{2\pi p}{\lambda}\left(|\vec{\ell}_2| - |\vec{\ell}_1|\right)$$

$$= \frac{2\pi p}{\lambda}\left(\langle \vec{\ell}_2, \vec{\ell}_2 \rangle^{\frac{1}{2}} - \rho_1\right)$$

$$\Delta\phi = \frac{4\pi}{\lambda}\left(\langle \vec{\ell}_1 + \vec{D} - \vec{b}, \vec{\ell}_1 + \vec{D} - \vec{b} \rangle^{\frac{1}{2}} - \rho_1\right)$$

Assuming that

$$\begin{aligned} |\vec{b}| &\leq \rho \\ |\vec{D}| &\leq \rho \\ |\langle \vec{b}, \vec{D} \rangle| &\leq \rho \end{aligned}$$

yields

$$\Delta\phi = \frac{4\pi}{\lambda}\left(-\langle \hat{\ell}, \vec{b} \rangle + \langle \hat{\ell}, \vec{D} \rangle\right)$$

Differential Interferometry and Topography

- Generally two observations are made from different locations in space and at different times, so the interferometric phase is proportional to topography and topographic change.

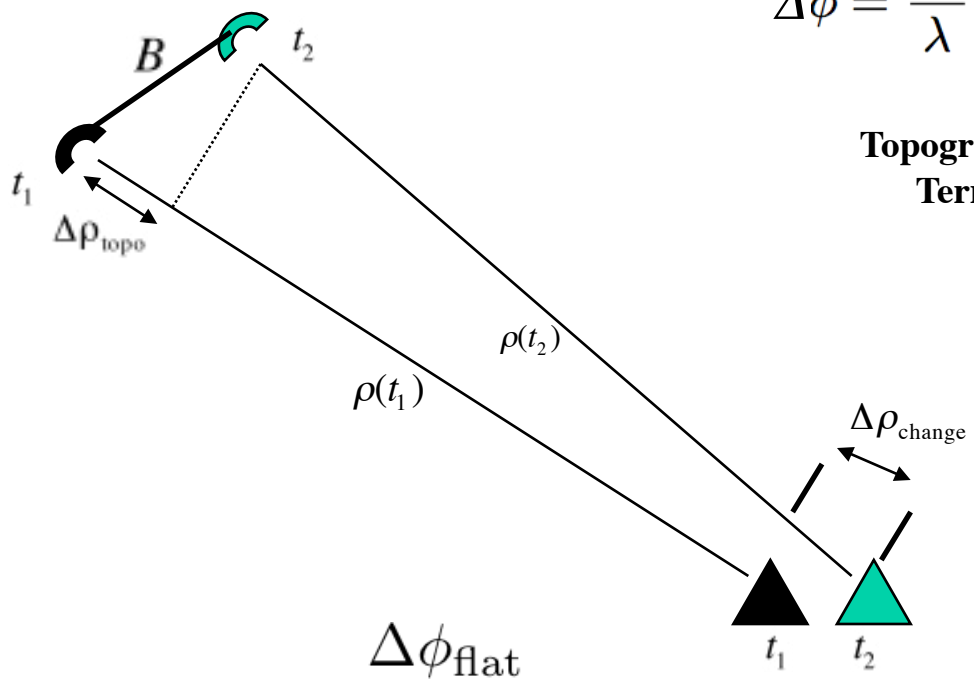

$$\Delta\phi = \frac{4\pi}{\lambda}\left(-\langle\hat{\ell},\vec{b}\rangle + \langle\hat{\ell},\vec{D}\rangle\right)$$

Topography Term **Change Term**

$$\Delta\phi = \frac{4\pi}{\lambda}(\Delta\rho_{change} - \Delta\rho_{topo})$$

$$\Delta\phi = \frac{4\pi}{\lambda}(\Delta\rho_{change} - b\sin(\theta-\alpha))$$

$$\Delta\phi_{flat} = \frac{4\pi}{\lambda}\left(\Delta\rho_{change} - \frac{b_\perp h_T}{\rho\sin\theta}\right)$$

Note: Sensitivity of phase with respect to change is much greater than with respect to topographic relief

If topography is known, then second term can be eliminated to reveal surface change

Extracting the Deformation Term - Pre-Existing DEM

$$\Delta\phi_{b_1} = \frac{4\pi}{\lambda}\left(-\langle\hat{\ell},\vec{b}_1\rangle + \langle\hat{\ell},\vec{D}\rangle\right)$$

Phase Simulated from DEM

$$\phi_{topo} = -\frac{4\pi}{\lambda}\langle\hat{\ell},\vec{b}_1\rangle$$

Using Unflattened Phases

$$\begin{aligned}\Delta\rho_{disp} &= \langle\hat{\ell},\vec{D}\rangle \\ &= \frac{\lambda}{4\pi}\left(\Delta\phi_{b_1} - \phi_{topo}\right)\end{aligned}$$

Using Flattened Phases

$$\begin{aligned}\Delta\phi_{flat_1} &= \frac{4\pi}{\lambda}b_{\perp_1}\frac{h_T}{\rho\sin\theta_o} + \frac{4\pi}{\lambda}\Delta\rho_{disp} \\ \Delta\phi_{flat_2} &= \frac{4\pi}{\lambda}b_{\perp_1}\frac{h_T}{\rho\sin\theta_o}\end{aligned}$$

$$\Delta\rho_{disp} = \frac{\lambda}{4\pi}\left(\Delta\phi_{flat_1} - \Delta\phi_{flat_2}\right)$$

Extracting the Deformation - Three Passes

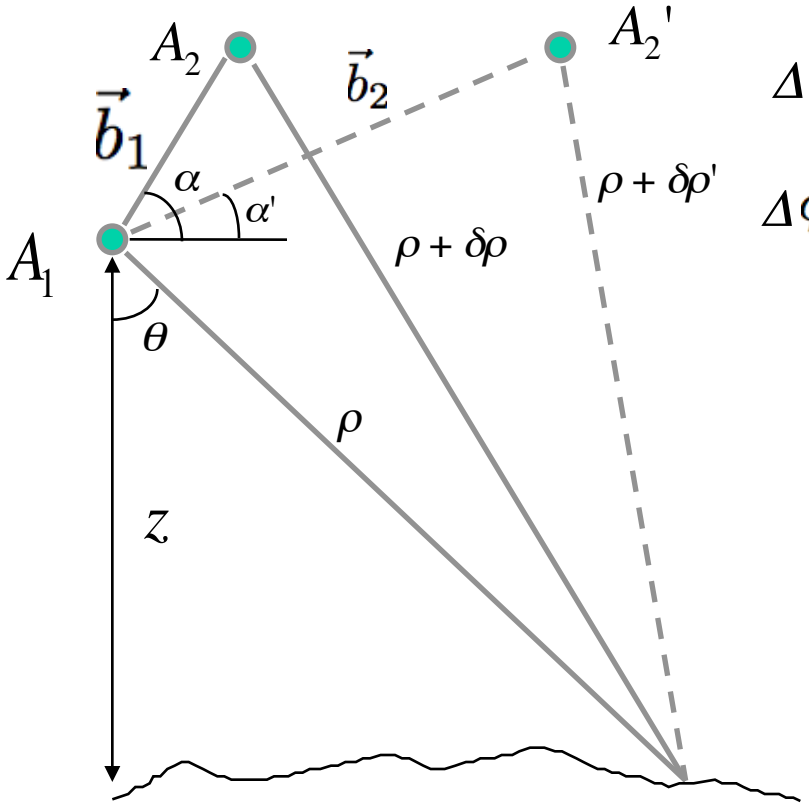

$$\Delta\phi_{b_1} = \frac{4\pi}{\lambda}\left(-\langle\hat{\ell}, \vec{b}_1\rangle + \langle\hat{\ell}, \vec{D}\rangle\right) \quad \text{Change Pair}$$

$$\Delta\phi_{b_2} = -\frac{4\pi}{\lambda}\langle\hat{\ell}, \vec{b}_2\rangle \quad \text{Topo Pair}$$

Using Unflattened Phases

$$\begin{aligned}\Delta\rho_{disp} &= \langle\hat{\ell}, \vec{D}\rangle \\ &= \frac{\lambda}{4\pi}\left(\Delta\phi_{b_1} - \frac{\langle\hat{\ell}, \vec{b}_1\rangle}{\langle\hat{\ell}, \vec{b}_2\rangle}\Delta\phi_{b_2}\right) \\ &= \frac{\lambda}{4\pi}\left(\Delta\phi_{b_1} - \frac{b_{||_1}}{b_{||_2}}\Delta\phi_{b_2}\right)\end{aligned}$$

Using Flattened Phases

$$\Delta\phi_{flat_1} = \frac{4\pi}{\lambda} b_{\perp_1} \frac{h_T}{\rho \sin\theta_o} + \frac{4\pi}{\lambda}\Delta\rho_{disp}$$

$$\Delta\phi_{flat_2} = \frac{4\pi}{\lambda} b_{\perp_2} \frac{h_T}{\rho \sin\theta_o}$$

$$\Delta\rho_{disp} = \frac{\lambda}{4\pi}\left(\Delta\phi_{flat_1} - \frac{b_{\perp_1}}{b_{\perp_2}}\Delta\phi_{flat_2}\right)$$

Differential Interferometry Sensitivities

- The reason differential interferometry can detect millimeter level surface deformation is that the differential phase is much more sensitive to displacements than to topography.

$$\frac{\partial \phi}{\partial h} = \frac{2\pi p b \cos(\theta - \alpha)}{\lambda \rho \sin\theta} = \frac{2\pi p b_{\perp}}{\lambda \rho \sin\theta}$$ Topographic Sensitivity

$(\phi \Leftrightarrow \Delta\phi)$

$$\frac{\partial \phi}{\partial \Delta\rho} = \frac{4\pi}{\lambda}$$ Displacement Sensitivity

$$\sigma_{\phi_{topo}} = \frac{\partial \phi}{\partial h}\sigma_h = \frac{4\pi}{\lambda}\frac{b_{\perp}}{\rho \sin\theta}\sigma_h$$ Topographic Sensitivity Term

$$\sigma_{\phi_{disp}} = \frac{\partial \phi}{\partial \Delta\rho}\sigma_{\Delta\rho} = \frac{4\pi}{\lambda}\sigma_{\Delta\rho}$$ Displacement Sensitivity Term

Since $\frac{b}{\rho} << 1$ ==> $\frac{\sigma_{\phi_{disp}}}{\sigma_{\Delta\rho}} >> \frac{\sigma_{\phi_{topo}}}{\sigma_h}$

Meter Scale Topography Measurement - Millimeter Scale Topographic Change

Strengths and Limitations

- The major strengths for using radar differential interferometry are
  - Wide area coverage
  - Millimeter scale accuracy locally
  - Geophysically useful even without other data sets
  - Complementary to established geodetic and seismic tools (e.g. GPS and leveling)
- Although there has been great success using radar differential interferometry for deformation measurement its application can be limited by
  - Temporal decorrelation of the surface
  - Other surface changes
  - Atmospheric and ionospheric effects
  - Poor DEM availability and Quality or lack of DEM pair

Some Examples of Deformation

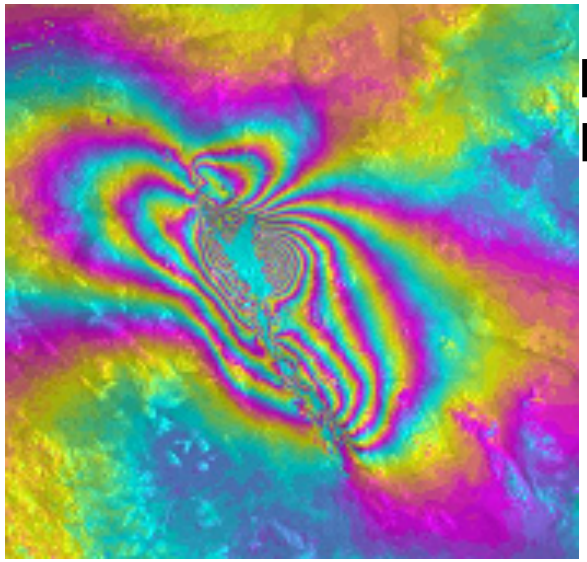

Hector Mine Earthquake

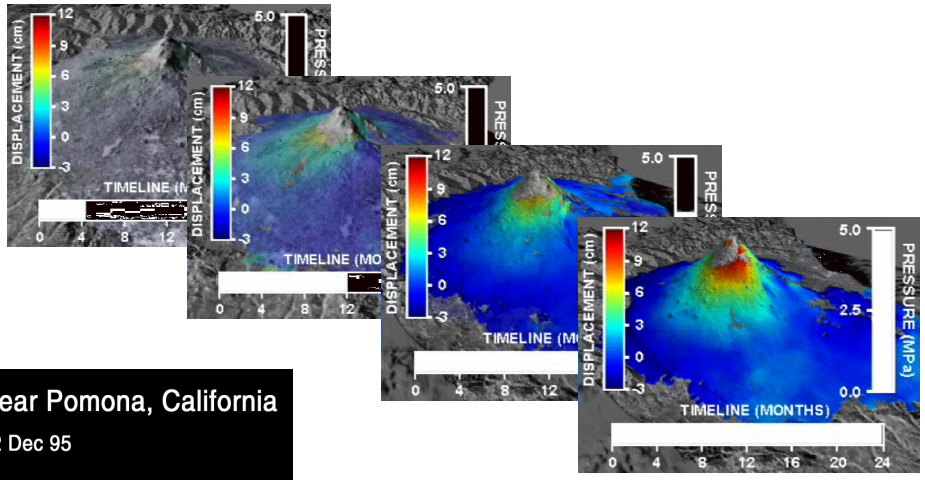

Etna Volcano

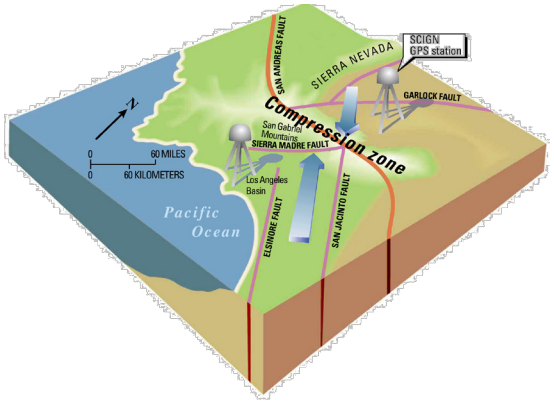

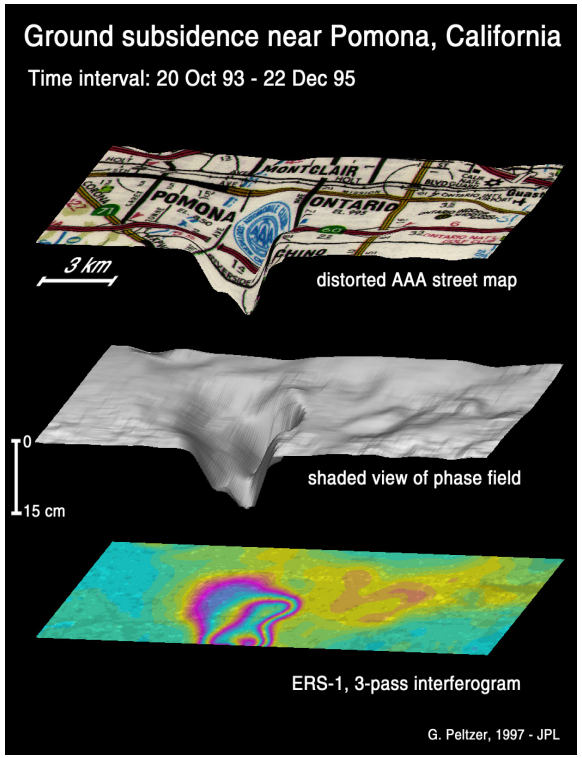

Example of SRTM DEM Improvement
Differential Interferometry

Using DTED+other DEM | **Using SRTM DEM**

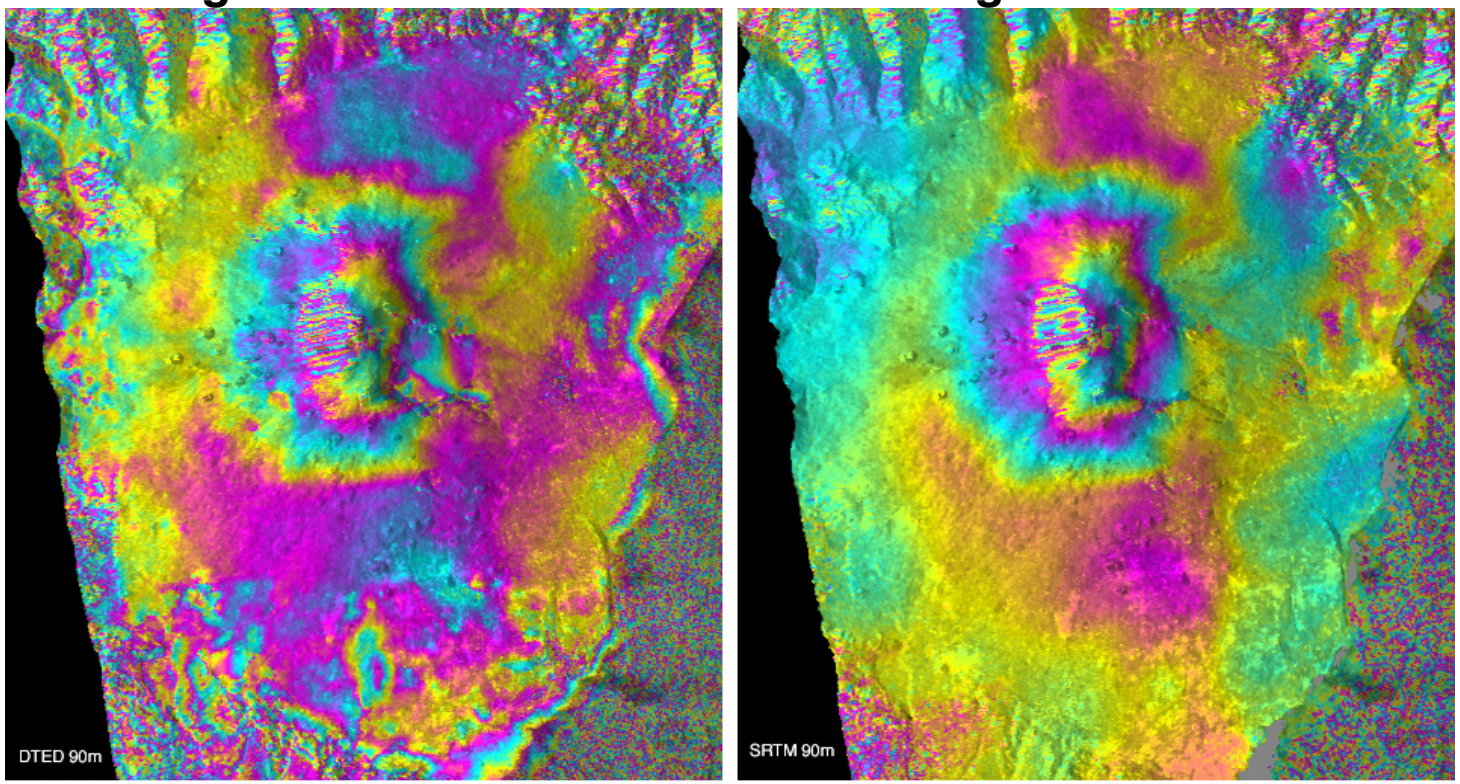

2000/10/04 - 2000/11/08 ERS Mt. Etna B_perp = 162m

ERS data courtesy ESA. P. Lundgren, JPL

Mount Etna inflation signature cleaned up considerably by using SRTM data to remove topographic signature.

The time evolution of ice stream flow variability is uniquely imaged by InSAR. Complete coverage by InSAR is needed to understand flow dynamics of the potentially unstable marine ice sheet.

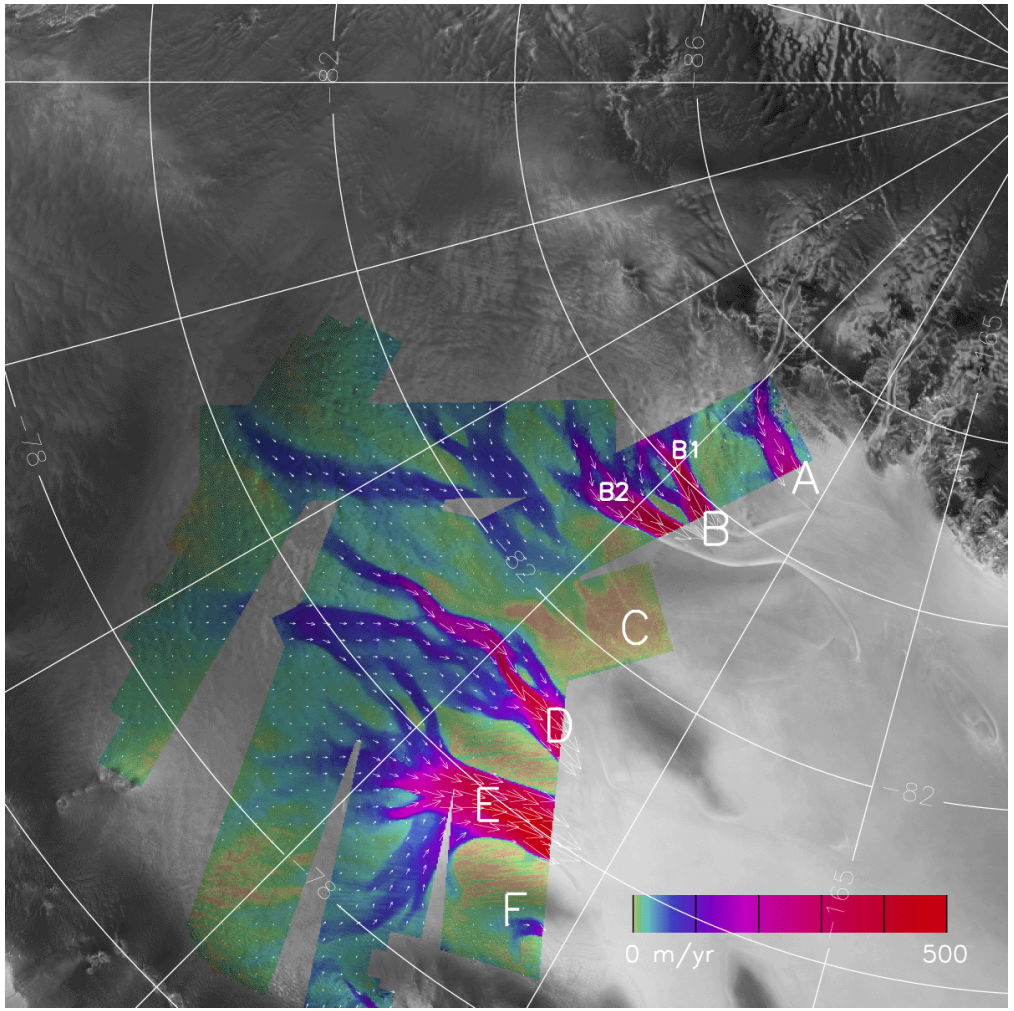

Joughin et al , 1999

Along Track Interferometry (ATI)

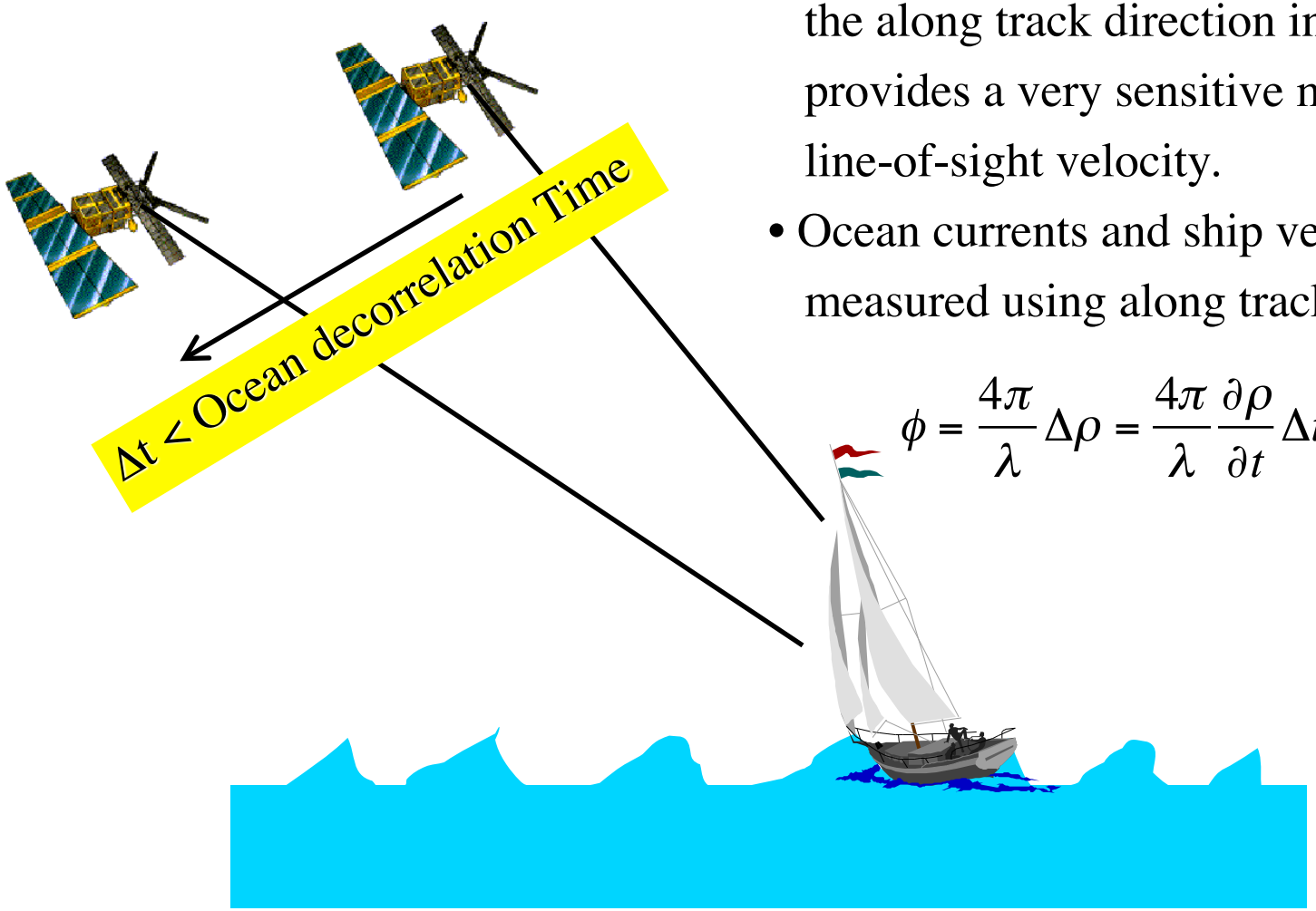

- By having antennas separated in the along track direction interferometry provides a very sensitive measure of the line-of-sight velocity.
- Ocean currents and ship velocities can be measured using along track interferometry.

$$\phi = \frac{4\pi}{\lambda}\Delta\rho = \frac{4\pi}{\lambda}\frac{\partial\rho}{\partial t}\Delta t = \frac{4\pi}{\lambda}V_{los}\frac{D}{V_{spc}}$$

ATI Experiment: Straits of Juan de Fuca

C-Band (AF/AA)

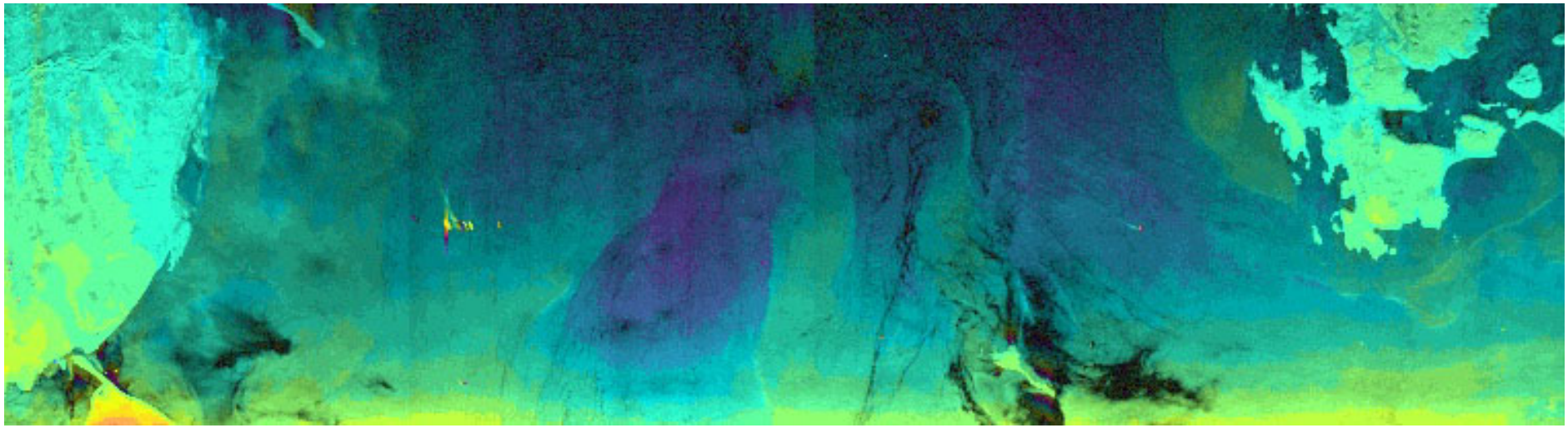

L-Band (AF/AA)

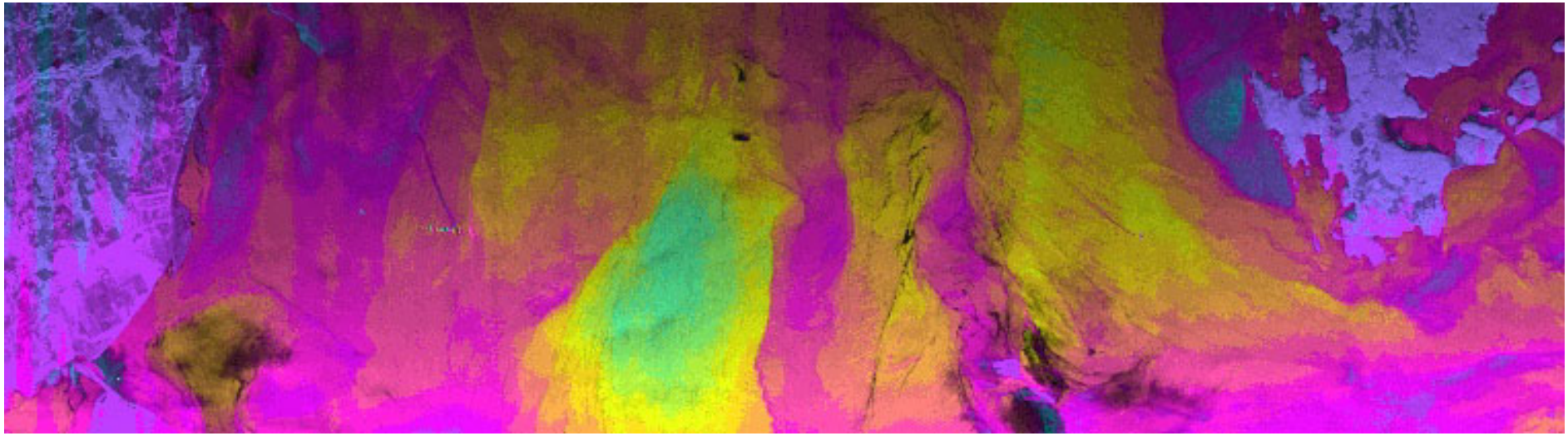

Phase Measurements in Interferometry

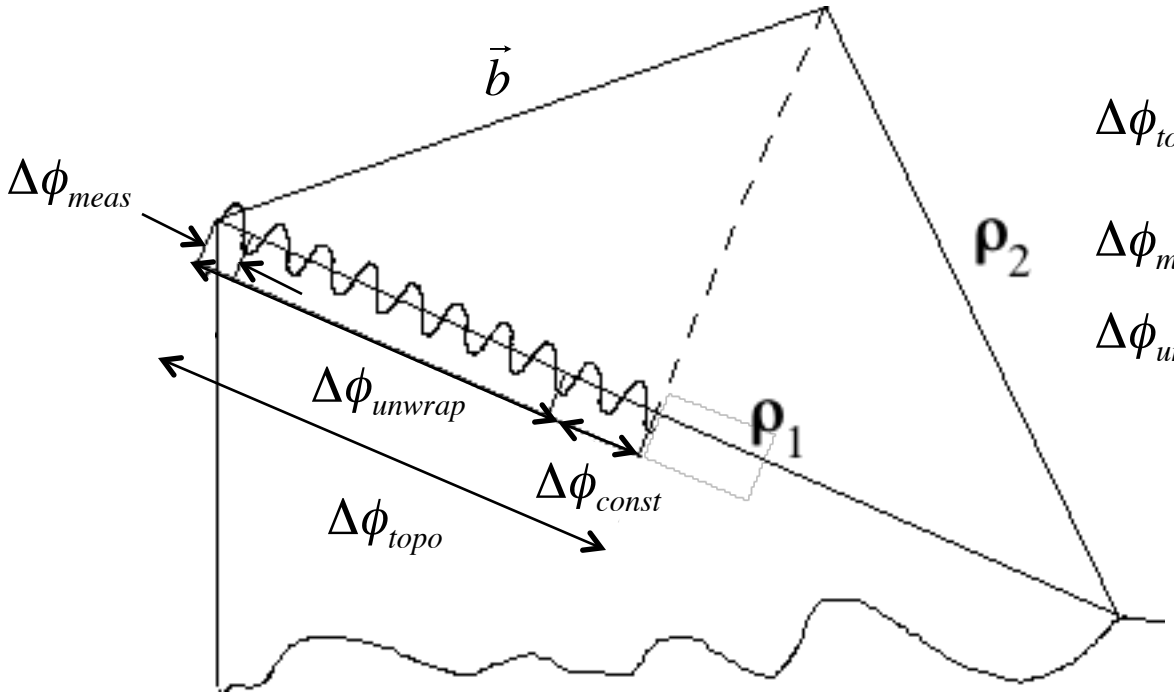

$$\Delta\phi_{topo} = \frac{2\pi p}{\lambda}\left(\rho_1 - \rho_2\right) = \frac{2\pi p}{\lambda}\vec{b} \bullet \vec{l}$$

$$\Delta\phi_{meas} = \mathrm{mod}\left(\Delta\phi_{topo}, 2\pi\right)$$

$$\Delta\phi_{unwrap}(s,\rho) = \Delta\phi_{topo}(s,\rho) + \Delta\phi_{const}$$

Unwrapping is conducted such that the unwrapped phase tracks the topographic phase except the entire image may be off by a constant $\Delta\phi_{const}$

The ROI_PAC Algorithmic Flow

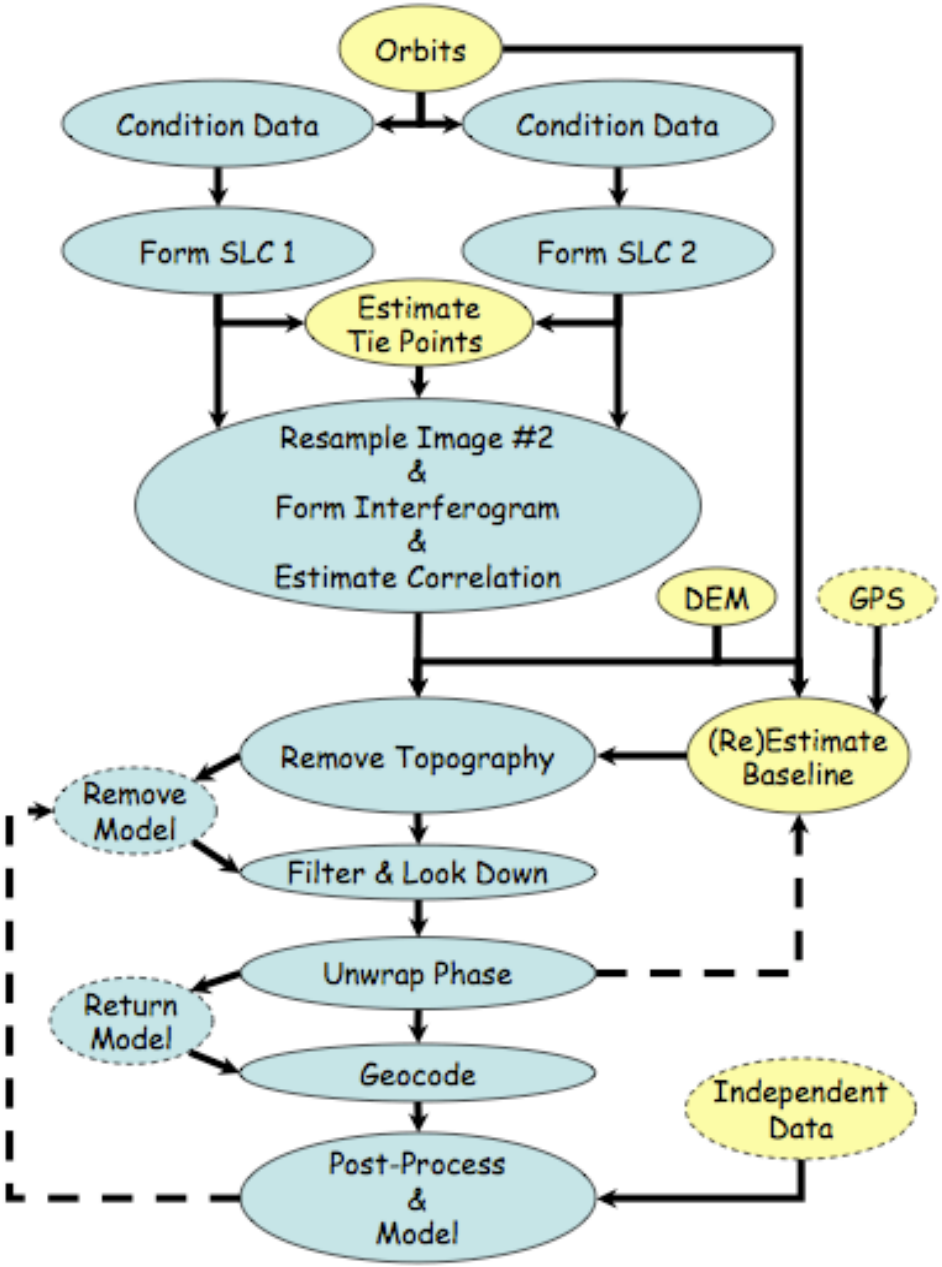

Radar Coherent Backscatter

Pixels in a radar image are a complex phasor representation of the coherent backscatter from the resolution element on the ground and the propagation phase delay

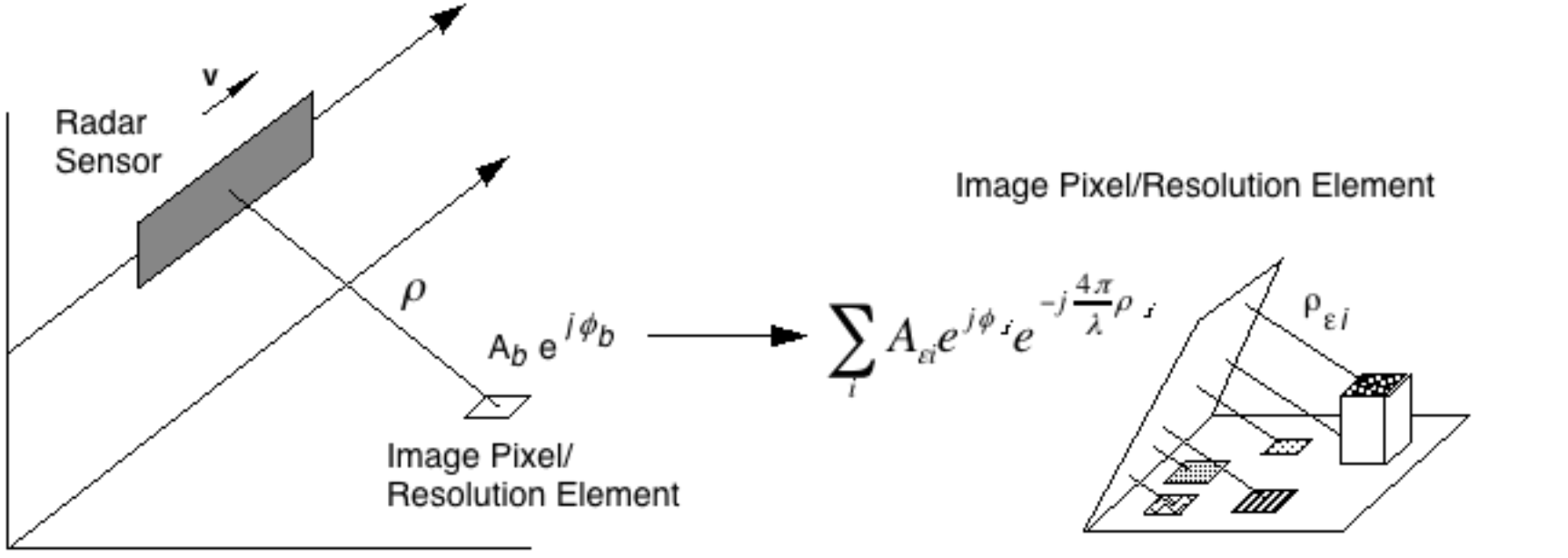

Propagation Phase Delay $\phi = -j\frac{4\pi}{\lambda}\rho$

Backscatter phase delay is coherent sum of contributions from all elemental scatterers in the resolution element with backscatter $A_{\varepsilon i} e^{j\phi_i}$ and their differential path delays $\rho_{\varepsilon i}$

Interferometric Phase Characteristics

Pixels in two radar images observed from nearby vantage points have nearly the same complex phasor representation of the coherent backscatter from a resolution element on the ground but a different propagation phase delay

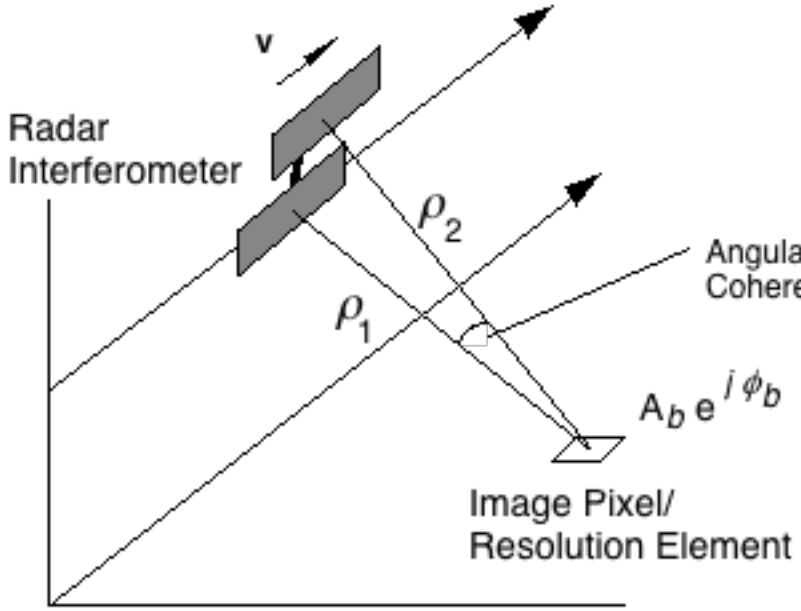

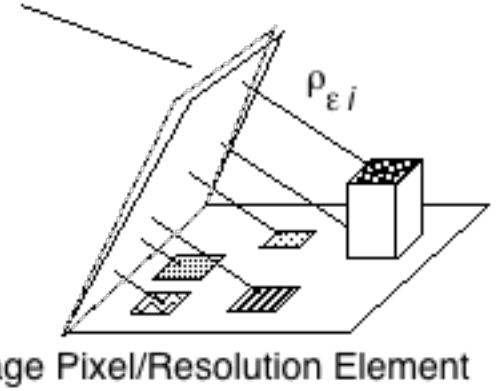

$$s_1 = A_b e^{j\phi_b} e^{-j\frac{4\pi}{\lambda}\rho_1} \qquad s_2 = A_b e^{j\phi_b} e^{-j\frac{4\pi}{\lambda}\rho_2}$$

Correlation Theory

SIGNALS DECORRELATE DUE TO

- **Thermal and Processor Noise**
- **Differential Geometric and Volumetric Scattering**
- **Rotation of Viewing Geometry**
- **Random Motions Over Time**

DECORRELATION OBSERVED AS PHASE STANDARD DEVIATION

- **Affects height and displacement accuracy and ability to unwrap phase**
- **Can define an effective SNR as thermal SNR degraded by other decorrelation effects**

Correlation Definition

For signals s_1 and s_2 observed at interferometer apertures 1 and 2, the correlation γ is given by

$$\gamma \equiv \frac{\left|\left\langle s_1 s_2^* \right\rangle\right|}{\sqrt{\left\langle s_1 s_1^* \right\rangle \left\langle s_2 s_2^* \right\rangle}}$$

Deterministic signals or combinations have perfect correlation

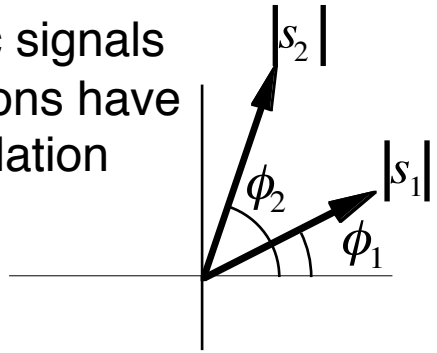

$$\gamma = \frac{\left|\left|s_1\right| e^{i\phi_1} \left|s_2\right| e^{-i\phi_2}\right|}{\sqrt{\left|s_1\right|^2 \left|s_2\right|^2}} = 1$$

Signals with random components have imperfect correlation

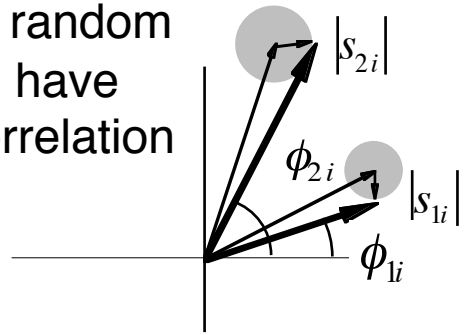

$$\gamma = \frac{\left|\left\langle \left|s_{1i}\right| e^{i\phi_{1i}} \left|s_{2i}\right| e^{-i\phi_{2i}} \right\rangle_i\right|}{\sqrt{\left\langle \left|s_{1i}\right|^2 \right\rangle_i \left\langle \left|s_{2i}\right|^2 \right\rangle_i}} \neq 1$$

Expectation Estimator

Expectation over the ensemble of realizations s_{1i} and s_{2i} cannot be calculated from a specific realization, that is, the observations s_1 and s_2. In general, an estimator derived from the image data must be devised.

The maximum likelihood estimator (MLE) of the interferometric *phase difference* between images forming an interferogram that have homogeneous backscatter and constant phase difference is

$$\hat{\phi} = \arg \sum_{l,m}^{N,M} s_{1l,m} s_{2l,m}^{*}$$

where *l* and *m* are image indices relative to some reference location and the sum is computed over a *N* x *M* box. *N* and *M* are known as the number of looks in their respective image dimensions.

Correlation Estimator

The standard estimator of the interferometric correlation between images forming an interferogram that have homogeneous backscatter and constant phase difference is

$$\hat{\gamma} = \frac{\left| \sum_{l,m}^{N,M} s_{1l,m} s_{2l,m}^{*} \right|}{\sqrt{\left| \sum_{l,m}^{N,M} s_{1l,m} s_{1l,m}^{*} \right| \left| \sum_{l,m}^{N,M} s_{2l,m} s_{2l,m}^{*} \right|}}$$

This estimator is biased. As an example, consider $N = 1$, $M = 1$. Then

$$\hat{\gamma} = \frac{\left| s_{1x,y} s_{2x,y}^{*} \right|}{\sqrt{\left| s_{1x,y} s_{1x,y}^{*} \right| \left| s_{2x,y} s_{2x,y}^{*} \right|}} = 1$$

where *x* and *y* are the coordinates of a particular image pixel. Other biases arise when backscatter homogeneity and phase constancy are violated.

Correlation Estimator Characteristics

A general set of curves of reveals the nature of the estimator bias when backscatter is homogeneous and phase is constant.

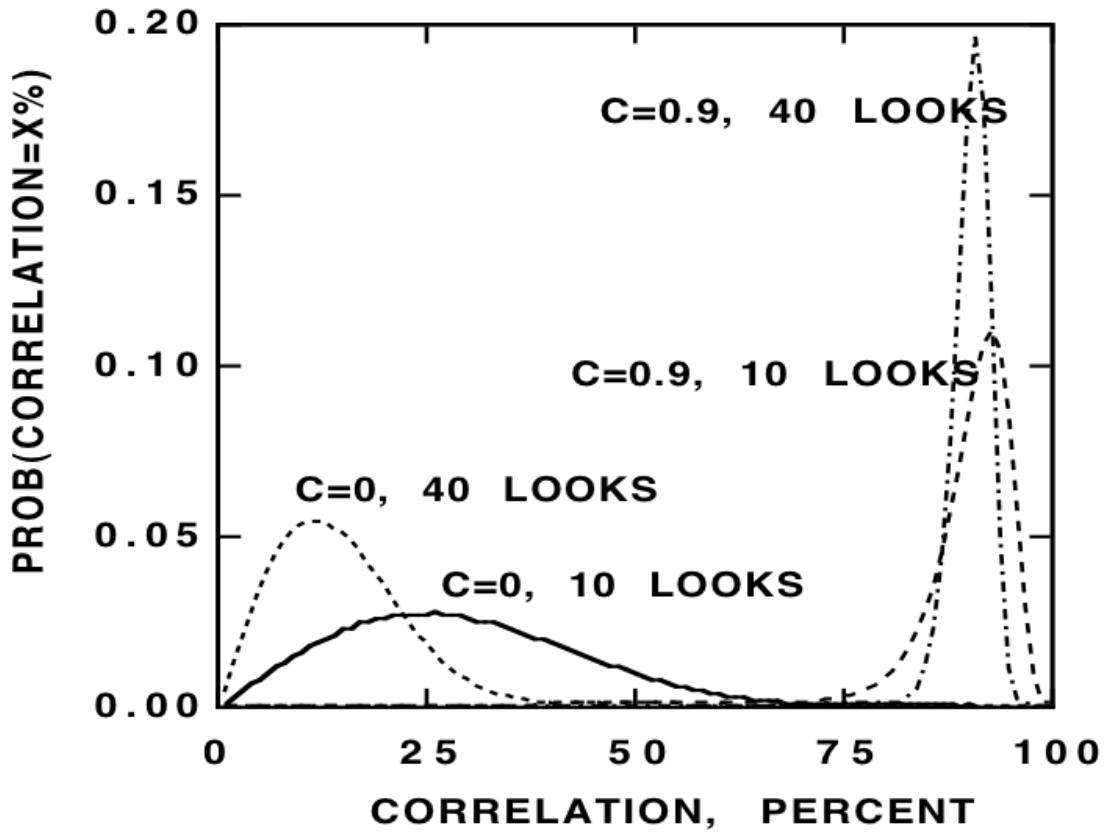

Relationship of Phase Noise and Decorrelation

- Increased decorrelation is associated with an increase in the interferometric phase noise variance
- If averaging $N > 4$ samples, the phase standard deviation approaches the Cramer-Rao bound on the phase estimator:

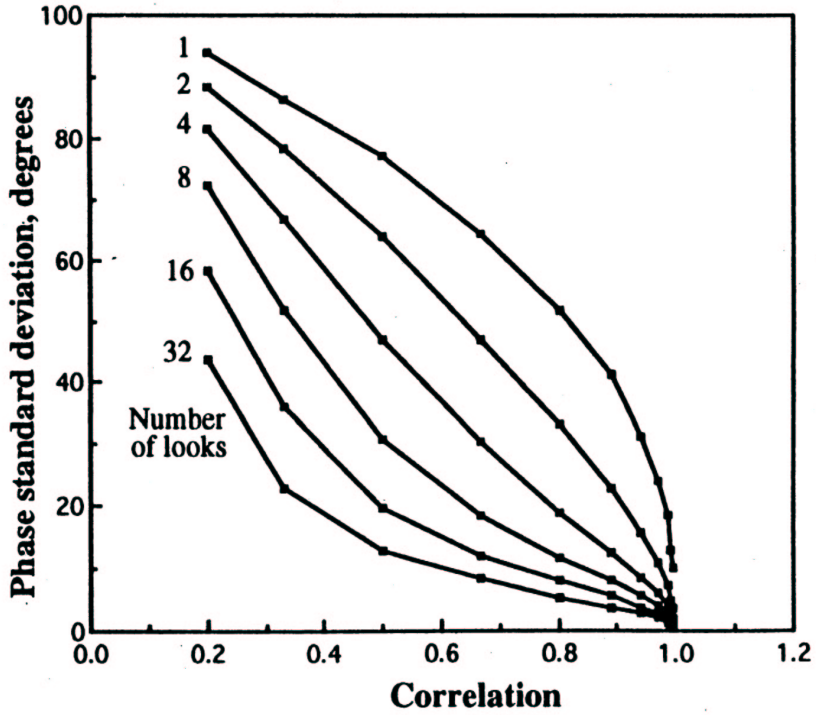

$$\sigma_\phi = \frac{1}{\sqrt{2N}} \frac{\sqrt{1-\gamma^2}}{\gamma}$$

Phase noise contributes to height errors in inter-ferometry as demonstrated in the sensitivity equations

Thermal Noise Decorrelation

Radar receiver electronics will add thermally generated noise to the image observations.

$$s_1' = A_b e^{j\phi_b} e^{-j\frac{4\pi}{\lambda}\rho_1} + n_1 \; ; \; s_2' = A_b e^{j\phi_b} e^{-j\frac{4\pi}{\lambda}\rho_2} + n_2$$

The added noise contributes randomly to the interferometric phase from pixel to pixel, causing thermal noise decorrelation. Assuming uncorrelated noise, the correlation between s_1' and s_2' is

$$\gamma = \frac{\left|\left\langle (s_1 + n_1)(s_2 + n_2)^* \right\rangle\right|}{\sqrt{\left\langle (s_1 + n_1)(s_1 + n_1)^* \right\rangle \left\langle (s_2 + n_2)(s_2 + n_2)^* \right\rangle}}$$

$$= \frac{|s_1 s_2|}{\sqrt{\left\langle (s_1^2 + n_1^2) \right\rangle \left\langle (s_2^2 + n_2^2) \right\rangle}}$$

$$= \frac{\sqrt{P_1}\sqrt{P_2}}{\sqrt{P_1 + N_1}\sqrt{P_{21} + N_2}} = \frac{1}{\sqrt{1 + N_1/P_1}} \frac{1}{\sqrt{1 + N_2/P_2}}$$

Thermal Noise Decorrelation

The correlation is related in a simple way to the reciprocal of the Signal-to-Noise Ratio (SNR). For observations with identical backscatter and equal noise power,

$$\gamma = \frac{1}{1 + N/P} = \frac{1}{1 + \mathrm{SNR}^{-1}}$$

Decorrelation is defined as

$$\delta = 1 - \gamma$$

The decorrelation due to thermal noise can vary greatly in a scene, not from thermal noise variations, but from variations in backscatter brightness. Extreme cases are:

- **Radar shadow, where no signal is returns; correlation is zero.**
- **Bright specular target, where signal dominates return; correlation is 1**

SNR from the Radar Equation

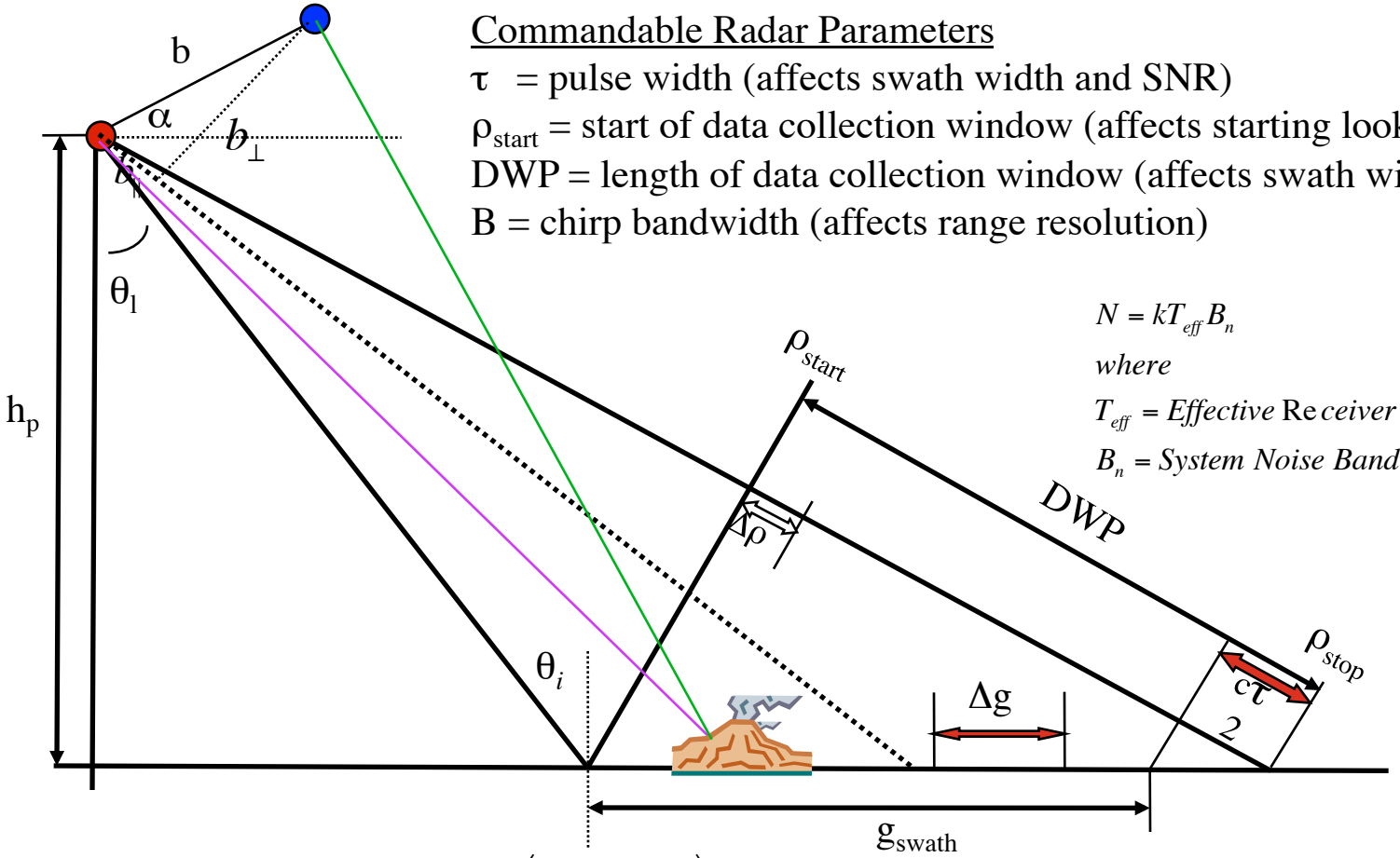

Commandable Radar Parameters

τ = pulse width (affects swath width and SNR)

ρ_{start} = start of data collection window (affects starting look angle)

DWP = length of data collection window (affects swath width)

B = chirp bandwidth (affects range resolution)

$N = kT_{eff}B_n$

where

T_{eff} = *Effective Receiver Temperature*

B_n = *System Noise Bandwidth*

$$SNR = \underbrace{\frac{P_t G_t G_r}{L_t L_r k T_{eff} B_n}} \frac{\lambda^2}{(4\pi)^3 \rho^4} \left(\frac{c\tau}{2\sin(\theta_i)} \right) \left(\rho \theta_{az}^{eff} \right) \sigma_o$$

P_{sys} - lumped effect of transmit gain and various losses

Baseline Decorrelation

Pixels in two radar images observed from nearby vantage points have *nearly* the same complex phasor representation of the coherent backscatter from a resolution element on the ground

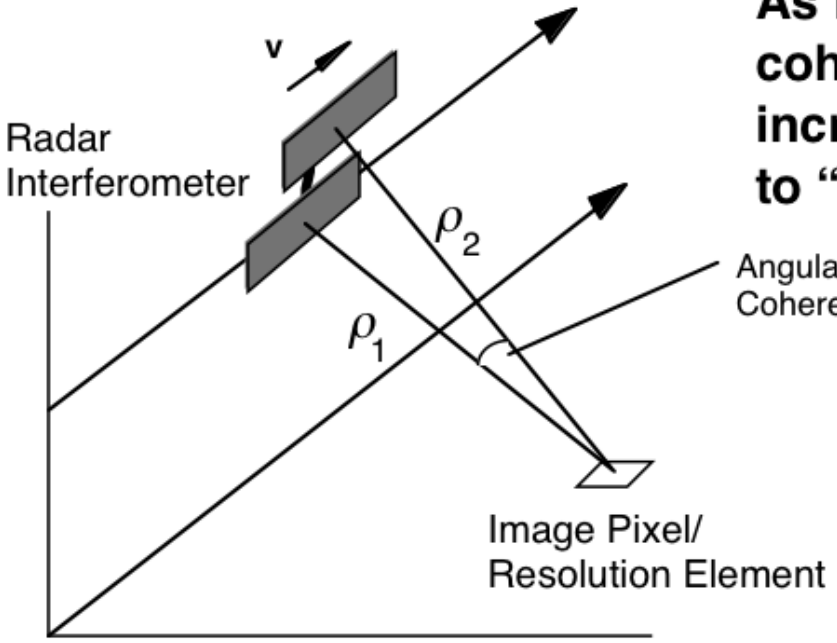

As interferometric baseline increases, the coherent backscatter phase becomes increasingly different randomly, leading to "baseline" or "speckle" decorrelation.

Angular separation << 1 degree
Coherent sum nearly unchanged

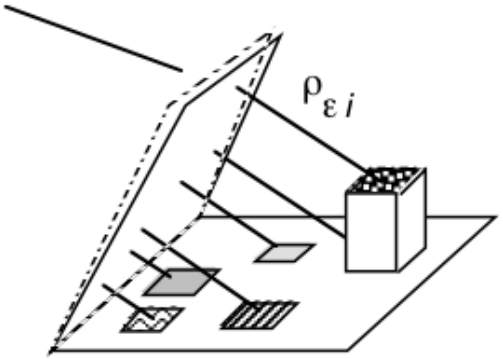

Image Pixel/Resolution Element

$$s_1 = A_{b1} e^{j\phi_{b1}} e^{-j\frac{4\pi}{\lambda}\rho_1} \qquad s_2 = A_{b2} e^{j\phi_{b2}} e^{-j\frac{4\pi}{\lambda}\rho_2}$$

Baseline Decorrelation: Resolution Cell

Interferometric geometry for a horizontal baseline in the cross-track plane

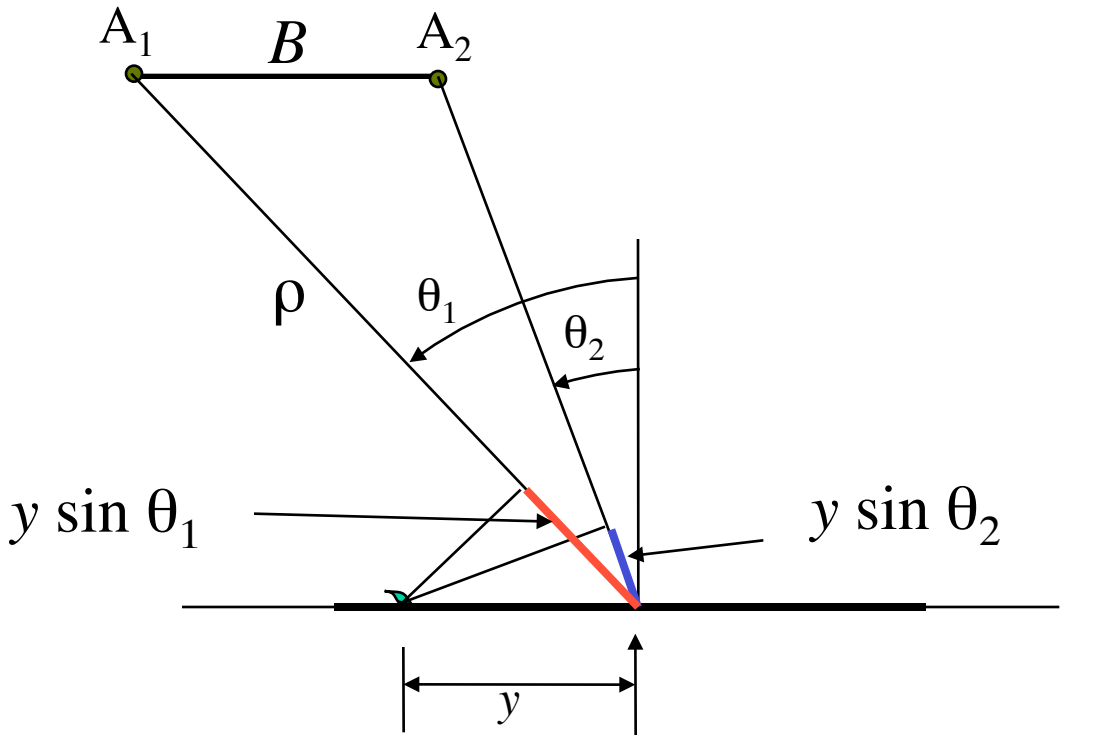

Baseline Correlation Formulation

Consider signals from the two antennas displaced in angle:

$$s_1(x_0, y_0) = \int dx \int dy f(x - x_0, y - y_0) e^{-j\frac{4\pi}{\lambda}(\rho + y \sin\theta_1)} W(x, y) + n_1(x_0, y_0)$$

$$s_2(x_0, y_0) = \int dx \int dy f(x - x_0, y - y_0) e^{-j\frac{4\pi}{\lambda}(\rho + y \sin\theta_2)} W(x, y) + n_2(x_0, y_0)$$

Cross-correlation yields:

$$s_1 s_2^\star = \int dx \int dy \int dx' \int dy' f(x - x_0, y - y_0) f^\star(x' - x_0, y' - y_0)$$

$$e^{-j\frac{4\pi}{\lambda}(y \sin\theta_1 - y' \sin\theta_2)} W(x, y) W^\star(x', y')$$

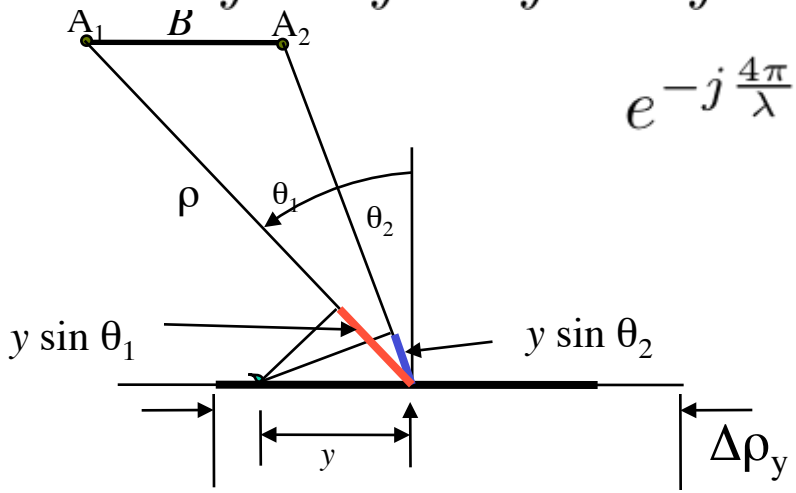

plus noise cross-products

$f(x,y)$ = the surface reflectivity function
$W(x,y)$ = the imaging point spread function

Surface Assumption for Correlation Formulation

If the surface is modeled as *uniformly distributed, uncorrelated* scattering centers, that is:

$$\langle f(x,y) f^{\star}(x',y') \rangle = \sigma_0 \delta(x-x', y-y')$$

where σ_0 is the mean backscatter cross section per unit area from the surface

Under this assumption, the correlation expression reduces to:

$$\langle s_1 s_2^{\star} \rangle = \sigma_0 \int dx \int dy \, |W(x,y)|^2 \, e^{-j \frac{4\pi}{\lambda} y \cos\theta \Delta\theta}$$

The shape of the correlation function as a function of angle is the Fourier Transform of the Image Point Spread Function

Form of Baseline Correlation Function

If $W(x,y)$ is assumed to be a sinc function, then the integral can be done in closed form (for ping-pong mode)

$$\gamma_B = 1 - \frac{2(B\cos\theta)(\Delta\rho_y \cos\theta)}{\lambda\rho}$$

$$= 1 - \frac{2B_\perp \Delta\rho_\perp}{\lambda\rho}$$

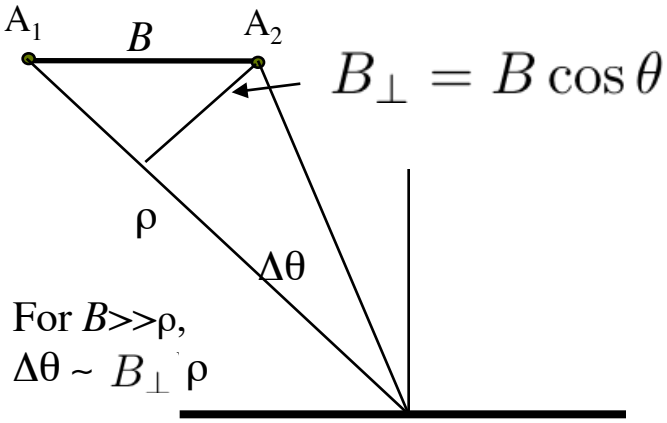

$$B_\perp = B\cos\theta$$

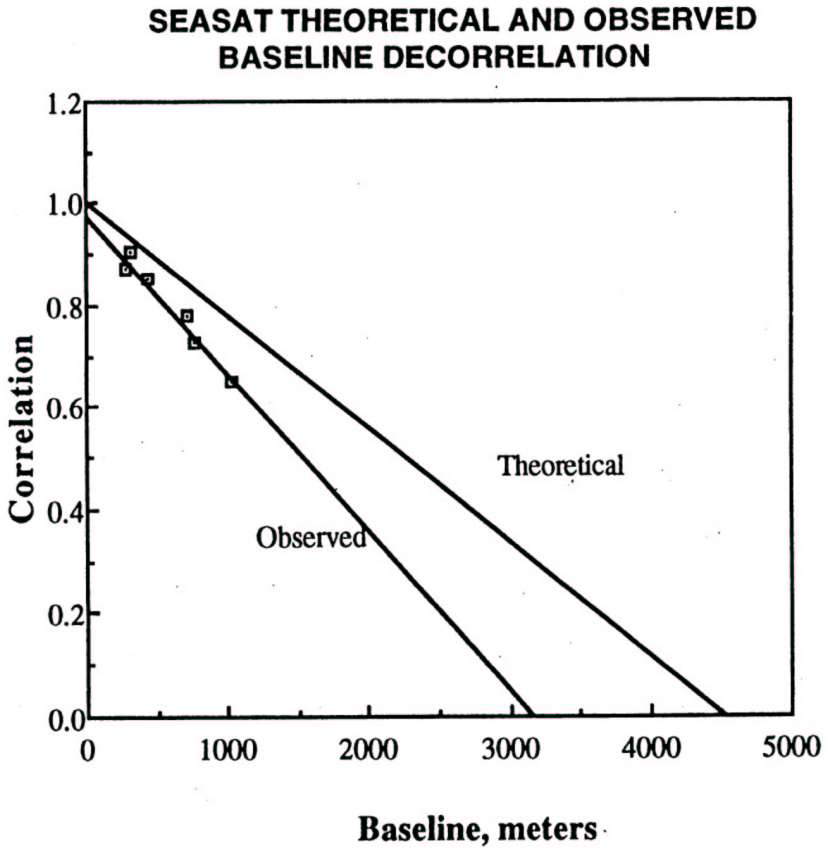

This function goes to zero at the *critical baseline*

$$B_{\perp,\mathrm{crit}} = \frac{\lambda\rho}{n\Delta\rho_\perp} \qquad n = 1, 2$$

The "Pixel Antenna" View of Baseline Decorrelation

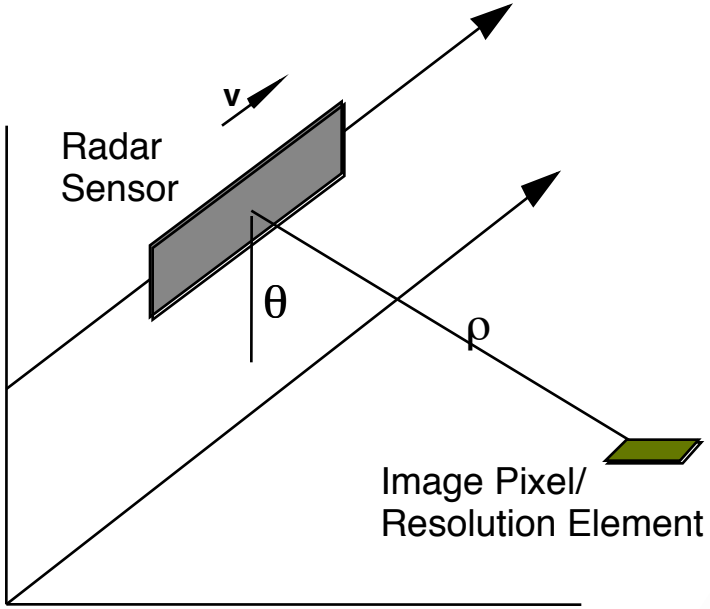

Each resolution element can be considered a radiating antenna with beamwidth of $\Delta\theta_{\Delta\rho_\perp}$, which depends on the range and local angle of incidence.

$$\Delta\theta = \frac{\lambda}{2\Delta\rho_\perp} \qquad n=1,2$$

$$\Delta\rho = \frac{c}{2\Delta f_{\mathrm{BW}}}$$

$$\Delta\rho_\perp = \Delta\rho / \tan\theta$$

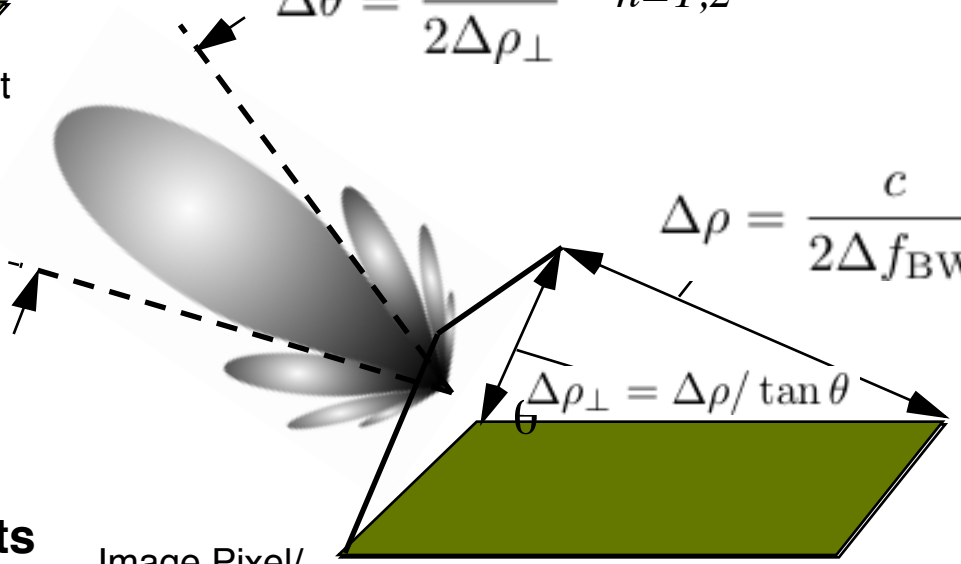

When the two apertures of the interferometer are within this beamwidth, coherence is maintained. Beyond this critical baseline separation, there is no coherence for distributed targets

Overcoming Baseline Decorrelation

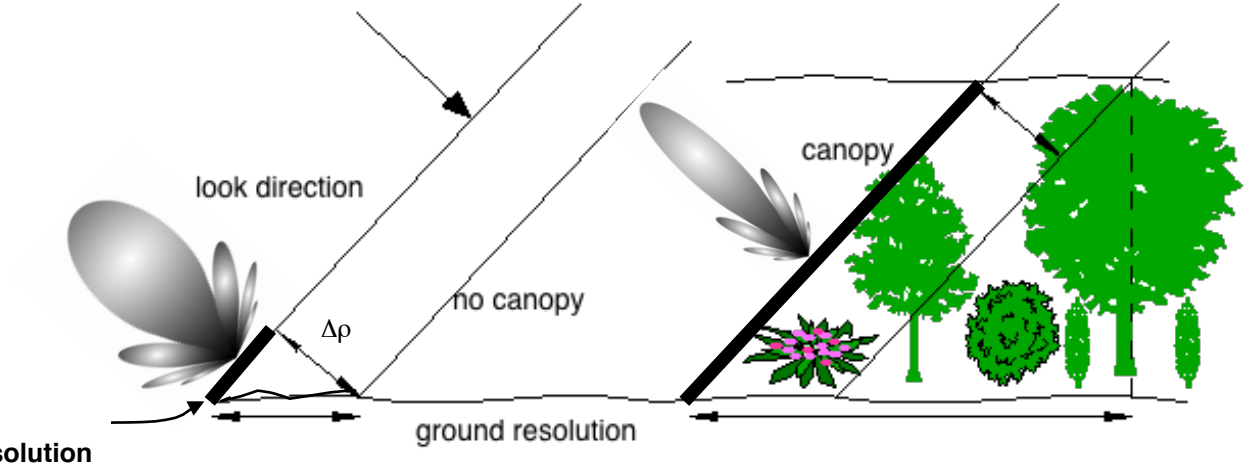

Distributed targets correlate over a narrow range of baselines

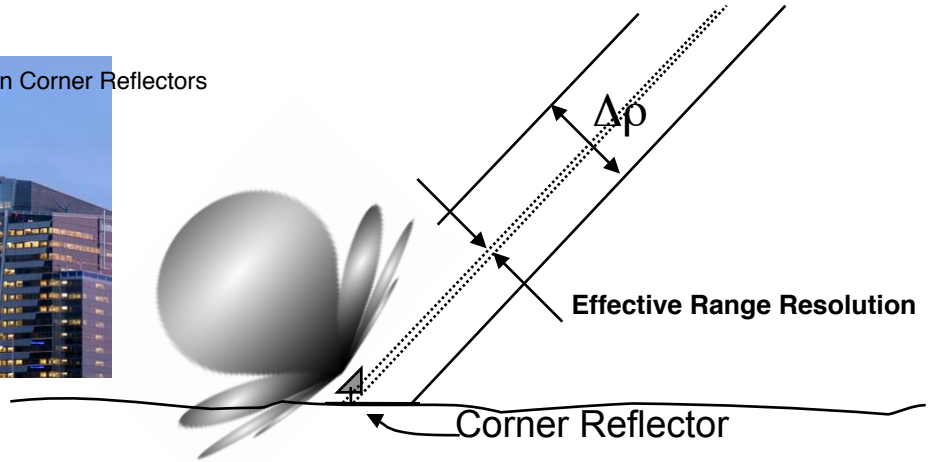

JPL Corner Reflector

Pixels dominated by single scatterers generally behave though imaged at much finer resolution

Critical Baseline

The critical baseline is the aperture separation perpendicular to the look direction at which the interferometric correlation becomes zero.

$$B_{\text{crit}} = \rho\Delta\theta_{\Delta\rho_\perp} = \frac{\lambda\rho\tan\theta}{n\Delta\rho} \qquad n=1,2$$

Interferometers with longer wavelengths and finer resolution are less sensitive to baseline decorrelation. When the critical baseline is reached, the interferometric phase varies as

$$\frac{\partial\phi_{\text{crit}}}{\partial\rho} = \frac{\partial\phi_{\text{crit}}}{\partial\theta}\frac{\partial\theta}{\partial\rho}$$

$$= \frac{2n\pi}{\lambda} B_{\text{crit}} \frac{1}{\rho\tan\theta} = \frac{2\pi}{\Delta\rho}$$

The relative phase of scatterers across a resolution element changes by a full cycle, leading to destructive coherent summation

Rotational Decorrelation

Rotation of scatterers in a resolution element can be thought of as observing from a slightly different azimuthal vantage point. As with baseline decorrelation, the change in differential path delay from individual scatterers to the reference plane produces rotational decorrelation.

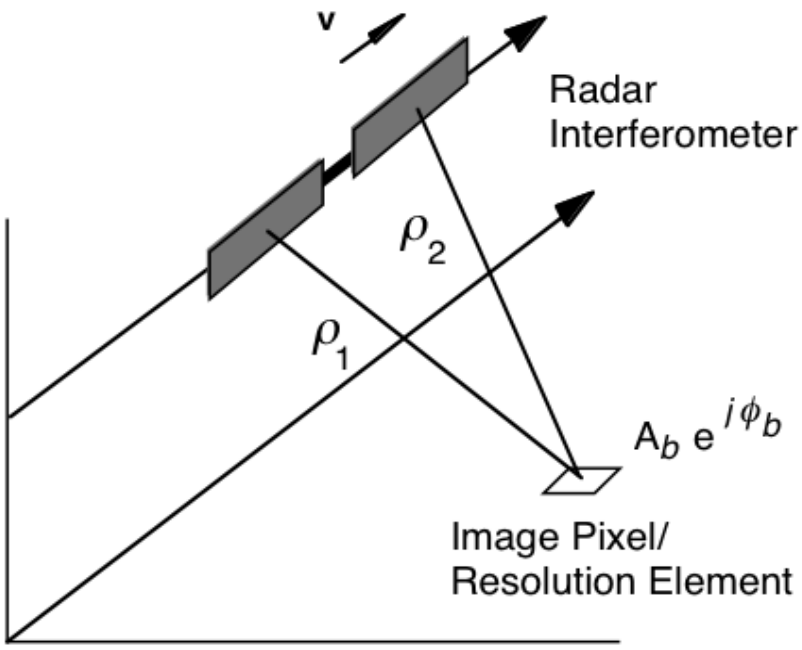

The critical rotational baseline is the extent of the synthetic aperture used to achieve the along track resolution.

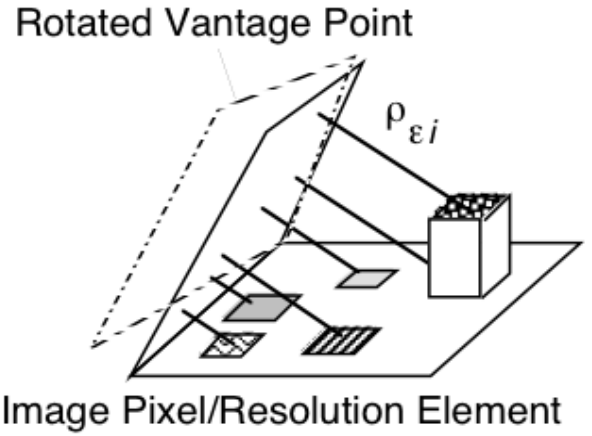

$$s_1 = A_{b1} e^{j\phi_{b1}} e^{-j\frac{4\pi}{\lambda}\rho_1} \qquad s_2 = A_{b2} e^{j\phi_{b2}} e^{-j\frac{4\pi}{\lambda}\rho_2}$$

Rotational Correlation Formulation

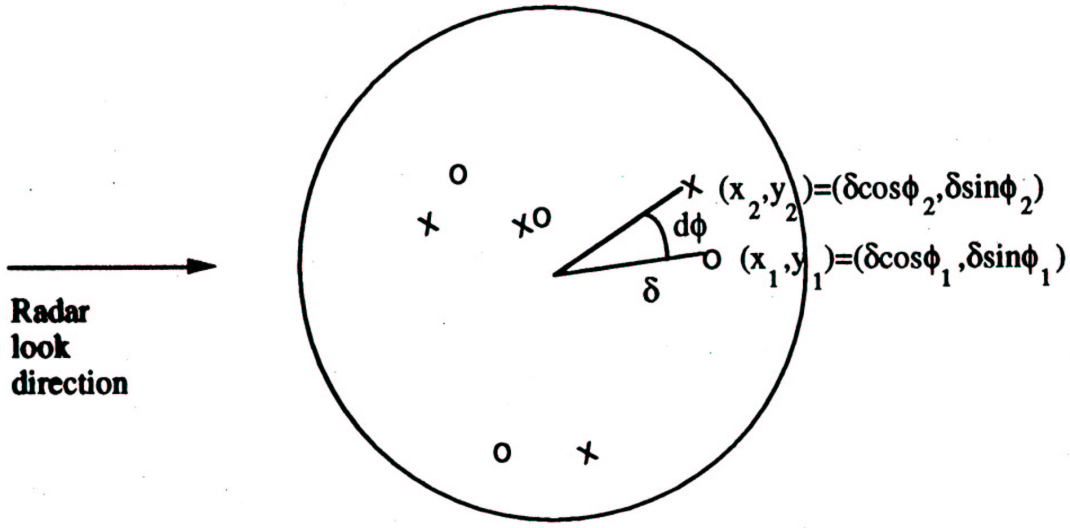

Cross-correlation for this case is:

$$s_1 s_2^\star = \int dx \int dy \int dx' \int dy' f(x - x_0, y - y_0) f^\star(x' - x_0, y' - y_0)$$
$$e^{-j\frac{4\pi}{\lambda}\delta \sin\theta(\sin\theta_1 - \sin\theta_2)} W(x,y) W^\star(x',y')$$

plus noise cross-products

Form of Rotational Correlation Function

A similar Fourier Transform relation as found in the baseline decorrelation formulation exists

$$\gamma_\phi = 1 - \frac{n \sin\theta B_\phi R_x}{\lambda\rho} \quad n = 1, 2$$

where R_x is the azimuth resolution and B_ϕ is the distance along track corresponding to the rotation angle of the look vector

This function goes to zero at the *critical rotational baseline*

$$B_{\phi,\mathrm{crit}} = \frac{\lambda\rho}{n\Delta\rho_\phi}, \Delta\rho_\phi \equiv R_x \sin\theta$$

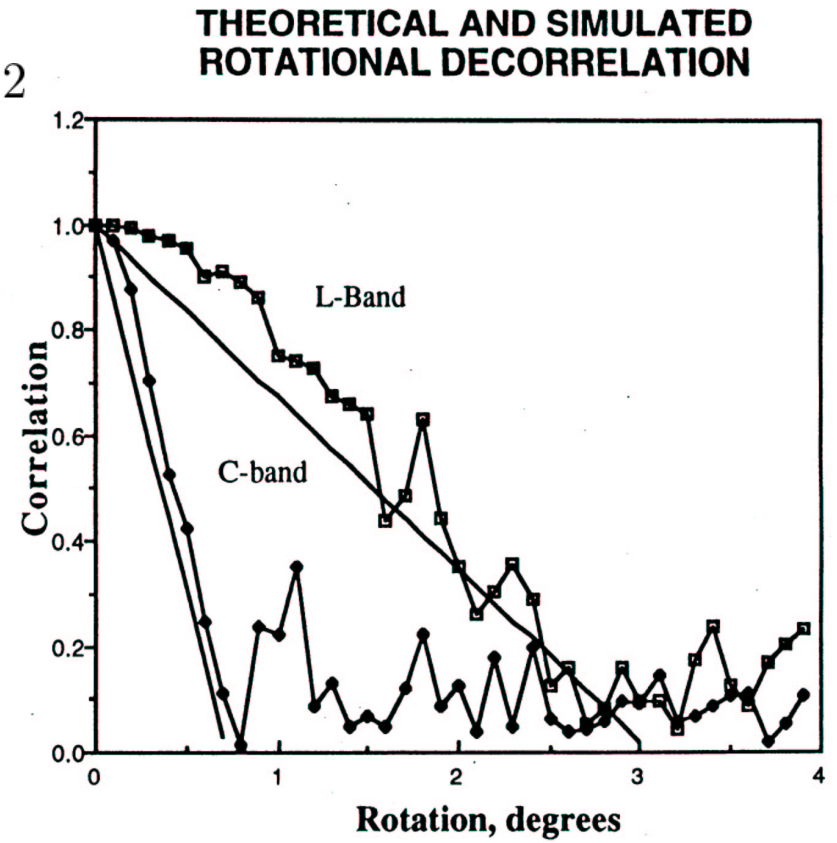

Scatterer Motion

Motion of scatterers within the resolution cell from one observation to the next will lead to randomly different coherent backscatter phase from one image to another, i.e. "temporal" decorrelation.

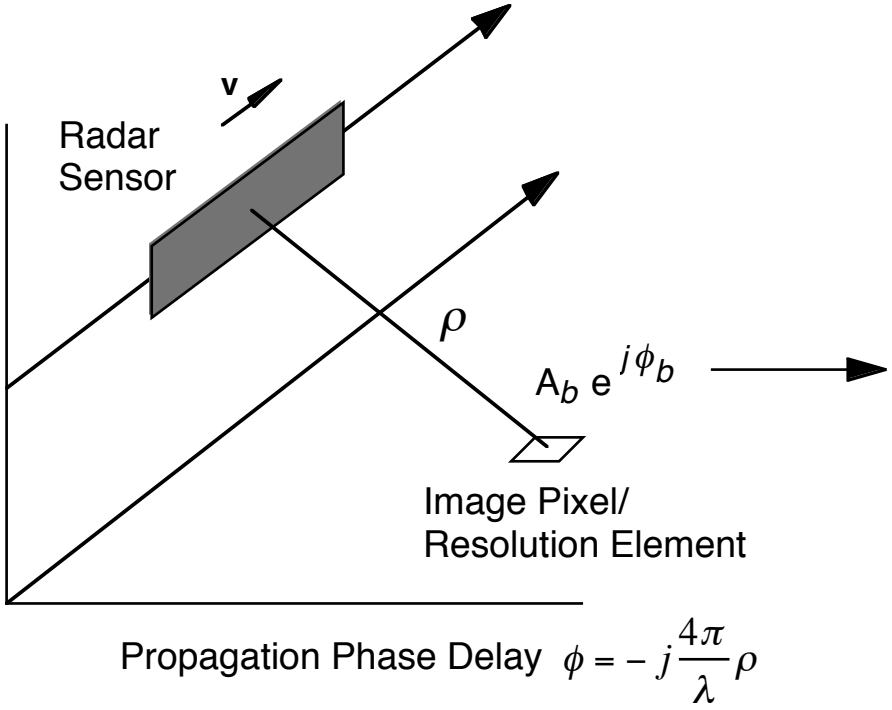

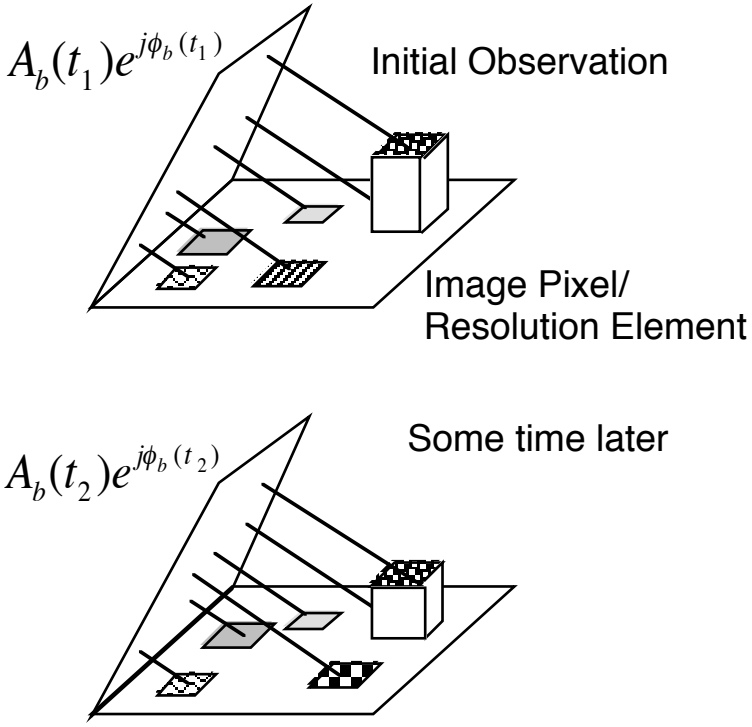

Motion Correlation Formulation

Assume the scatterers move in the cross-track and vertical directions by random displacements from one observation to the next by δy and δz. The cross-correlation for this case is:

$$s_1 s_2^\star = \int dx \int dy \int dz \int dx' \int dy' \int dz' f(x-x_0, y-y_0, z-z_0) f^\star(x'-x_0, y'-y_0, z-z_0)$$

$$e^{-j\frac{4\pi}{\lambda}(\delta y \sin\theta + \delta z \cos\theta)} W(x,y,z) W^\star(x',y',z')$$

plus noise cross-products

If the motions are independent and unrelated to position

$$\langle s_1 s_2^\star \rangle = \sigma_0 \int d\delta x \int d\delta y \quad e^{-j\frac{4\pi}{\lambda}(\delta y \sin\theta + \delta z \cos\theta)} p_y(\delta y) p_z(\delta z)$$

where p_y and p_z are the probability distributions of the scatterer locations

Form of Motion Correlation Function

The Fourier Transform relation can be evaluated if Gaussian probability distributions for the motions are assumed

$$\gamma_t = e^{-\frac{1}{2}\left(\frac{4\pi}{\lambda}\right)^2(\sigma_y^2 \sin^2\theta + \sigma_z^2 \cos^2\theta)}$$

where $\sigma_{y,z}$ is the standard deviation of the scatterer displacements cross-track and vertically

Note correlation goes to 50% at about 1/4 wavelength displacements

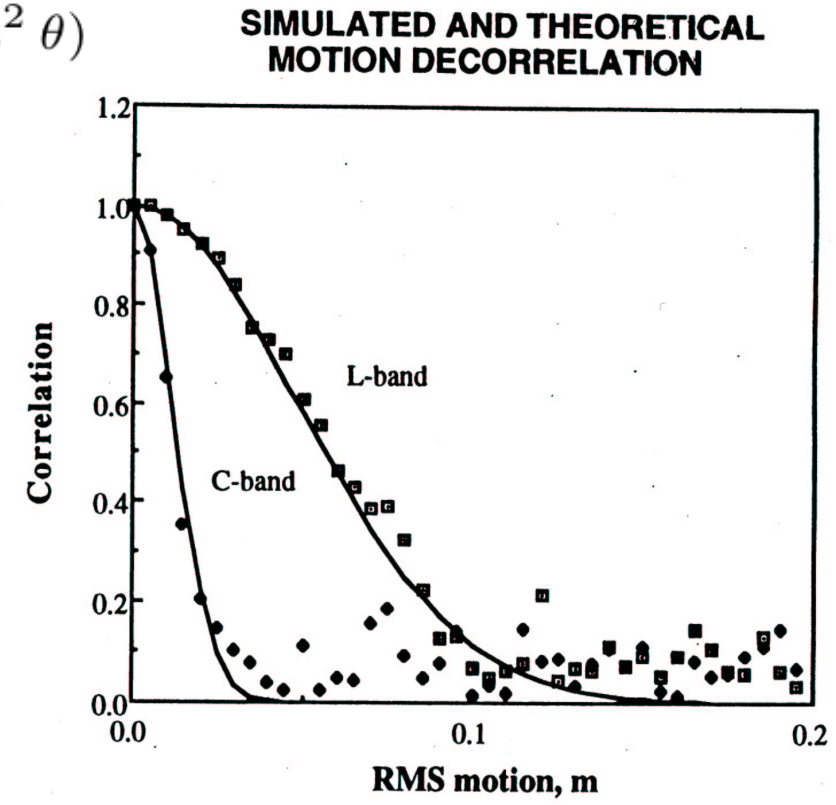

Repeat-pass Interferometry and Coherent Change Detection

L-Band low frequency improves correlation in vegetated areas

Most radars do well in areas of sparse vegetation

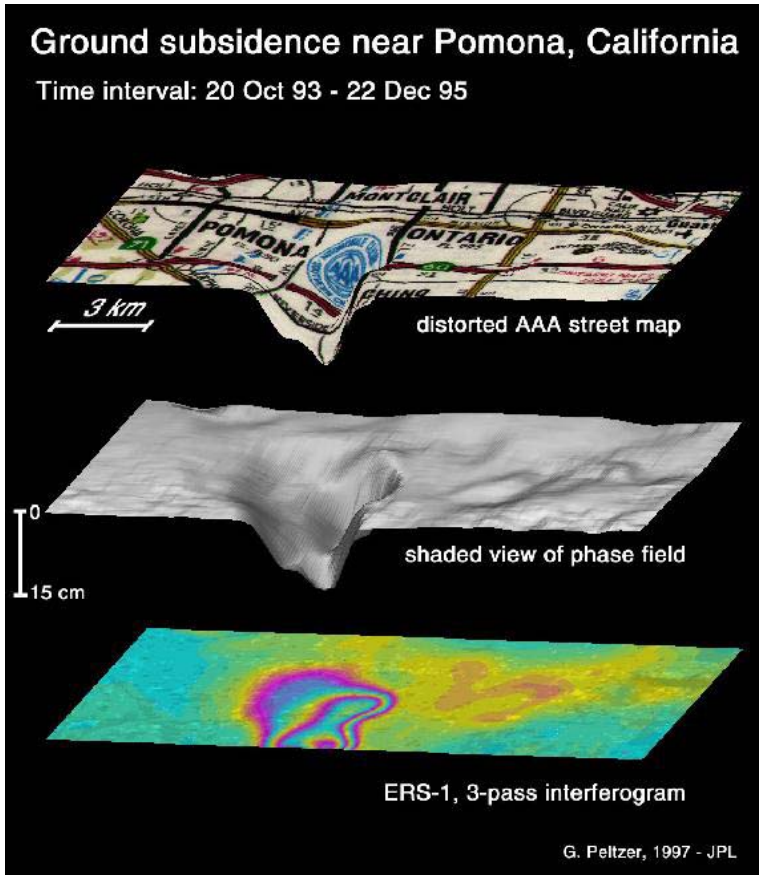

But maintaining correlation in dense vegetation requires longer wavelengths

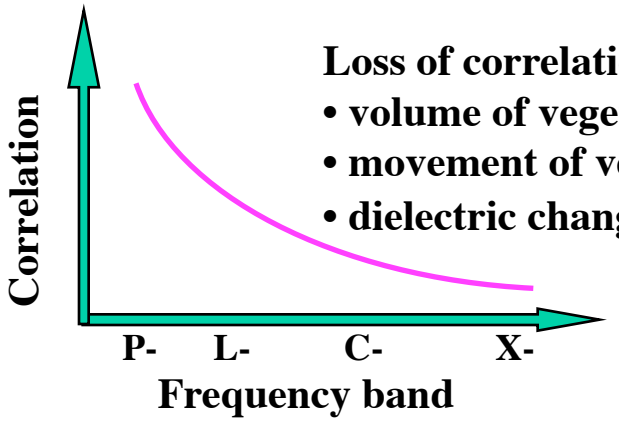

Loss of correlation is due to:

- volume of vegetation
- movement of vegetation
- dielectric change (moisture)

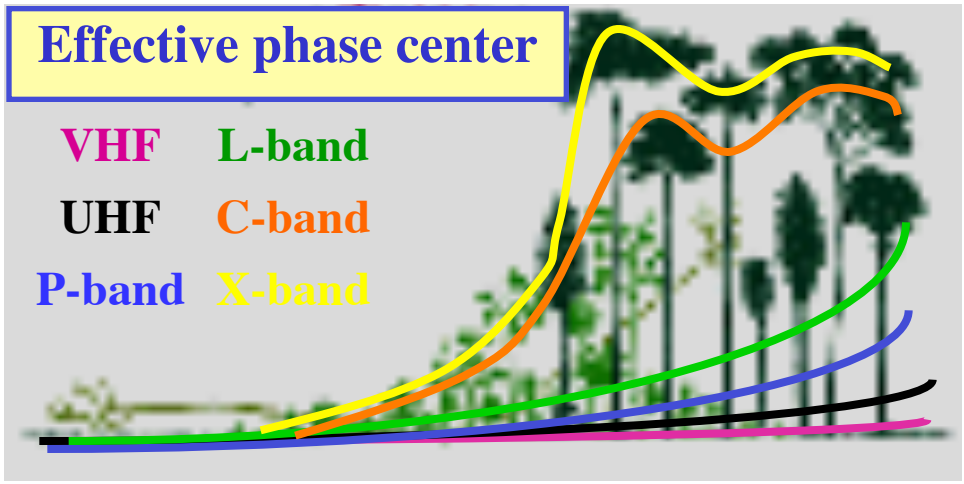

Coherent Change Detection
SIR-C L and C-band Interferometry

6 month time separated observations to form interferograms
Simultaneous C and L band

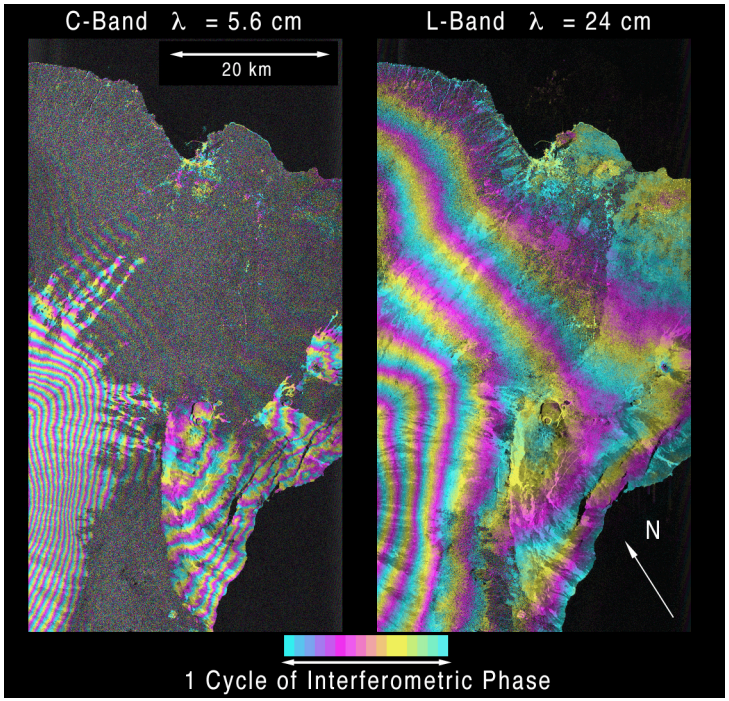

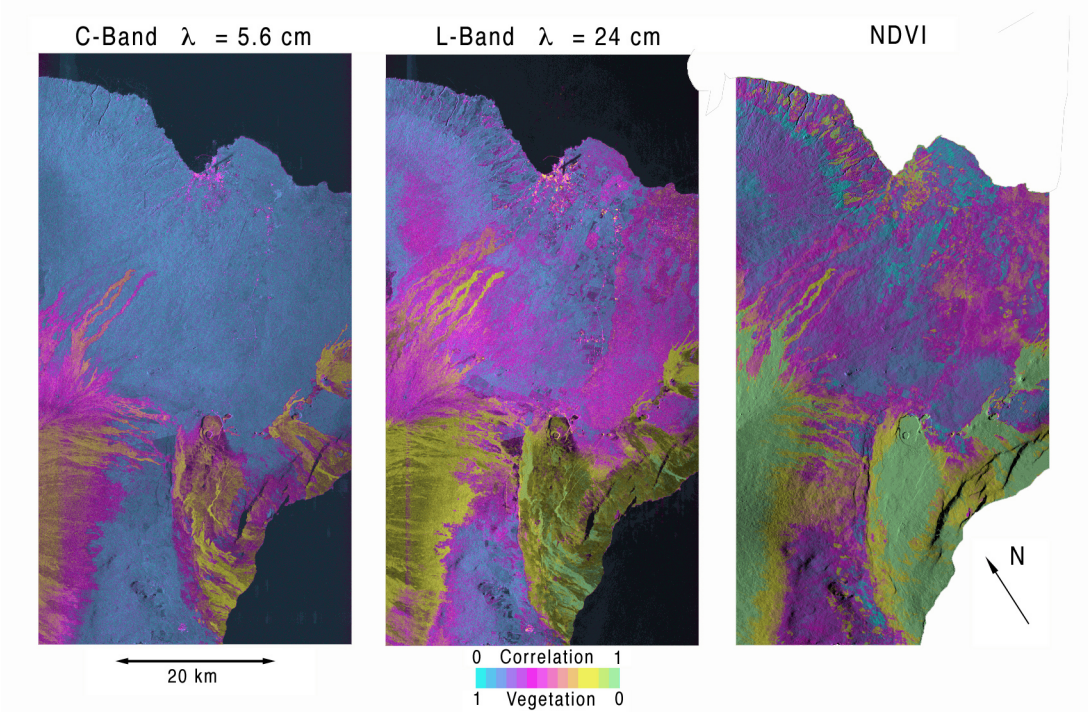

InSAR experiments have shown good correlation at L-band

AIRSAR Coherent Change Detection

Interferograms

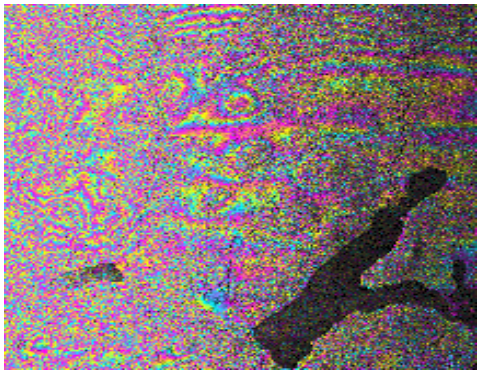

C-band

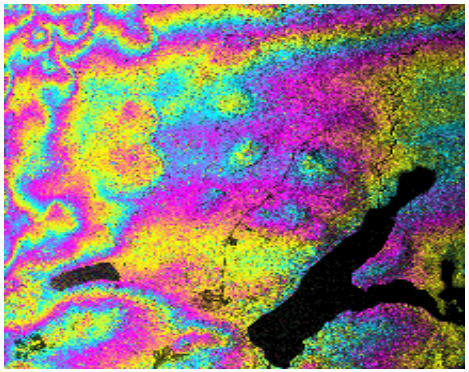

L-band

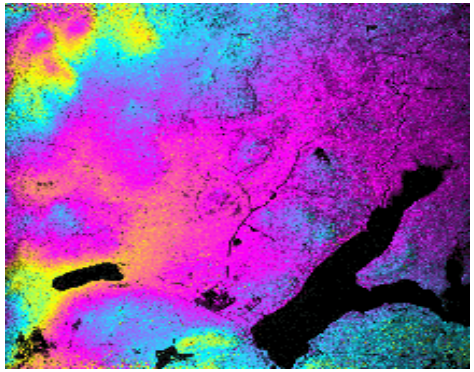

P-band

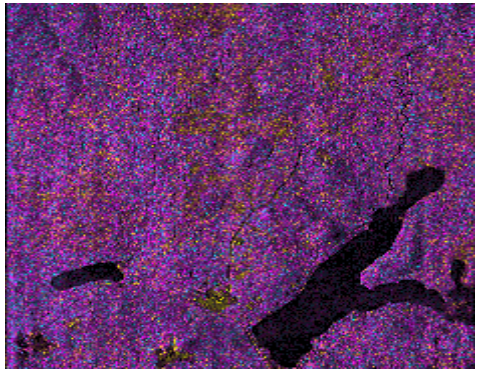

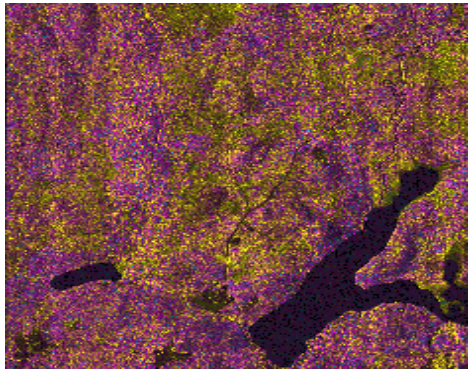

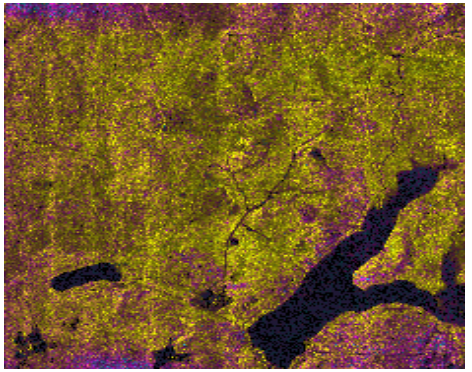

Correlation

Airborne InSAR experiments have shown good correlation at L-band

A Correlation Test:
What were the interferometric observation conditions?

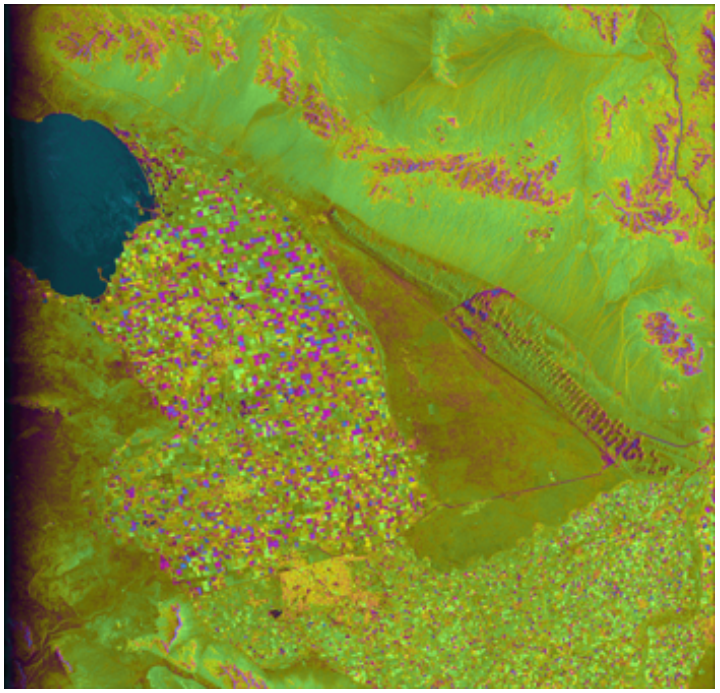

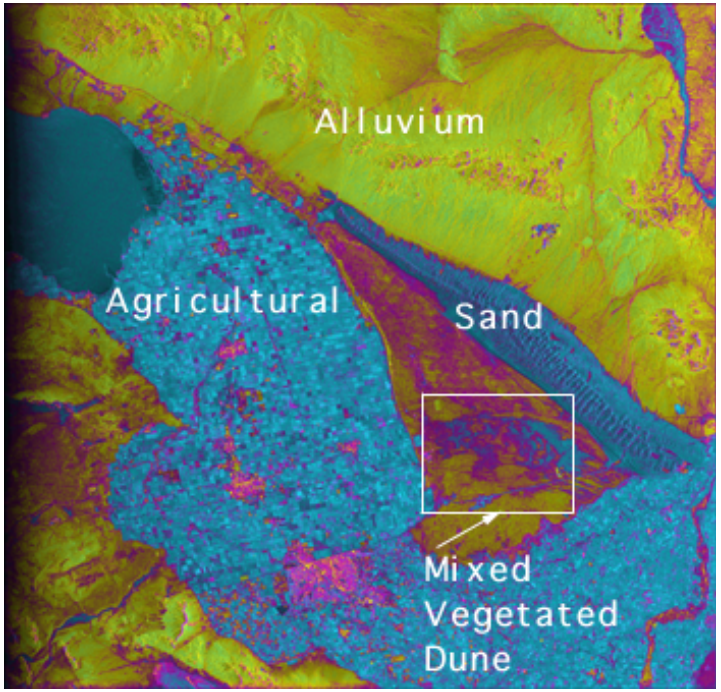

Correlation in Practical Systems

- For Single-Pass Two-Aperture Interferometer Systems
  - System noise and baseline/volumetric decorrelation are particularly relevant
  - Proper design of system can control
    - noise, by increasing SNR and minimizing shadow
    - baseline decorrelation, by choosing proper wavelength and geometry
  - Volumetric decorrelation can be inferred and used as a diagnostic of the vertical distribution of scatterers
- For Multi-Pass Single-Aperture Interferometer Systems
  - All decorrelation effects may occur
  - Time series analysis and some assumptions may be useful in distinguishing decorrelation contributors

Correlation Discrimination

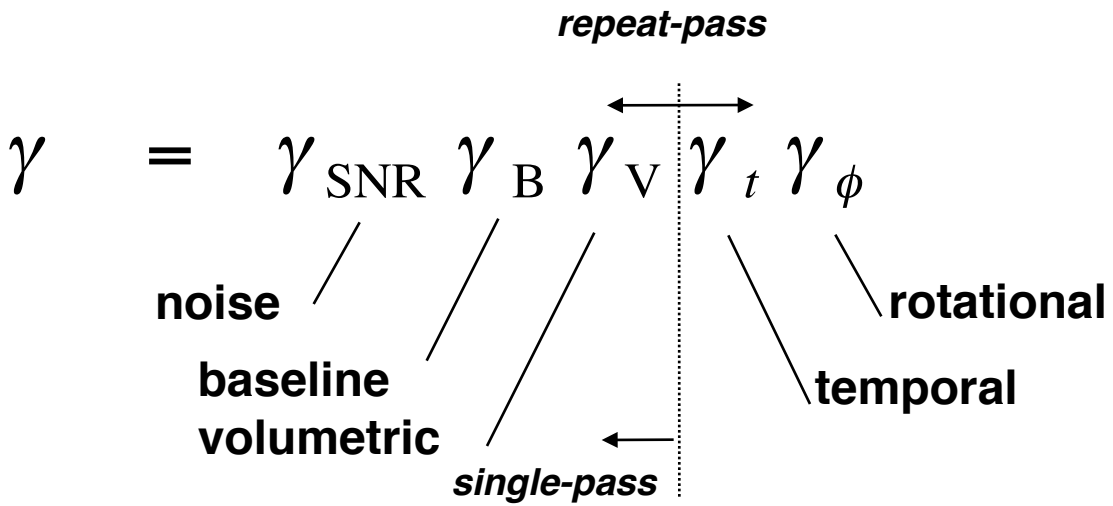

For a calibrated interferometer, γ_{SNR} can be calculated for each pixel. For single-pass systems, $\gamma_t = 1$ and γ_ϕ is usually nearly unity. The baseline decorrelation can be computed from the known geometry, leaving the volumetric correlation, which can used as a diagnostic of surface scatterers.

For calibrated repeat-pass systems with no rotational decorrelation, the product $\gamma_V \gamma_t$ is separable only if $\gamma_t \neq 0$ and γ_V estimates from several baselines are compared.

Interferometric Error Sources

- Interferometric Decorrelation

In addition to the decorrelation contributions, several other sources of error exist in interferometry. These include

- Layover and shadow in radar imagery from slant range geometry
- Multiple scattering within and among resolution cells
- Range and Azimuth sidelobes due to bandwidth/resolution constraints
- Range and azimuth ambiguities due to design constraints
- Multipath and channel cross-talk noise as low-level interference
- Phase unwrapping errors
- Calibration errors
- Propagation delay errors from atmosphere and ionosphere

Hawaii SIR-C One Day Repeat Pass Data Showing Tropospheric Distortion

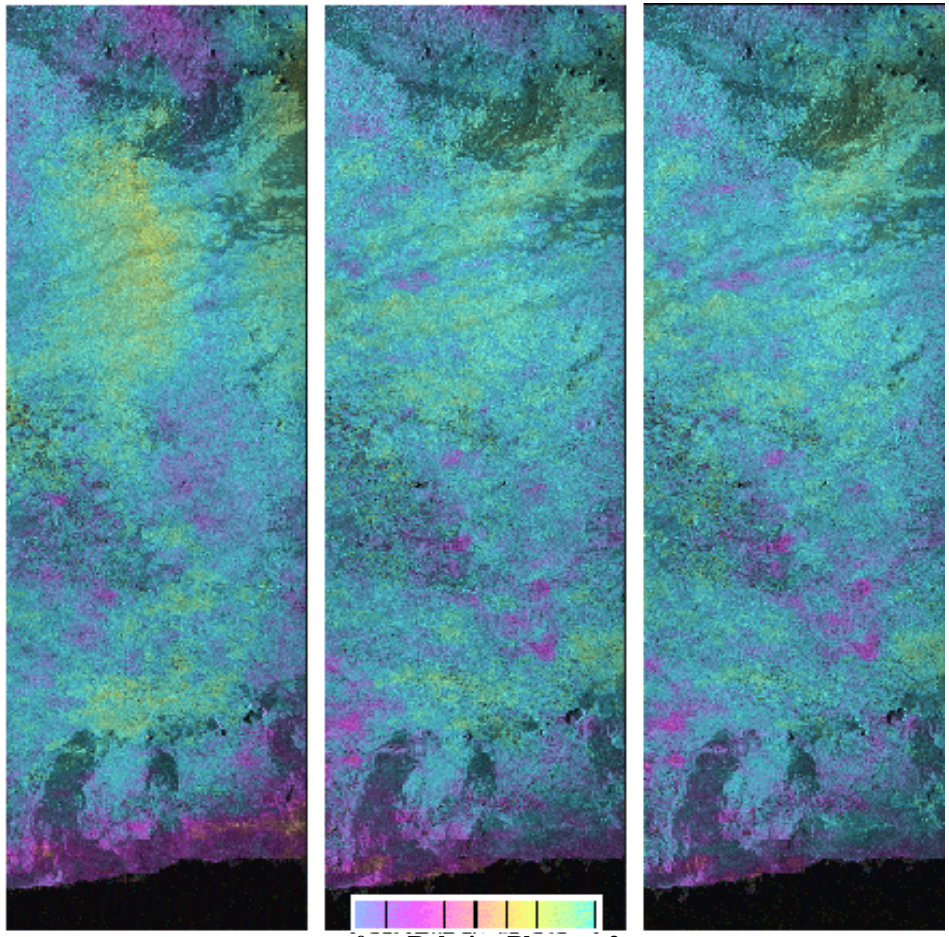

DAYS 7-8 TWO-PASS | DAYS 7-10 TWO-PASS | DAYS 7-8-10 THREE-PASS

The ROI_PAC Algorithmic Flow

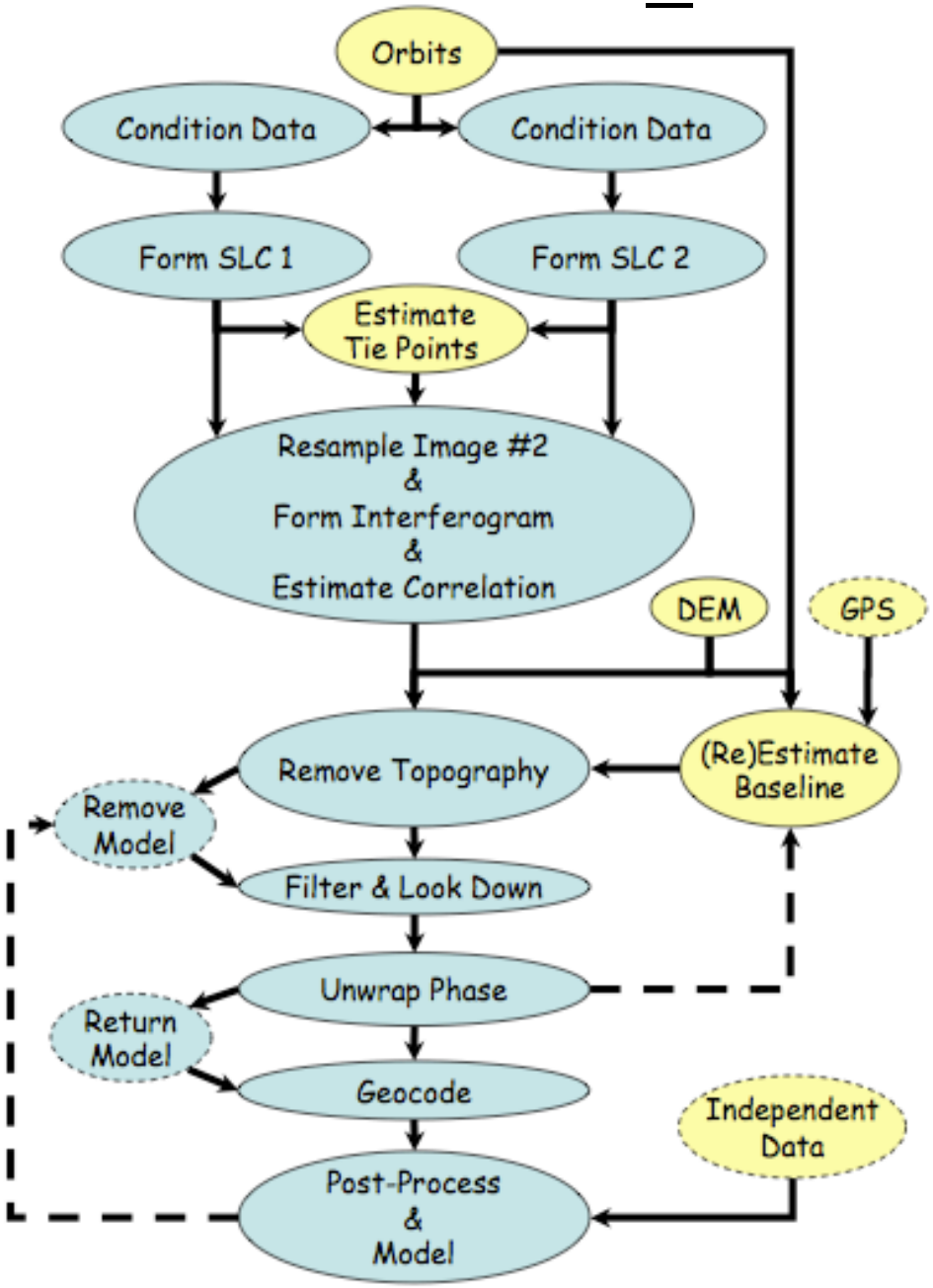

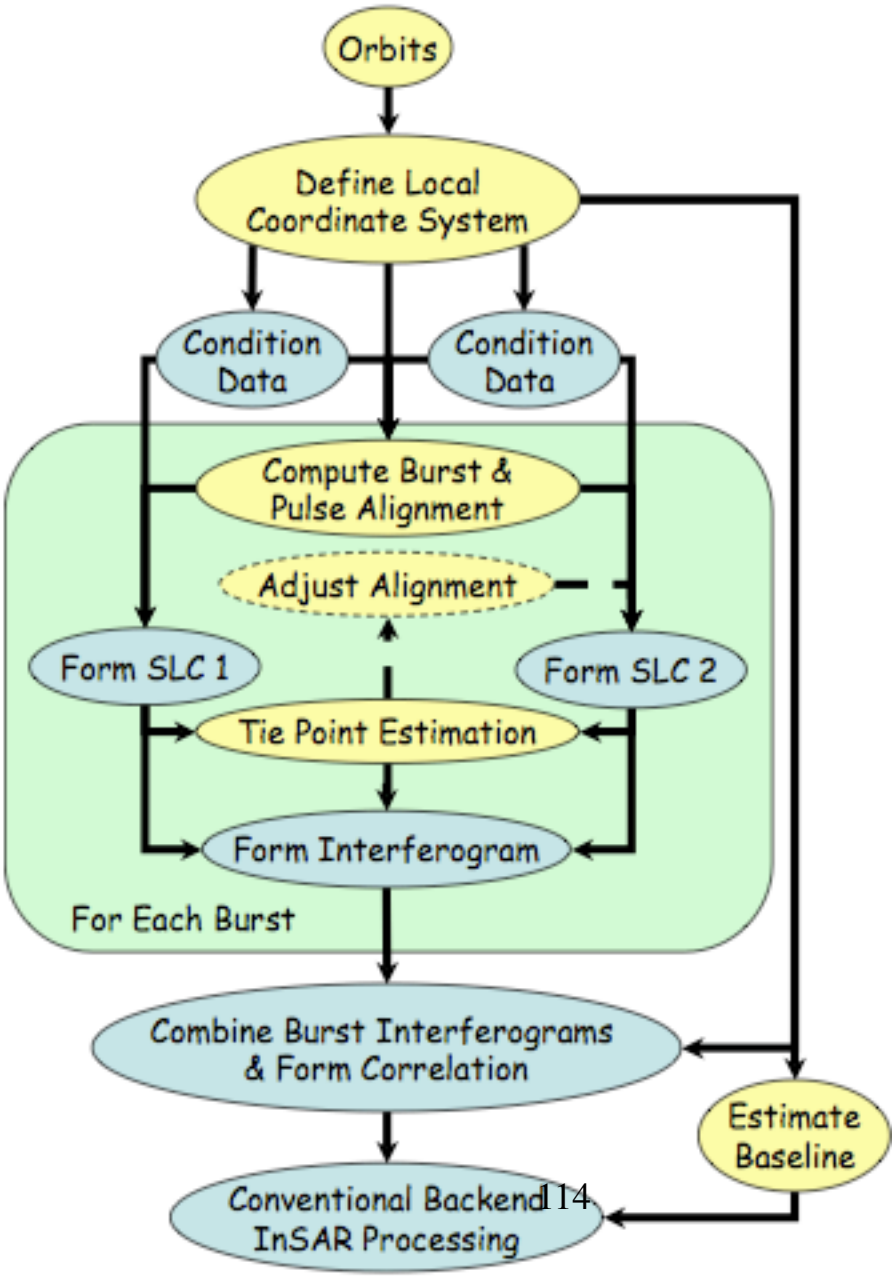

Scene Matching and Coregistration

Cross-correlate images by expedient method

- **Tie-points by eye**
- **Fringe visibility**
- **Amplitude correlation**
- **Amplitude difference**

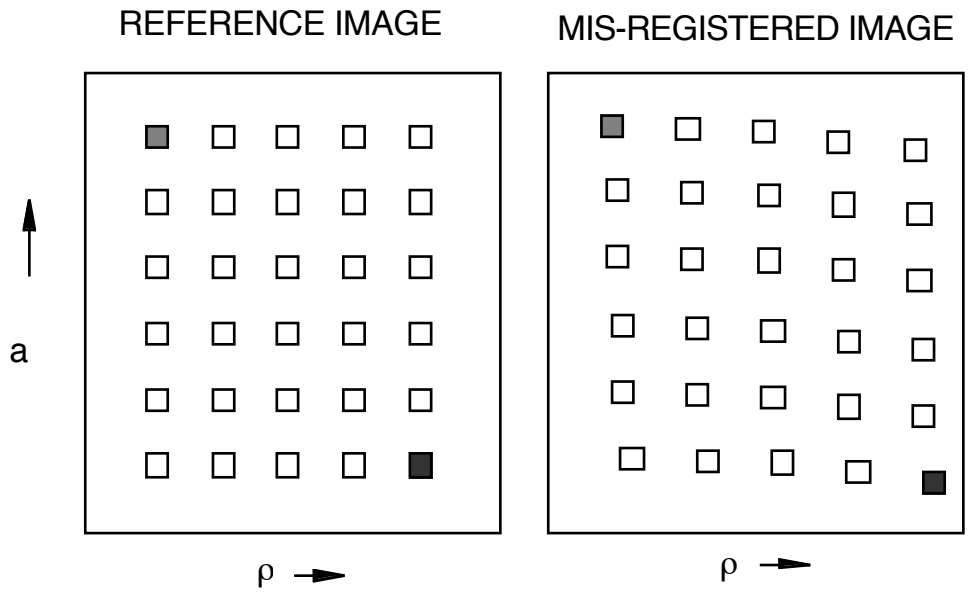

Fit a 2-D function (polynomial) to ($\Delta\rho$,Δa) offset field

Scene Matching on Imagery

- There are a plethora of algorithms in existence for automatic scene matching, each with particular strengths and weaknesses
- SAR scenic matching for interferometry applications is difficult for several reasons:
  - Thermal noise causes the fine structure of two SAR images to differ, adding noise to the correlation measurements.
  - Geometric speckle noise is similar in images acquired in nearly the same geometry, but as the interferometric baseline increases, differing speckle noise corrupts the matching correlation.
  - Scene decorrelation is another form of speckle noise difference that corrupts matching correlation.
- SAR scenic matching for mosaicking applications involves greater challenges, including severe speckle noise differences, layover and shadow effects.

Automatic Scene Matching

- Find overlap region and sample points at specified spacing in along track and cross track direction.
- Typical window sizes are 64x64 pixels for image data and 64x64 or 128x128 pixels for height data.
- Uses a modified Frankot's method for rejecting bad matches and to provide an estimate of the match covariance matrix.
- Cross correlation uses a normalized mean correlation function, mean of search window is calculated over the region in common with the reference window.

Mean of reference is constant

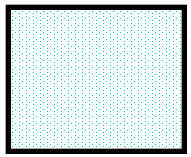

Reference Window

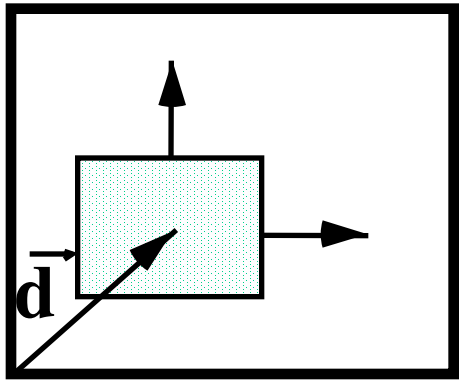

Search Window

Mean of search varies with position

Match Correlation Estimate

- Correlation is computed in the spatial domain using a normalized cross correlation algorithm.
- Let $I_1(\vec{x})$ be the image values at a point $\vec{x}$ in the reference window in the first data set, $\bar{I}_1$, the mean of the intensities in that window.
- Let $I_2(\vec{x}+\vec{d})$ be the image value at point $\vec{x}+\vec{d}$ in the search window of the second data set, and $\bar{I}_2(\vec{d})$ the mean of the intensities in that window.
- Viewing each image as a vector in an n-dimensional vector space then the cross correlation is computed as

$$c(\vec{d}) = \frac{\left\langle I_1 - \bar{I}_1 , I_2(\vec{d}) - \bar{I}_2(\vec{d}) \right\rangle}{\sqrt{\left\| I_1 - \bar{I}_1 \right\| \left\| I_2(\vec{d}) - \bar{I}_2(\vec{d}) \right\|}} = \frac{\left\langle I_1 - \bar{I}_1 , I_2(\vec{d}) - \bar{I}_2(\vec{d}) \right\rangle}{\sigma_{I_1} \sigma_{I_2(\vec{d})}}$$

where σ_{I_1} and $\sigma_{I_2(\vec{d})}$ are the standard deviations of the image intensities in data sets 1 and 2, respectively.

Space-domain correlation used for speed and because large irregular data gaps are trouble free.

JPL

Baseline Estimation from Offsets

- Baseline estimation in repeat pass interferometry is a rich subject. Briefly:
- Offset field determined from scene matching carries information sufficient to reconstruct the baseline to an accuracy com-mensurate with ability to co-register images.
- For nearly parallel, smoothly varying, orbit tracks, the baseline can be modeled as a simple function of the range ρ

$$B_{\parallel}(\rho) \approx B\sin(\theta_0(\rho) - \alpha) = \Delta\rho(\rho)$$

$$B_{\perp}(\rho) \approx B\cos(\theta_0(\rho) - \alpha) = \frac{d\Delta\rho}{d\theta}(\rho)$$

- **Solve two equations for two unknowns:** B, α
- **Evaluating baseline at several widely-spaced along-track (azimuth) locations gives azimuth history of the baseline.**

Converging Baselines

- For orbit tracks with substantial convergence, azimuth offsets strongly characterize convergence rates.

Observation vector:

$$\{\cdots, \Delta\rho(\rho_i, a_i), \Delta a(\rho_i, a_i), \Delta\rho(\rho_{i+1}, a_{i+1}), \Delta a(\rho_{i+1}, a_{i+1}), \cdots\}$$

Parameter vector: $$\{B_{s0}, B_{c0}, B_{h0}, \gamma, \frac{\partial B_c}{\partial s}, \frac{\partial B_h}{\partial s}\}$$

where γ is an image scaling factor resulting from velocity differences between the tracks, and (*s,c,h*) are local coordinates defined by the orbit track (see notes on coordinate systems).

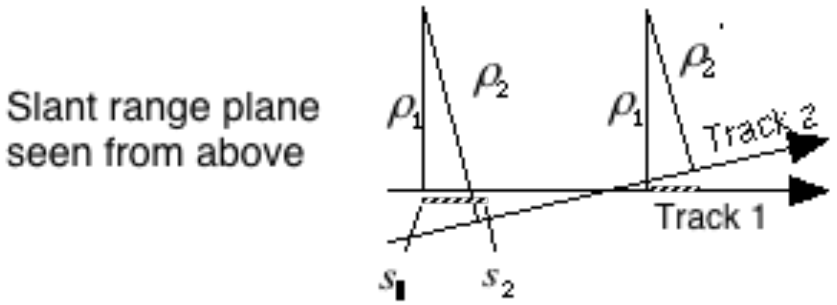

Baseline Accuracy from Offsets

- Baselines determined from offset fields are typically accurate to a fraction of the scene matching accuracy that depends on the model function and the number of offset estimates. Example:
  - Zero baseline image pair with 10 match points across range.
  - Scene matching accuracy of 1/20 pixel resolution at typical single look resolution of 15 meters: 75 cm / $\sqrt{3}$ = 25 cm
- This accuracy is insufficient for topographic mapping applications

$$\sigma_h = \frac{\rho}{B}\sin\theta\cos\alpha\sigma_{B_z}$$

$$= 320 \text{ m} \quad ; \quad \rho = 830 \text{ km}, \; B = 250 \text{ m}, \theta = 23^\circ, \alpha = 0, \sigma_{B_z} = 25 \text{ cm}$$

These geometric parameters are typical of ERS with baselines suitable for topography. Generally, ground control points tied to the unwrapped interferometric phase are required for mapping.

Interferogram Formation

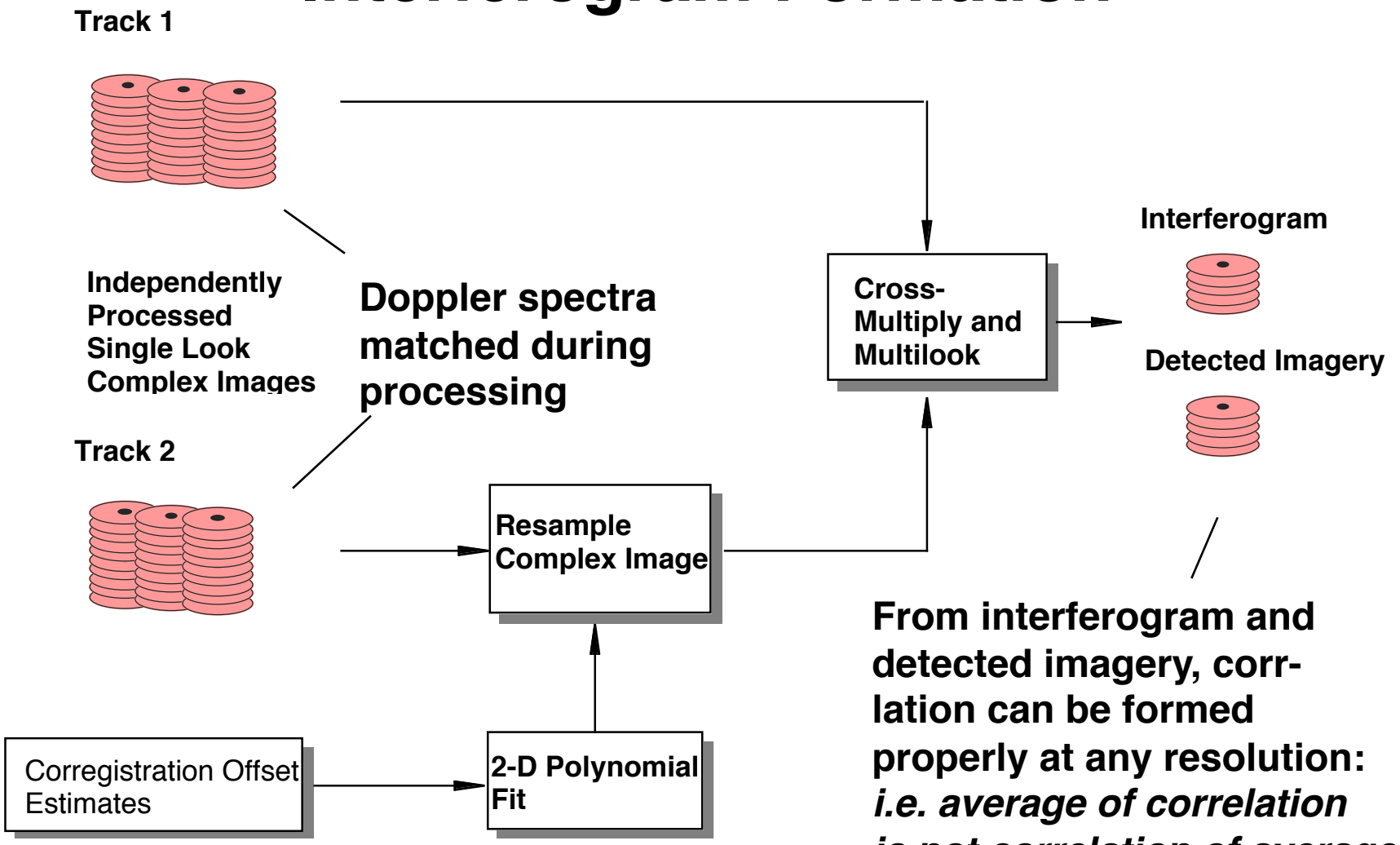

Registration Implementation

- In resampling single look complex image to register properly with the reference image, care must be taken in interpolation of complex data
  - The azimuth spectrum of squinted SAR data is centered at the Doppler centroid frequency - a band-pass signal
  - Simple interpolators, such as linear or quadratic interpolators, are low-pass filters and can destroy band-pass data characteristics
- Band-pass interpolators or spectral methods preserve phase fidelity

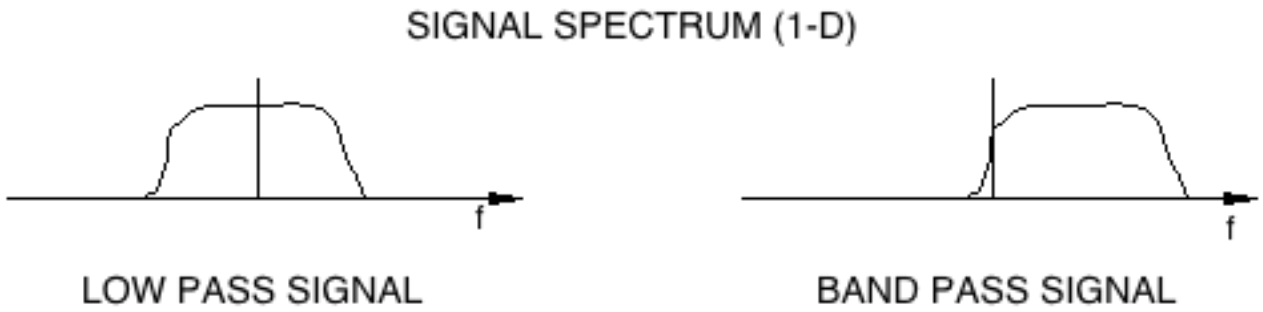

Repeat Pass Interferometry Back-end Processing

Performance Summary:
L-band: good over most terrain
C-band: poor over most terrain

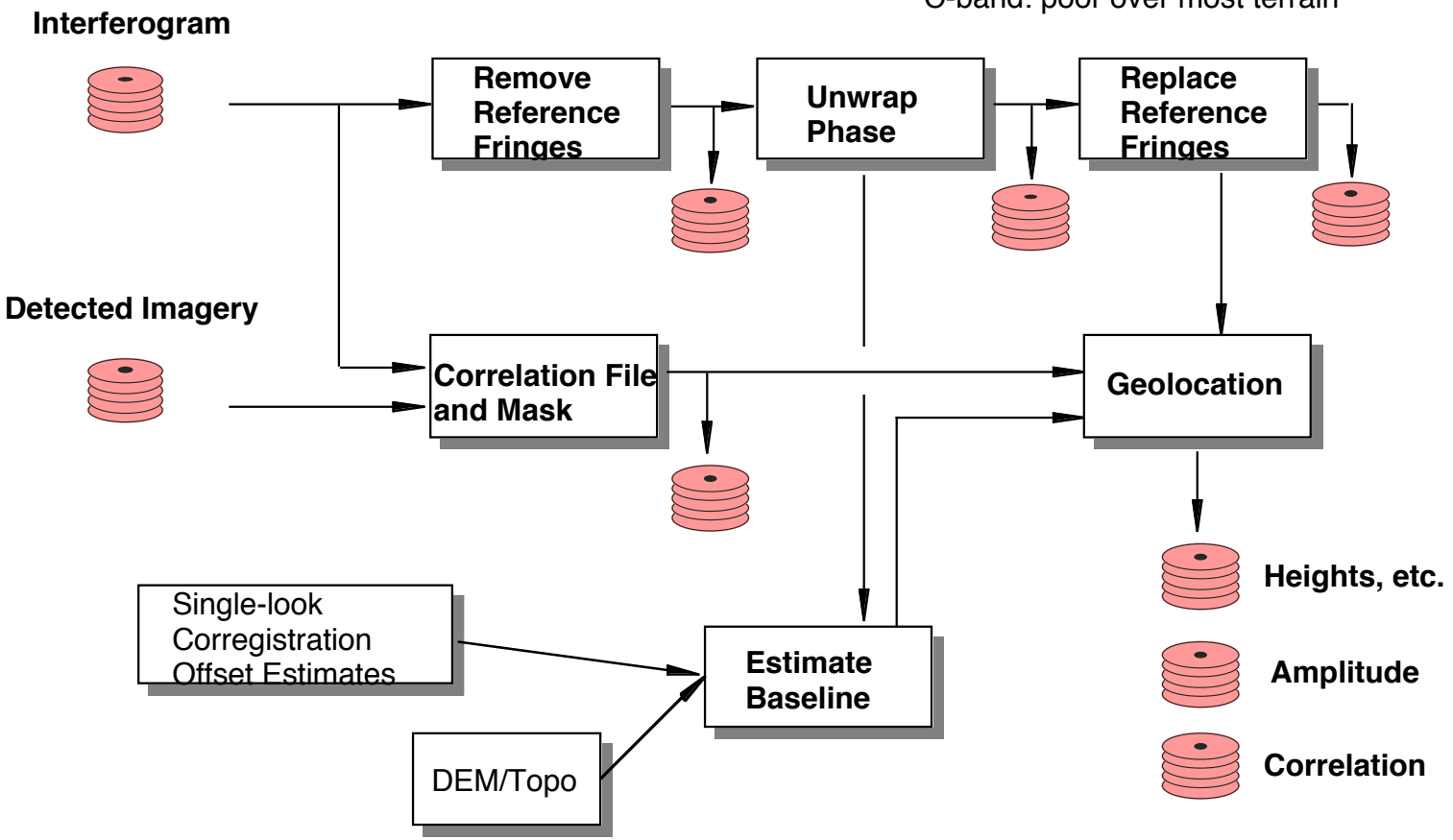

2-Pass Differential Processing

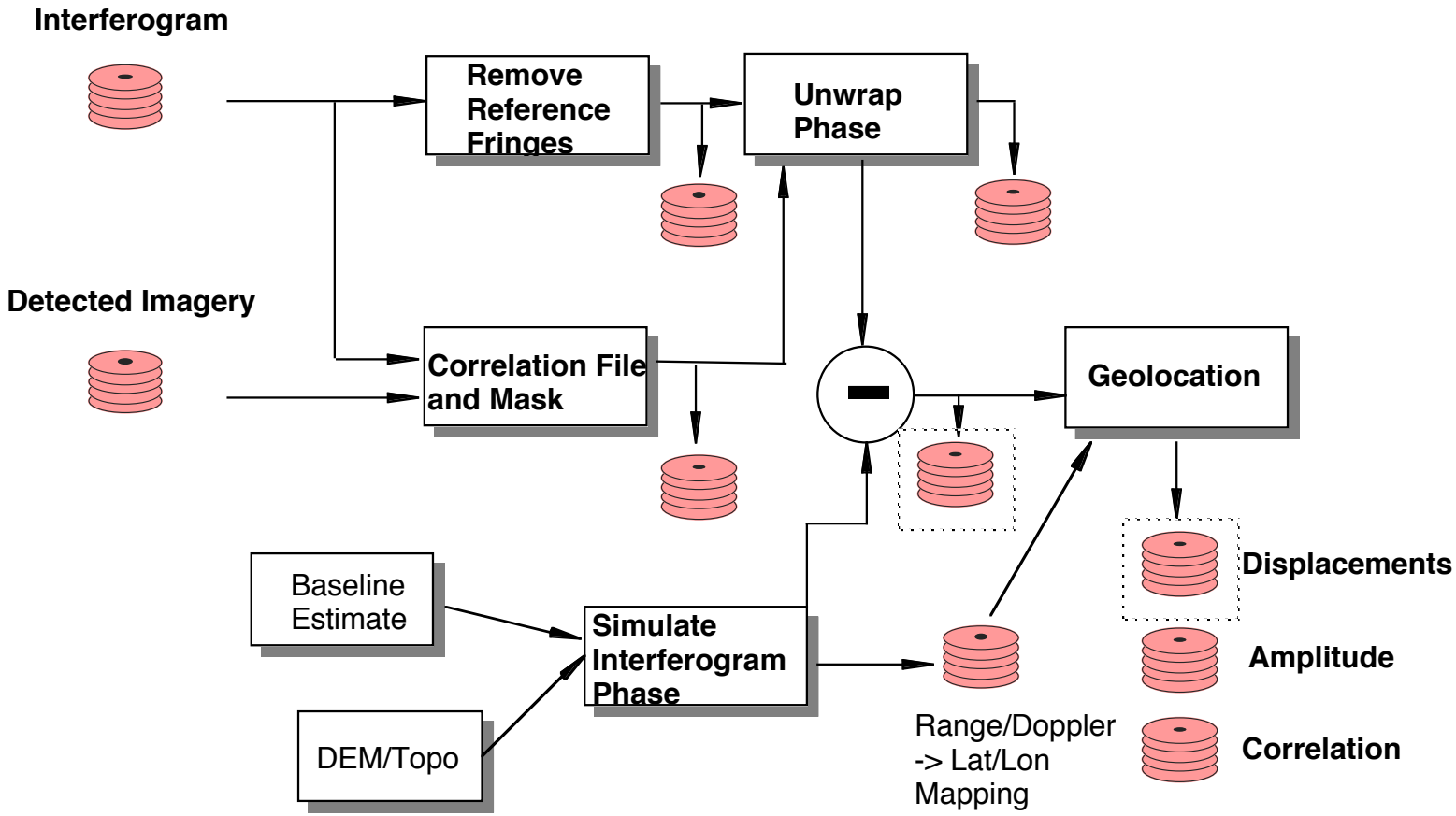

Phase Unwrapping

- Elements of the phase unwrapping problem: From the measured, wrapped phase, unwrap the phase from some arbitrary starting location, then determine the proper ambiguity cycle.

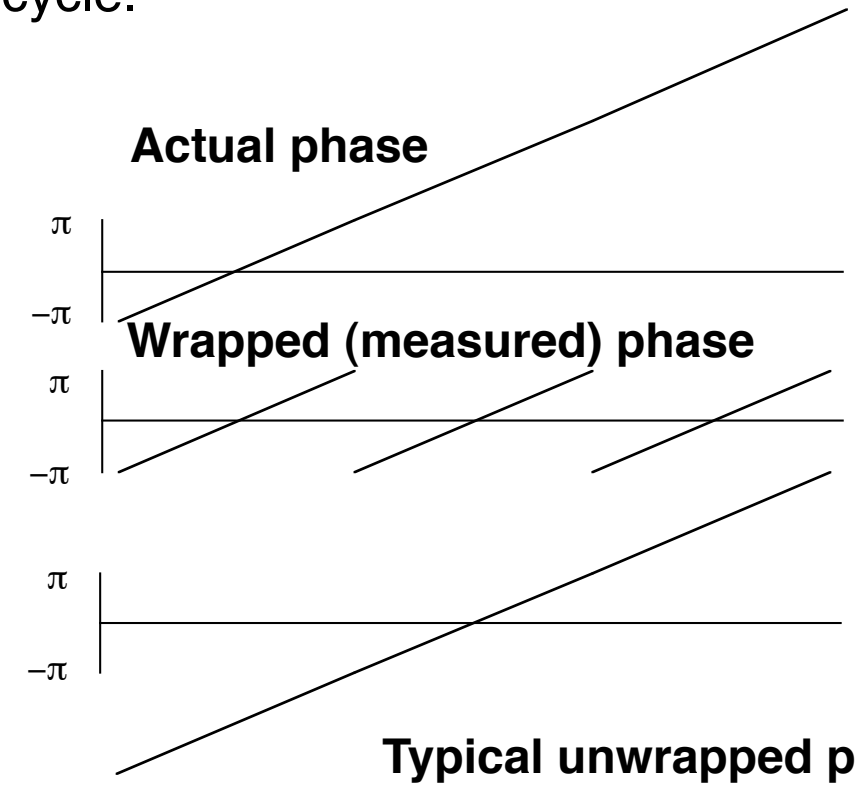

$$\phi = -\frac{4\pi}{\lambda}(\rho_1 - \rho_2) \cong -\frac{4\pi}{\lambda}\vec{B}\cdot\hat{n}_{los}$$

$$\phi_{meas} = \mathrm{mod}(\phi, 2\pi)$$

$$\phi_{unw} = \bigcup(\phi_{meas}) = \phi + 2\pi k$$

where k is an integer to return the absolute phase

Two-Dimensional Phase Unwrapping

- Two dimensional phase field values below are in units of cycles
- One-dimensional unwrapping criterion of half-cycle proximity is inconsistent in two dimensions

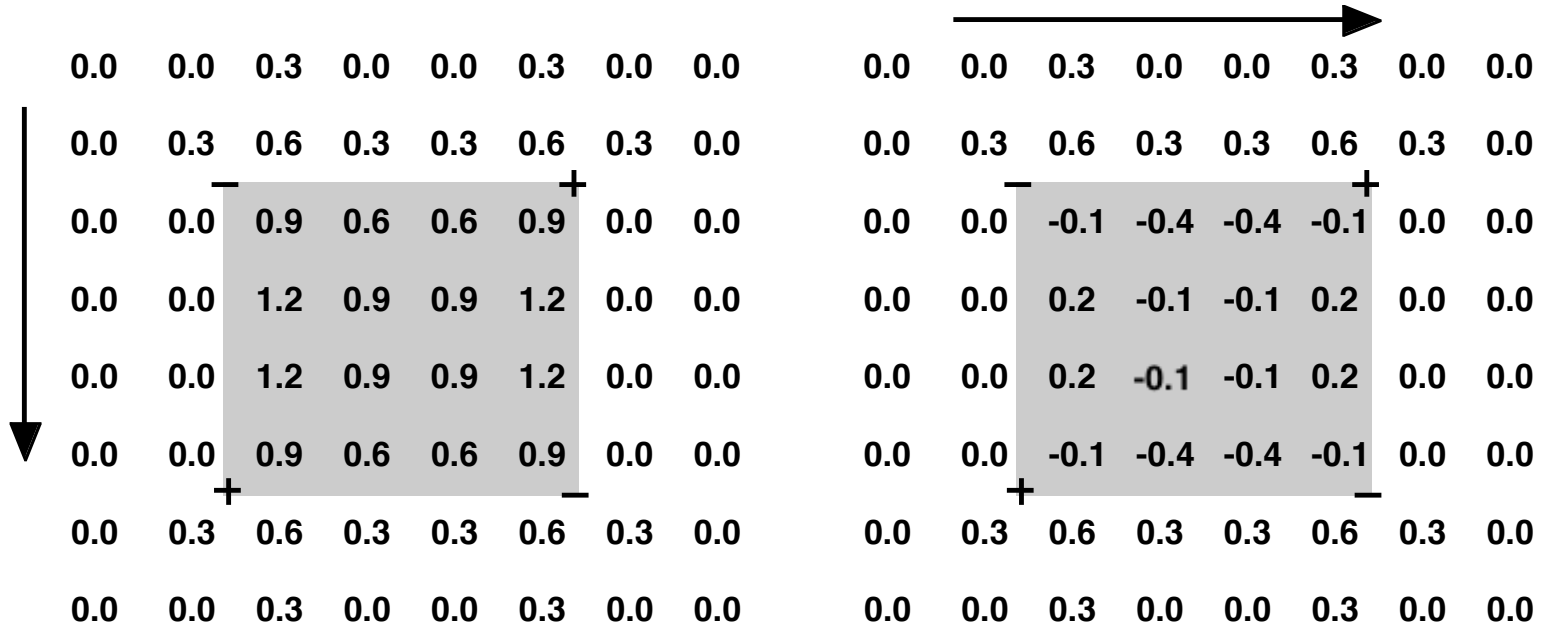

- **Residues, marked with + and -, define ambiguous boundaries.**

Residues in Phase Unwrapping

- The wrapping operator delivers the true phase modulo 2 π, in the interval $-\pi < \phi < \pi$.
- The true phase gradient is conservative: $\nabla \times \nabla \phi = 0$
- The wrapped gradient of the measured, wrapped phase, however, may not be conservative: $\nabla \times W\{\nabla \phi_w\} \neq 0$
- When this function is non-conservative, its integration becomes path dependent.
- Residues occur at locations of high phase noise and/or phase shear such that the wrapped gradient of the measured, wrapped phase is no longer conservative.

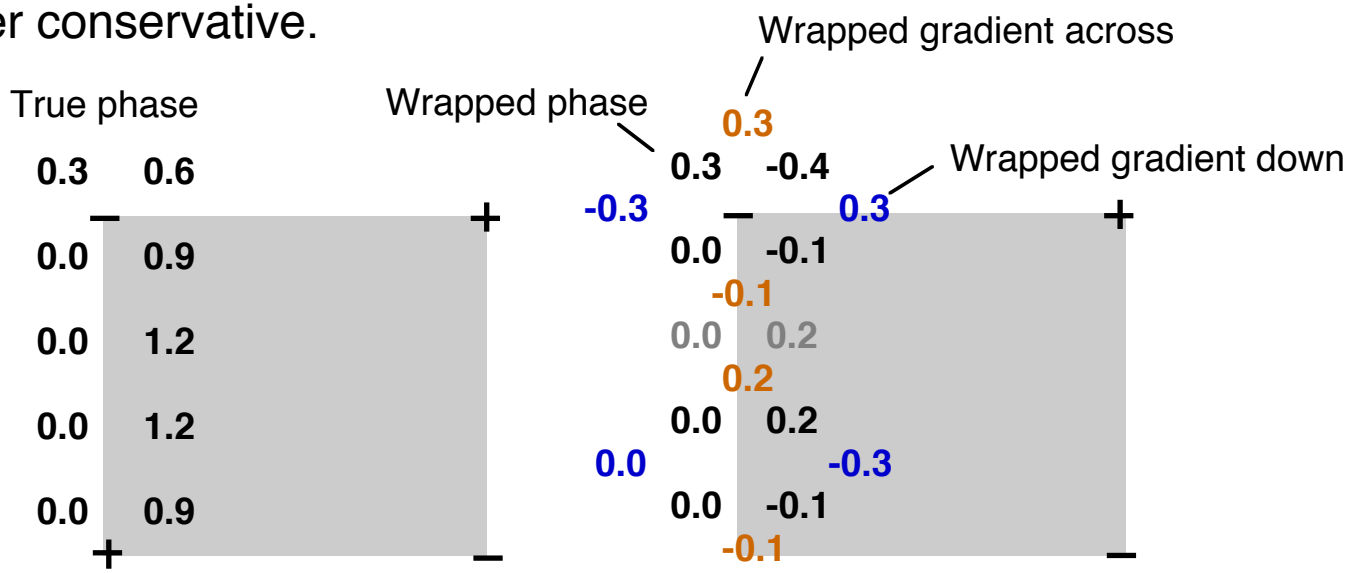

Branch Cuts in Phase Unwrapping

- Branch-cut algorithms (Goldstein, Zebker, and Werner 1986) seek to neutralize these regions of inconsistency by connecting residues of opposite solenoidal sense with cuts, across which integration may not take place.
- Branch cut connections force path independence in the integration of the wrapped phase gradient.
- If done properly, the integrated phase field will be correct. But which is correct?

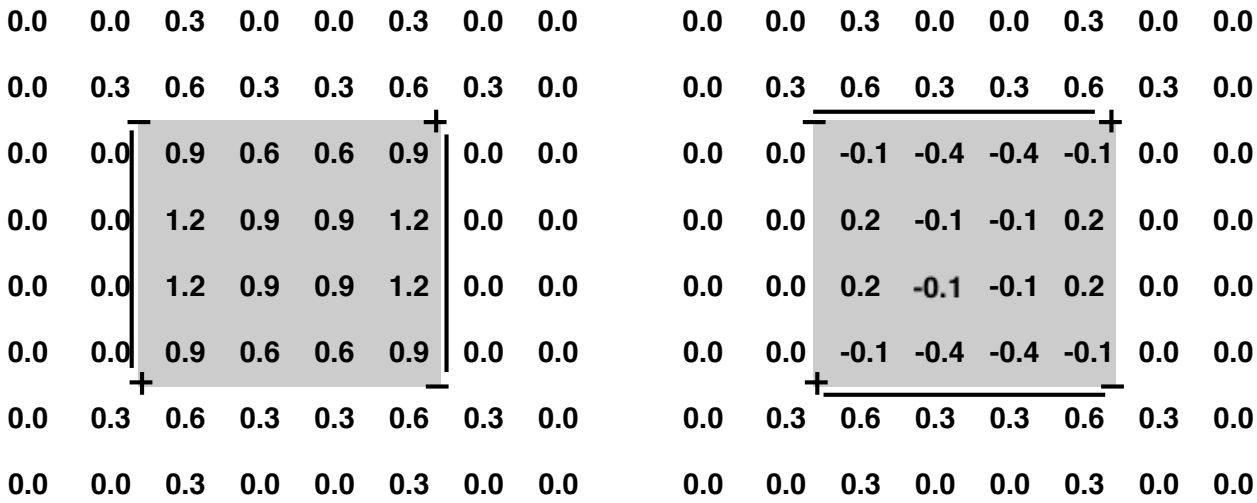

Illustration of Branch Cut Algorithm

Connect all simple pairs

Expand search window and connect where possible

Initiate search from every residue encountered

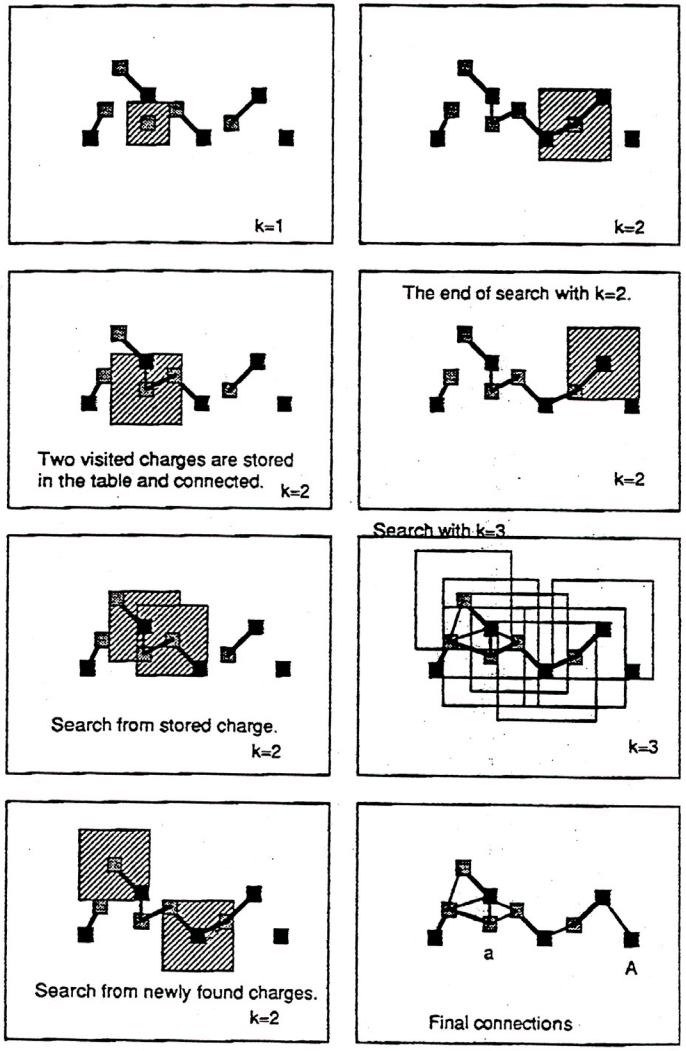

Could not connect last residue with this search window size

Repeat all steps with larger search window size

Branch Cut Strategies

- The standard GZW algorithm is designed to connect residues into a neutral network into the shortest possible connection tree, i.e. to minimize the length of the individual branch cuts comprising a tree
- This will not necessarily create the shortest possible tree, since GZW makes many unnecessary connections in its search for neutrality
- Various criteria have been devised to place guiding centers (unsigned residues) along expected paths to facilitate the right choice in branch cut connection

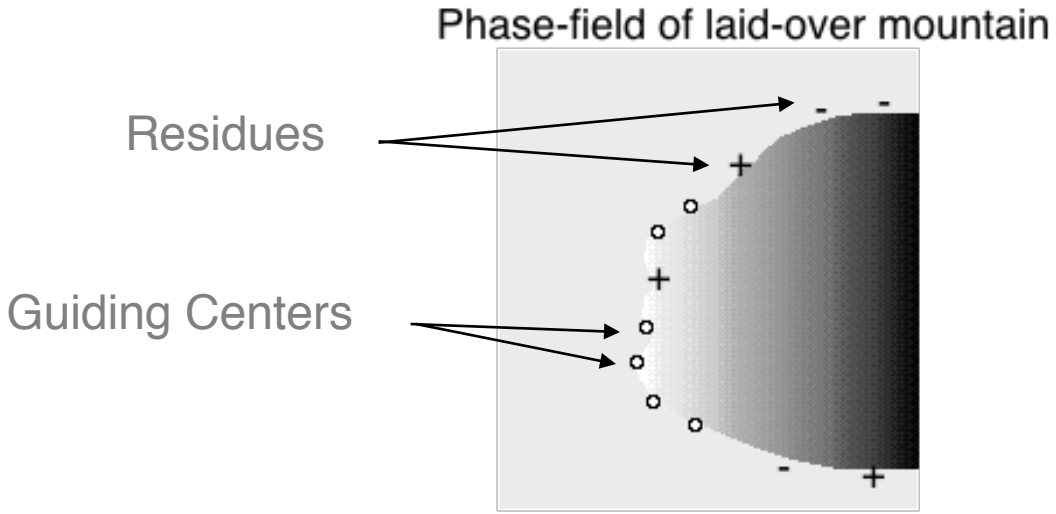

Guiding Center Criteria

- A number of criteria have been devised for selecting guiding centers, each more or less tailored to characteristics of SAR data:
  - when phase slope exceeds threshold (implies layover)
  - when derivative of phase slope exceeds threshold
  - when radar brightness exceeds threshold (implies layover)
  - when decorrelation estimator exceeds threshold (implies noise and/or layover
- Some guiding center selections help in some cases
- Difficult to assess performance in a quantitative way

Absolute Phase Determination

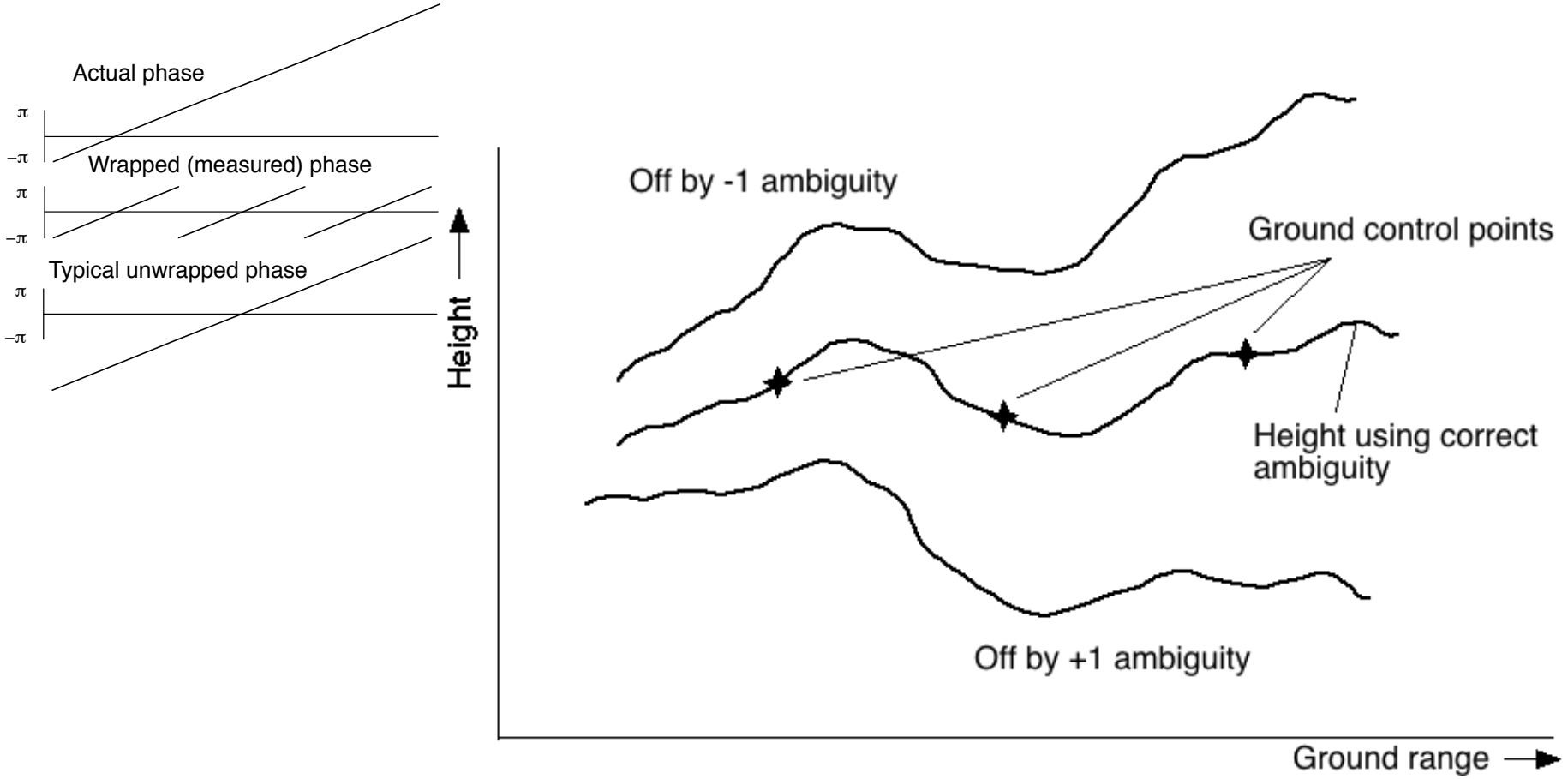

Ground control reference points can be used to determine the absolute phase ambiguity

The ROI_PAC Algorithmic Flow

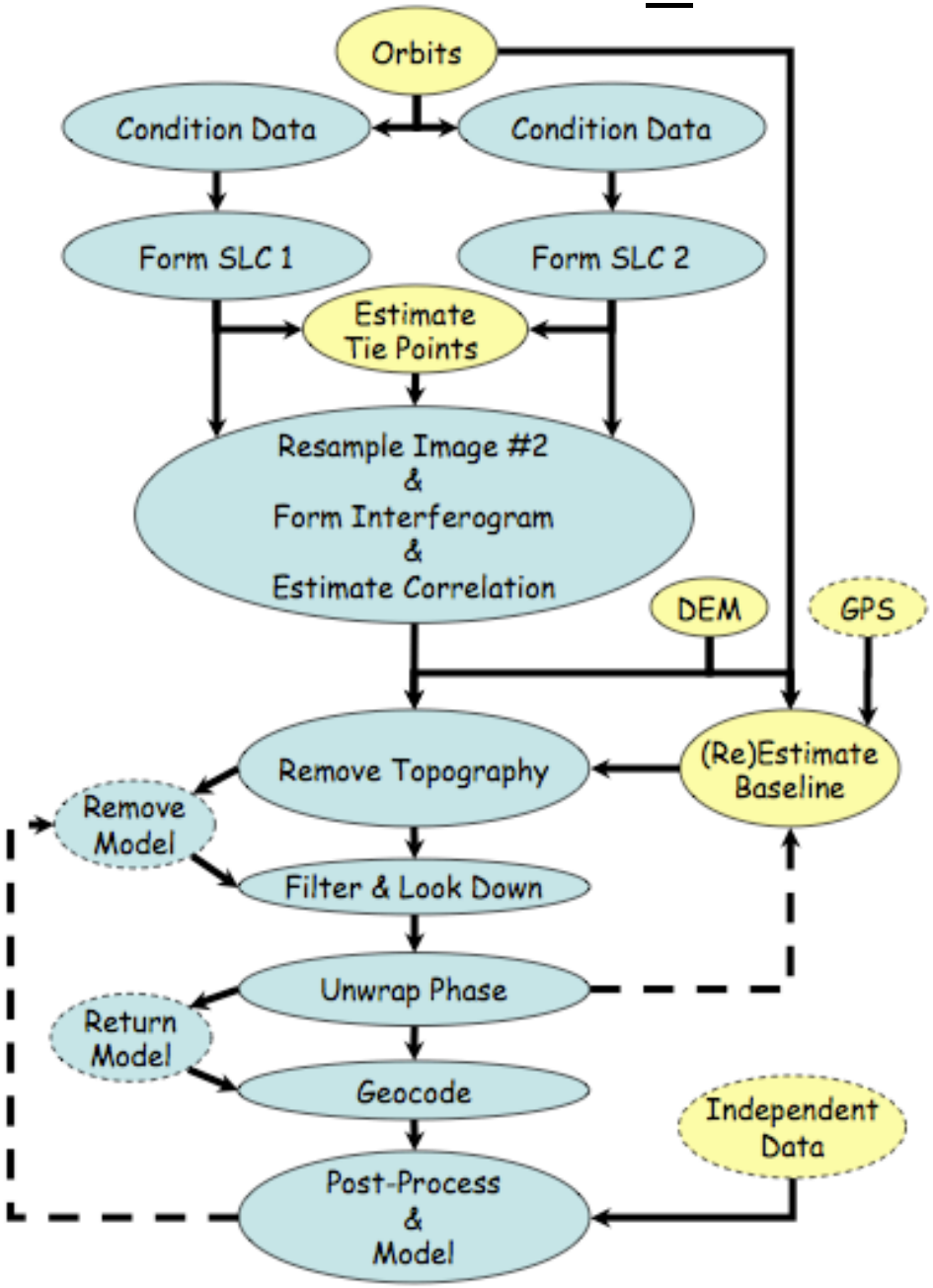

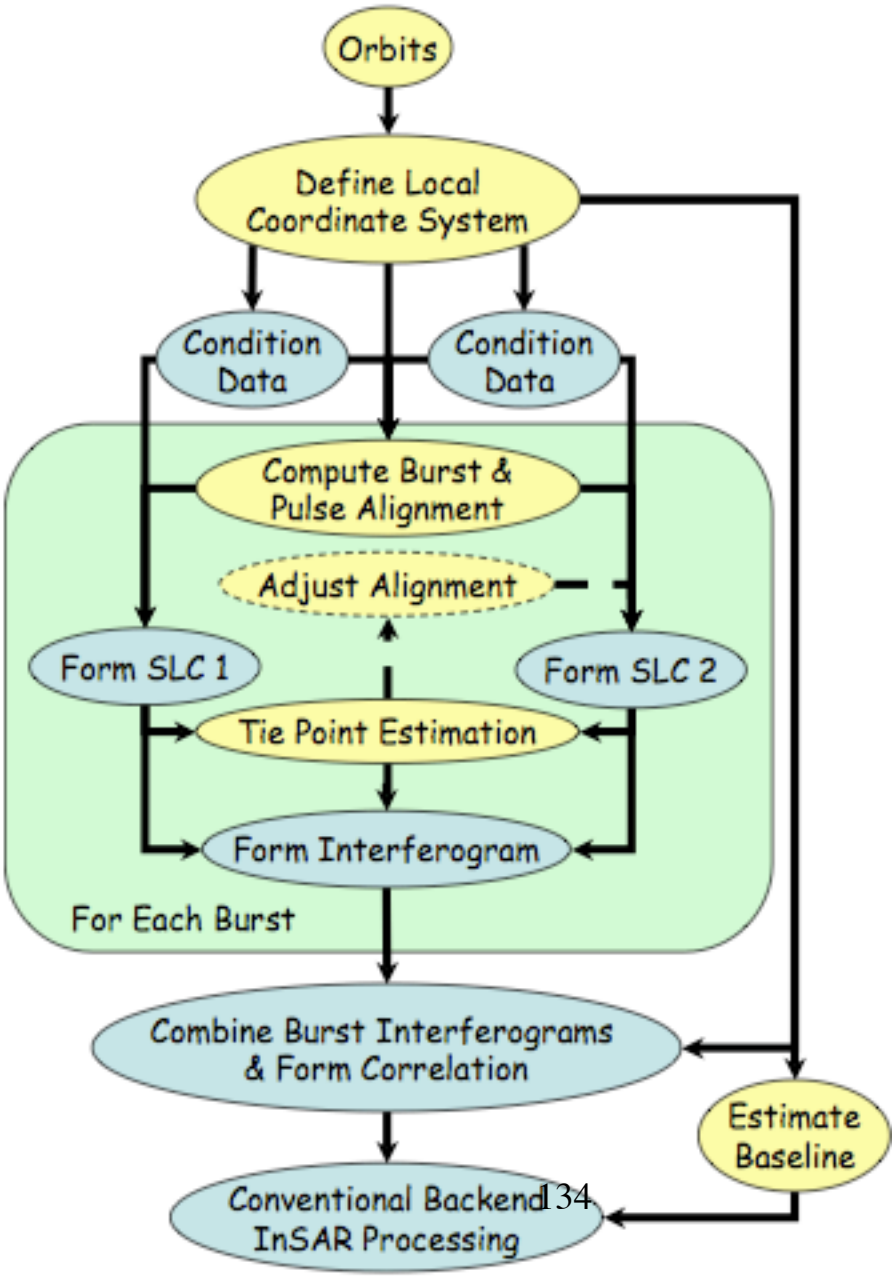

Other Resources

M. Simons and P. Rosen,
Interferometric Synthetic Aperture Radar Geodesy
Treatise on Geophysics, Schubert, G. (ed.), Volume 3- Geodesy, Elsevier Press, pp. 391-446, 2007
http://www.gps.caltech.edu/~simons/pdfs/Simons_Treatise.pdf

Rosen, P. A.; Hensley, S.; Joughin, I. R.; Li, F. K.; Madsen, S. N.; Rodriquez, E. & Goldstein, R. M.
Synthetic Aperture Radar Interferometry
Proc. IEEE, 2000***, 88*****, 333-382**

Burgmann, R.; Rosen, P. & Fielding, E.
Synthetic Aperture Radar Interferometry to measure Earth's surface topography and its deformation
Ann.~Rev.~Earth Planet.~Sci., 2000***, 28*****, 169-209**

Madsen, S. N. & Zebker, H. A.
Synthetic Aperture Radar Interferometry: Principles and Applications
Manual of Remote Sensing, Artech House, **1999***, 3*

Massonnet, D. & Feigl, K. L.
Radar interferometry and its application to changes in the earth's surface
Reviews of Geophysics, **1998***, 36*, 441-500

Bamler, R. & Hartl, P.
Synthetic Aperture Radar Interferometry
Inverse Problems, 1998***, 14*****, 1-54**

What's Next

- Having been exposed to the principles and theory of InSAR, you will spend a day learning to use the roipac software and becoming familiar with
  - images, image pairs and registration offsets
  - interferograms and phase
  - correlation and noise
  - phase ramps and estimating baselines
  - deformation signals and error signals